2023

IRRIGATION IN THE WESTERN UNITED STATES: OCCURRENCE, IMPACTS, AND SUSTAINABILITY

David Granger Ketchum

IRRIGATION IN THE WESTERN UNITED STATES: OCCURRENCE, IMPACTS, AND SUSTAINABILITY

By

DAVID GRANGER KETCHUM

Bachelor of Arts: Environmental Studies, Western Washington University, Bellingham, WA, 2007

&

Masters of Science: Hydrology, New Mexico Institute of Mining and Technology, Socorro, NM, 2016

Dissertation

presented in partial fulfillment of the requirements
for the degree of

Doctor of Philosophy

The University of Montana
Missoula, MT

May, 2023

Approved by:

Scott Whittenburg,
Graduate School Dean

Dr. Kelsey Jencso, Chair
W.A. Franke College of Forestry and Conservation, University of Montana

Dr. John Kimball
Department of Ecosystem and Conservation Sciences

Dr. Douglas Brinkerhoff
Department of Computer Science

Dr. Marco Maneta
Department of Geosciences

Dr. Justin Huntington
Desert Research Institute

ABSTRACT

Ketchum, David Granger, Ph.D., Spring 2023 *Systems Ecology*

Irrigation in the Western United States: Occurrence, Impacts, and Sustainability

Chairperson: Dr. Kelsey G. Jencso

Irrigation represents our greatest intervention in the hydrological cycle, accounting for over 80% of extracted freshwater in the Western U.S. Despite its economic and ecological importance, irrigation's spatial and temporal occurrence, magnitude, impacts on streamflow, and response during water shortages has not been characterized in our region. The major objective of this dissertation was to systematically assess irrigation over the Western US to answer the following questions: 1) Where and when does irrigation occur within the study region? 2) How has the intensity, area, and distribution of irrigation changed over the course of the past 35 years? 3) What impact is irrigation having on surface water (i.e., rivers) in the region, how do impacts differ across basins, and what is driving them? 4) Finally, how do irrigators respond to drought and what can be expected of the irrigated system during water scarce times? To answer these questions, we developed a 35-year dataset covering the western U.S. consisting of high resolution satellite-derived irrigation and evapotranspiration data alongside streamflow, field-scale agricultural boundaries, and detailed climate information. We used a combination of data-driven methods to infer the behavior of irrigation in time and space, Bayesian regression modeling to define relationships between climate, irrigation and streamflow, and detailed geospatial and economic data analysis to explore drivers of the behavior of irrigated systems. We show that both climate change and irrigation are impacting streamflows, and that contrary to government statistics, irrigation is expanding in intensity, area, and water use. We show evidence for the large-scale operation of the 'paradox of irrigation efficiency', where despite increasing on-farm irrigation efficiency enabled by advances in irrigation infrastructure, basin-scale crop water use increases. We show how streamflow is changing and where the changes are driven by changes in climate and irrigation. Finally, we show that crop prices appear to drive crop planting decisions (and thus irrigated water use) to a greater degree than seasonal climate conditions and that intensely irrigated regions are unresponsive to drought. This dissertation contributes to our understanding of the systems-level impact of irrigation and provides opportunities for basin-specific management actions to mitigate irrigation and climate impacts on streamflow.

TABLE OF CONTENTS

LIST OF TABLES

LIST OF FIGURES

Chapter 1

DISSERTATION OVERVIEW

1.1 Chapter 1

Irrigation represents the largest consumptive use of water in the Western United States by our society, and enables the production of enormous quantities of food and fiber in regions otherwise too dry to sustain intensive agriculture. Development of large-scale infrastructure serving irrigated agricultural systems in the arid and semi-arid regions of the Western US (the West) have supported the rapid expansion of the human population and the development of a large and diverse economy. The vast economic benefits of irrigation in the West have been accompanied by costs associated with reservoir operations, large scale water diversion from rivers and extraction from aquifers, and increased evapotranspiration (ET) and reduced runoff from irrigated regions. Ecological impacts include the modification of wetlands [1, 2], changes to stream flow and surface water temperature regimes [3, 4], alteration of sedimentation [5], and modification of local weather patterns [6, 7, 8, 9].

Despite the societal importance and ecological impact of irrigation, its occurrence and behavior over time have been poorly quantified in the scientific literature. I created a system to accurately map the occurrence of irrigation through time at high resolution, a prerequisite step to enable the detection of irrigation water use (IWU) patterns through time. I then used our irrigated lands mapping system (IrrMapper), to quantify the water use of irrigated agriculture within the variable areal extent over which irrigation is applied each year to examine the IWU in the context of changing climate and its role in changing streamflow in the West. Finally, I used our datasets to examine the response of irrigation to drought at the large river basin and individual irrigated field scales to determine how irrigation responds to drought and whether factors such as crop type, federal irrigation project management, and on-field irrigation infrastructure type determine water use.

The most robust accounting of irrigated area has been made since the 1840s by the National Agricultural Statistics Service (and its predecessors; NASS), a US Department of Agriculture branch that tracks revenue-producing farms in the US [10]. As a survey-based estimate of irrigated area, NASS's Census of Agriculture is subject to errors of nonresponse, undercoverage, and misclassification of farm operations, and excludes small operations and non-farm irrigation (golf courses, playing fields) [11]. Further, the survey tabulates data at the county scale, hindering the correlation of specific irrigated areas with estimates of production, water use, and planting decisions. Satellite remote sensing (SRS) offers the advantages of spatiotemporally resolved information about changing conditions on the landscape, and has been used in several efforts to map the spatial and temporal extent of irrigation using SRS information in algorithms capable of classifying irrigation based in part on spectral information gathered by SRS [12, 13, 14, 15, 16]. While several of these irrigated lands classification systems cover part or all of the West, they either lack the long period of record, annual temporal resolution, or fine spatial resolution necessary to estimate multidecadal, field-scale irrigated area requisite to fully characterize IWU over the West.

In Chapter 1, we describe IrrMapper, our approach to mapping annual irrigated area at high resolution over the West using an automatic classifier implemented on Google Earth Engine [17]. We used a supervised machine learning approach to classify irrigated lands based on Landsat surface reflectance data, gridded climate information, and existing land use information. We used the Random Forest algorithm, an ensemble decision tree classifier that has been shown in other studies to be a reliable and fast classifier suitable for use with large input data sets containing correlated features. We developed an unprecedented database of verified irrigated field boundaries to use as training data, and developed IrrMapper independently of survey estimates of irrigated area. IrrMapper classifies irrigation at 30 m resolution, was initially produced at an annual time step from 1986-2018 (and eventually through 2021), and has an overall accuracy of over 97%. IrrMapper was built using an accessible set of open-source Python software packages that allow for easy iteration

and re-processing of training data and deployment of updated predictions, and was updated frequently throughout this dissertation research.

1.2 Chapter 2

Studies characterizing the impact on streamflow by irrigation operations are few and limited to relatively short periods at the basin scale [3, 18, 19]. Where large scale characterization of irrigation impacts has been undertaken, approaches have been dependent on coarse spatiotemporal information and proxies for crop water use [20, 21, 22]. Studies examining the sustainability of irrigation in the Western U.S. have primarily addressed groundwater and salinity issues [23, 24, 25]. Large-scale assessment of crop water use trends in the US has been hindered by a lack of information detailing the rate, time and place of irrigation; most studies in the region rely on the aforementioned NASS census that provides data only at the county scale and quantifies only irrigated area and water application rates, not consumptive use [26, 27]. Advances in scalable evapotranspiration and irrigation area mapping techniques using long-period, high resolution satellite remote sensing, and Landsat in particular, have enabled the systematic estimate of crop water use on a large scale [28, 29].

In Chapter 2, we exploit the resolution and period of IrrMapper to make estimates of large-scale IWU in the Colorado, Columbia, and Upper Missouri river basins and to connect the irrigated landscape's large-scale water use to streamflow in the context of climate change. In order to estimate IWU, we applied the Simplified Surface Energy Balance (Operational; SSEBop [30]) to our 1.6 M km^2 study area to find monthly growing season crop ET, and developed a simple approach to estimate the amount of water lost to crop ET ultimately derived from in place precipitation (i.e., effective precipitation). The monthly, 30 m resolution pixel-wise difference of effective precipitation and total ET is IWU, which we aggregated to basin scale to relate with streamflow. We accounted for climate using the Climatic Water Balance, the difference between reference evapotranspiration (ETr) and precipitation. We analyzed climate, streamflow, and IWU trends, showing climate and

flow trends differ by region, but that increases in irrigated area and intensity are nearly ubiquitous. We find systems where climate change does not explain the change in streamflow and attribute those changes to IWU. Further, we link changes in streamflow and IWU to the modernization of irrigation infrastructure, and suggest the impacts we observe are in part due to the operation of 'irrigation efficiency paradox', where improvements in on-farm irrigation efficiency counterintuitively lead to increases in basin-scale water use [31, 32, 33]. Comparison of streamflow and IWU trends offer a metric of sustainability, and indicate the Snake and Colorado river basins follow a systematically unsustainable trajectory in water use and supply, a cause for concern and consideration of alternative management strategies. This study offers avenues through which irrigation management can be tailored to basin-specific characteristics in order to mitigate negative impacts of water scarcity.

1.3 Chapter 3

Irrigation management decisions can have important implications for the sustainability of surface water supplies; as documented in Chapter 2. While our results regarding trends in IWU reveal the change in our irrigated system through time, it is as important to define the response of the system when water is least plentiful and the consequences of the tradeoff between irrigation and other uses are most acute [22]. The response of irrigation to water scarcity depends on local, field-scale management by producers, who consider a plethora of factors that ultimately determine their planting and irrigation decisions, and ultimately their water use. These factors include the potential water deliveries, crop yields, the price of inputs and crop products, and drought conditions [34, 35, 36].

In Chapter 3, we characterize the link between climate state as expressed in two drought metrics (Standardized Precipitation Index (SPI), and Standardized Precipitation and Evapotranspiration Index (SPEI)) and a novel measure of irrigation intensity, Standardized Irrigation Management Index (SIMI). SIMI is calculated using the anomaly in remote sensing-based estimates of crop coefficient, or the fraction of ETr a crop experiences. SIMI allows us to remove the direct functional dependence of crop ET on ETr, thus providing a means to

isolate management-induced differences in irrigated crops. We applied the drought metrics and SIMI at the basin and field scale. We show that irrigation management at the basin scale responds weakly to SPI and SPEI, with the strongest correlation at short time scales (3-4 months), implying seasonal meteorology is more explanatory of irrigated crop water use than longer term climate. This further implies that irrigation management is largely unresponsive to interannual variation in water supply, which depends to a greater extent on longer meteorological time scales, as shown in Chapter 2. At the field scale, SIMI response to SPEI was found to be highly varied at the local scale, but differentiated at the basin scale between the Upper Colorado, Columbia, and Upper Missouri systems. We found that when we calculated SIMI at the field scale, differences were found based on field-scale attributes; irrigation type, inclusion in federal irrigation infrastructure projects, and crop category all showed differences in the relationship between SIMI during different drought states according to a common classification (i.e., SPEI-based classification into 'wet', 'normal', and 'dry' growing seasons). Using a classifier based on price and climate data to predict crop transitions, we show that among the standardized coefficients, those associated with price are more often of greater magnitude than the climate coefficient, suggesting that prices are a stronger driver of crop planting decisions and subsequent water use.

REFERENCES

[1] M. Reisner, *Cadillac desert: The American West and its disappearing water*. Penguin, 1993.

[2] D. E. Peck and J. R. Lovvorn, "The importance of flood irrigation in water supply to wetlands in the laramie basin, wyoming, usa," *Wetlands*, vol. 21, no. 3, pp. 370–378, 2001.

[3] H. I. Essaid and R. R. Caldwell, "Evaluating the impact of irrigation on surface water–groundwater interaction and stream temperature in an agricultural watershed," *Science of the total environment*, vol. 599, pp. 581–596, 2017.

[4] B. R. Scanlon, I. Jolly, M. Sophocleous, and L. Zhang, "Global impacts of conversions from natural to agricultural ecosystems on water resources: Quantity versus quality," *Water resources research*, vol. 43, no. 3, 2007.

[5] D. J. Stanley and A. G. Warne, "Nile delta: recent geological evolution and human impact," *Science*, vol. 260, no. 5108, pp. 628–634, 1993.

[6] W. J. Sacks, B. I. Cook, N. Buenning, S. Levis, and J. H. Helkowski, "Effects of global irrigation on the near-surface climate," *Climate Dynamics*, vol. 33, no. 2-3, pp. 159–175, 2009.

[7] B. Yang, Y. Zhang, Y. Qian, J. Tang, and D. Liu, "Climatic effects of irrigation over the huang-huai-hai plain in china simulated by the weather research and forecasting model," *Journal of Geophysical Research: Atmospheres*, vol. 121, no. 5, pp. 2246–2264, 2016.

[8] Z. Yang, F. Dominguez, X. Zeng, H. Hu, H. Gupta, and B. Yang, "Impact of irrigation over the california central valley on regional climate," *Journal of Hydrometeorology*, vol. 18, no. 5, pp. 1341–1357, 2017.

[9] Z. Yang, Y. Qian, Y. Liu, L. K. Berg, H. Hu, F. Dominguez, B. Yang, Z. Feng, W. I. Gustafson Jr, M. Huang, *et al.*, "Irrigation impact on water and energy cycle during dry years over the united states using convection-permitting wrf and a dynamical recycling model," *Journal of Geophysical Research: Atmospheres*, vol. 124, no. 21, pp. 11220–11241, 2019.

[10] "Quick stats: United states department of agriculture national agricultural statistics service," 2020.

[11] L. J. Young, A. C. Lamas, and D. A. Abreu, "The 2012 census of agriculture: a capture–recapture analysis," *Journal of Agricultural, Biological and Environmental Statistics*, vol. 22, no. 4, pp. 523–539, 2017.

[12] Y. Xie, T. J. Lark, J. F. Brown, and H. K. Gibbs, "Mapping irrigated cropland extent across the conterminous united states at 30 m resolution using a semi-automatic training approach on google earth engine," *ISPRS Journal of Photogrammetry and Remote Sensing*, vol. 155, pp. 136–149, 2019.

[13] M. S. Pervez and J. F. Brown, "Mapping irrigated lands at 250-m scale by merging modis data and national agricultural statistics," *Remote Sensing*, vol. 2, no. 10, pp. 2388–2412, 2010.

[14] M. S. Pervez, M. Budde, and J. Rowland, "Mapping irrigated areas in afghanistan over the past decade using modis ndvi," *Remote sensing of environment*, vol. 149, pp. 155–165, 2014.

[15] J. M. Deines, A. D. Kendall, and D. W. Hyndman, "Annual irrigation dynamics in the us northern high plains derived from landsat satellite data," *Geophysical Research Letters*, vol. 44, no. 18, pp. 9350–9360, 2017.

[16] J. M. Deines, A. D. Kendall, M. A. Crowley, J. Rapp, J. A. Cardille, and D. W. Hyndman, "Mapping three decades of annual irrigation across the us high plains aquifer

using landsat and google earth engine," *Remote Sensing of Environment*, vol. 233, p. 111400, 2019.

[17] D. Ketchum, K. Jencso, M. P. Maneta, F. Melton, M. O. Jones, and J. Huntington, "IrrMapper: A machine learning approach for high resolution mapping of irrigated agriculture across the western U.S," *Remote Sensing*, vol. 12, p. 2328, July 2020.

[18] F. Wen and X. Chen, "Evaluation of the impact of groundwater irrigation on streamflow in nebraska," *J. Hydrol.*, vol. 327, pp. 603–617, Aug. 2006.

[19] R. Zeng and X. Cai, "Analyzing streamflow changes: irrigation-enhanced interaction between aquifer and streamflow in the republican river basin," *Hydrol. Earth Syst. Sci. Discuss.*, vol. 10, pp. 7783–7807, June 2013.

[20] S. M. Vicente-Serrano, M. Peña-Gallardo, J. Hannaford, C. Murphy, J. Lorenzo-Lacruz, F. Dominguez-Castro, J. I. López-Moreno, S. Beguería, I. Noguera, S. Harrigan, and J.-P. Vidal, "Climate, irrigation, and land cover change explain streamflow trends in countries bordering the northeast atlantic," *Geophys. Res. Lett.*, vol. 46, pp. 10821–10833, Oct. 2019.

[21] Y. Wada, L. P. H. van Beek, N. Wanders, and M. F. P. Bierkens, "Human water consumption intensifies hydrological drought worldwide," *Environ. Res. Lett.*, vol. 8, p. 034036, Sept. 2013.

[22] B. D. Richter, D. Bartak, P. Caldwell, K. F. Davis, P. Debaere, A. Y. Hoekstra, T. Li, L. Marston, R. McManamay, M. M. Mekonnen, B. L. Ruddell, R. R. Rushforth, and T. J. Troy, "Water scarcity and fish imperilment driven by beef production," *Nature Sustainability*, vol. 3, pp. 319–328, Mar. 2020.

[23] B. R. Scanlon, R. C. Reedy, and J. B. Gates, "Effects of irrigated agroecosystems: 1. quantity of soil water and groundwater in the southern high plains, texas," *Water Resour. Res.*, vol. 46, Sept. 2010.

[24] B. R. Scanlon, C. C. Faunt, L. Longuevergne, R. C. Reedy, W. M. Alley, V. L. McGuire, and P. B. McMahon, "Groundwater depletion and sustainability of irrigation in the US high plains and central valley," *Proc. Natl. Acad. Sci. U. S. A.*, vol. 109, pp. 9320–9325, June 2012.

[25] G. Schoups, J. W. Hopmans, C. A. Young, J. A. Vrugt, W. W. Wallender, K. K. Tanji, and S. Panday, "Sustainability of irrigated agriculture in the san joaquin valley, california," *Proc. Natl. Acad. Sci. U. S. A.*, vol. 102, pp. 15352–15356, Oct. 2005.

[26] A. Hrozencik and M. Aillery, "Trends in irrigated agriculture reveal sector's ability to adapt to evolving climatic, resource, and market conditions," *Amber Waves*, vol. 2022, no. 1490-2022-276, 2022.

[27] I. K. Mpanga and O. J. Idowu, "A decade of irrigation water use trends in southwestern USA: The role of irrigation technology, best management practices, and outreach education programs," *Agric. Water Manage.*, vol. 243, p. 106438, Jan. 2021.

[28] M. C. Anderson, R. G. Allen, A. Morse, and W. P. Kustas, "Use of landsat thermal imagery in monitoring evapotranspiration and managing water resources," *Remote Sensing of Environment*, vol. 122, pp. 50–65, 2012.

[29] F. S. Melton, J. Huntington, R. Grimm, J. Herring, M. Hall, D. Rollison, T. Erickson, R. Allen, M. Anderson, J. B. Fisher, A. Kilic, G. B. Senay, J. Volk, C. Hain, L. Johnson, A. Ruhoff, P. Blankenau, M. Bromley, W. Carrara, B. Daudert, C. Doherty, C. Dunkerly, M. Friedrichs, A. Guzman, G. Halverson, J. Hansen, J. Harding, Y. Kang, D. Ketchum, B. Minor, C. Morton, S. Ortega-Salazar, T. Ott, M. Ozdogan, P. M. ReVelle, M. Schull, C. Wang, Y. Yang, and R. G. Anderson, "OpenET: Filling a critical data gap in water management for the western united states," *J. Am. Water Resour. Assoc.*, Nov. 2021.

[30] G. B. Senay, S. Bohms, R. K. Singh, P. H. Gowda, N. M. Velpuri, H. Alemu, and J. P. Verdin, "Operational evapotranspiration mapping using remote sensing and weather

datasets: A new parameterization for the sseb approach," *JAWRA Journal of the American Water Resources Association*, vol. 49, no. 3, pp. 577–591, 2013.

[31] R. Q. Grafton, J. Williams, C. J. Perry, F. Molle, C. Ringler, P. Steduto, B. Udall, S. A. Wheeler, Y. Wang, D. Garrick, and R. G. Allen, "The paradox of irrigation efficiency," *Science*, vol. 361, pp. 748–750, Aug. 2018.

[32] C. A. Scott, S. Vicuña, I. Blanco-Gutiérrez, F. Meza, and C. Varela-Ortega, "Irrigation efficiency and water-policy implications for river basin resilience," *Hydrol. Earth Syst. Sci.*, vol. 18, pp. 1339–1348, Apr. 2014.

[33] F. A. Ward and M. Pulido-Velazquez, "Water conservation in irrigation can increase water use," *Proc. Natl. Acad. Sci. U. S. A.*, vol. 105, pp. 18215–18220, Nov. 2008.

[34] D. J. Molden, R. Sakthivadivel, C. J. Perry, and C. de Fraiture, *Indicators for Comparing Performance of Irrigated Agricultural Systems*. IWMI, 1998.

[35] J. D. Oster and D. Wichelns, "Economic and agronomic strategies to achieve sustainable irrigation," *Irrig. Sci.*, vol. 22, pp. 107–120, Nov. 2003.

[36] P. Wurster, M. Maneta, S. Beguería, K. Cobourn, B. Maxwell, N. Silverman, S. Ewing, K. Jensco, P. Gardner, J. Kimball, *et al.*, "Characterizing the impact of climatic and price anomalies on agrosystems in the northwest united states," *Agricultural and Forest Meteorology*, vol. 280, p. 107778, 2020.

Chapter 2

IRRMAPPER: A MACHINE LEARNING APPROACH FOR HIGH RESOLUTION MAPPING OF IRRIGATED AGRICULTURE ACROSS THE WESTERN U.S.

2.1 Abstract

High frequency and spatially explicit irrigated land maps are important for understanding the patterns and impacts of consumptive water use by agriculture. We built annual, 30 m resolution irrigation maps using Google Earth Engine for the years 1986–2018 for 11 western states within the conterminous U.S. Our map classifies lands into four classes: irrigated agriculture, dryland agriculture, uncultivated land, and wetlands. We built an extensive geospatial database of land cover from each class, including over 50,000 human-verified irrigated fields, 38,000 dryland fields, and over 500,000 km^2 of uncultivated lands. We used 60,000 point samples from 28 years to extract Landsat satellite imagery, as well as climate, meteorology, and terrain data to train a Random Forest classifier. Using a spatially independent validation dataset of 40,000 points, we found our classifier has an overall binary classification (irrigated vs. unirrigated) accuracy of 97.8%, and a four-class overall accuracy of 90.8%. We compared our results to Census of Agriculture irrigation estimates over the seven years of available data and found good overall agreement between the 2832 county-level estimates ($r^2 = 0.90$), and high agreement when estimates are aggregated to the state level ($r^2 = 0.94$). We analyzed trends over the 33-year study period, finding an increase of 15% (15,000 km^2) in irrigated area in our study region. We found notable decreases in irrigated area in developing urban areas and in the southern Central Valley of California and increases in the plains of eastern Colorado, the Columbia River Basin, the Snake River Plain, and northern California.

2.2 Introduction

In the Western U.S., over 80% of extracted freshwater is used for irrigation (i.e., artificial application of water to crops by humans), 56% of which is consumed by crops (i.e., lost to the atmosphere) [1]. In this region, only one third of total cropland area is irrigated, yet irrigated farmland accounted for nearly two thirds of total commodities revenue in 2012 [2]. Irrigation is necessary to agricultural production in arid areas where precipitation is insufficient to grow food crops. Irrigation increases yields and decouples crop yields from climatic constraints [3, 4], buffers against extreme weather events [5, 6], and modifies temperature, humidity, and precipitation regimes at local to regional scales [7, 8, 9, 10] and evapotranspiration (ET) globally [11]. Irrigation may also cause significant environmental impacts, including the draining or maintaining of wetlands [12, 13], disrupted sedimentation [14], increased soil salinity [15], altered stream temperatures [16], changes in water table elevation [17, 18], decreased stream flow [19], and changes in peak runoff rates and base flows [20, 21]. Despite its economic and ecological importance, the extent and distribution of irrigation is poorly mapped in the U.S.

The most robust accounting of irrigated area in the U.S. are county-level statistics included in the Census of Agriculture, an effort undertaken since 1840 by the precursor to the U.S. Census Bureau, and currently conducted and managed by the U.S. Department of Agriculture, National Agricultural Statistics Service (NASS) [22]. NASS produces a semi-decadal estimate of per-county irrigated area based on survey responses from agricultural producers. These data lack any explicit spatial information indicating where irrigation occurs within each county. In addition, the irrigation survey is subject to potential error resulting from undercoverage, nonresponse, and misclassification of farm operations. One example of this potential error is from the 2012 census, which required an adjustment of the estimated number of operating farms of nearly 35% to correct for undercoverage [23]. Irrigated areas are self-reported and only required for farm operations meeting a revenue threshold, and therefore exclude irrigation operations on non-revenue-generating agricul-

tural operations. The infrequency and lack of explicit spatial information of the Census of Agriculture creates a need for explicit spatial and temporal estimates of irrigated areas to improve census statistics, consumptive water use estimates, and agricultural, ecological, and water resource management.

Satellite remote sensing (SRS) is finding increasing use in approaches to identify and monitor ecological and agricultural processes at global to local scales, utilizing a variety of instruments [24, 25, 26]. Researchers have found utility in SRS to monitor many surface and atmospheric phenomena, including soil moisture [27], water quality [28], snow cover [29], and stream flow [30]. Advances in estimating ET using SRS methods [31, 32, 33, 34] have enabled explicit spatial and temporal accounting of consumptive water use rates from irrigation, however lack of frequent, high-resolution maps of irrigated areas has limited the ability to accurately estimate and summarize consumptive water use volumes from irrigated areas. Volumes of consumptive water use are ultimately needed for improving natural resource management, modeling, and prediction.

SRS is well suited for efficiently identifying irrigation in space and time due to the fact that irrigated areas often have a distinct spectral signature when compared to surrounding natural vegetation or unirrigated lands, and can be identified by orbiting satellites that acquire imagery at regular and frequent intervals, and are free and open for scientific use [35, 36, 37]. Freely available satellite data are subject to trade-offs among overpass frequency, period of record, and spatial resolution. For example, the Moderate Resolution Imaging Spectroradiometer (MODIS) instruments on board Terra and Aqua satellites have daily, morning and afternoon overpass frequency, but the 250-m spatial resolution of the images makes identification of irrigation for individual fields difficult due to mixed pixel and field edge effects [35]. The MultiSpectral Instrument (MSI) on board Sentinel 2a and 2b satellites acquires images at 10 m spatial resolution, and has an overpass frequency of five days since the launch of Sentinel 2b in 2017. While Sentinel's short record limits the utility for mapping irrigation history, it acquires data in comparable spectral bands to Landsat, and thus can

be harmonized to map historical irrigated areas into the future [38]. Landsat Thematic Mapper (TM), Enhanced Thematic Mapper Plus (ETM+), Optical Land Imager (OLI), and Thermal Infrared Sensor (TIRS) observations provide an unmatched consistent and continuous data record of optical and thermal imagery from 1984 to present at 8–16-day frequency, and at 30-m spatial resolution—a scale well suited for observing the spatial extent and variability of individual agricultural fields and associated volumes of consumptive water use [39].

Previous SRS studies focused on mapping regional to global-scale irrigation often depend on census estimates of irrigated land area or existing land-use and land-cover datasets to parameterize irrigation models. Examples include the Global Irrigated Area Map (GIAM [40, 41, 42]), Landsat-based irrigation dataset (LANID [43]), and the Moderate Resolution Imaging Spectroradiometer Irrigated Agriculture Dataset for the U.S. (MIrAD-US [44, 45]). These studies aim to reproduce the reported irrigated extent with added spatial detail, often using a greenness index threshold in which pixels are considered irrigated. While several studies produce annual irrigated lands data [46, 47, 48, 49, 50, 51], to our knowledge, none are available for the Western U.S. A significant advance in annual, high resolution mapping of irrigated areas was recently achieved over the High Plains Aquifer (HPA) of the Central U.S. by Deines et al. [50, 51]. This approach used an independently developed dataset to train a Random Forest (RF) model, a non-parametric ensemble decision tree classification and regression algorithm [52]. They mapped historical irrigated lands annually from 1984 to 2017 at 30-m resolution within a 625,000 km^2 study area with 91.4% overall accuracy. They used a novel approach to overcome imagery gaps and commission errors, and parameterized their model with neighborhood greenness indices and many ancillary datasets. Drivers of irrigated area [50] and projections of High Plains Aquifer decline [51] were also studied.

RF has been successfully implemented in many SRS-based land classification studies on mixed land types [53, 54, 55], and for classification of agricultural land uses [56, 57, 58, 59, 60]. RF has been shown to be a reliable and fast algorithm for remote sensing applica-

tions, suited to handling high-dimensional and colinear data, insensitive to overfitting, and explanatory of variable importance [61].

Here, we describe a Landsat-based irrigation detection RF model, IrrMapper, to map annual irrigation status at 30-m resolution. We use a similar approach and build on the previous work of Deines [50], by expanding the spatial scope and parameterizing the RF model with more extensive training, climate, land use, and other geospatial datasets. IrrMapper produces irrigation status wall-to-wall across the Western U.S., and is independent of USDA NASS irrigation statistics, allowing for an independent comparison to Census of Agriculture data as described in the following sections.

2.3 Data and Methods

2.3.1 Methodological Overview

IrrMapper uses a RF modeling approach to predict four land classes of irrigated agriculture, dryland agriculture (i.e., crops receiving water only from precipitation), uncultivated lands, and wetlands at an annual time step, and at 30-m spatial resolution across the Western U.S. The RF model is parameterized using a large set of training data of both the target class (i.e., irrigation) and non-target classes (e.g., uncultivated), and numerous geospatial and climatic datasets. The training data consist of manually developed Geographic Information System (GIS) field boundary polygons and attributes of irrigation-equipped and unirrigated lands developed by numerous state and federal agencies, and research institutions. Input parameter data are geospatial and climate datasets including Landsat and aerial imagery, terrain and land use data, and precipitation, temperature, and evaporative demand. We sampled 132 parameter values from geospatial and climate datasets at 60,000 randomly distributed training points within our field polygon training dataset, and used them to train and apply the RF algorithm to predict and perform accuracy assessment of irrigation status classes across the Western U.S. We used Google Earth Engine (GEE [62]), a cloud-based geospatial analysis platform and multi-petabyte catalog of geospatial data

and satellite imagery to access all imagery used in training data development, compile all model input data, to parameterize and train the RF model, to predict land class, and to extract results and validation data. All services from GEE were free.

2.3.2 Study Area

The study area consists of 11 Western U.S. states of Arizona, California, Colorado, Idaho, Montana, New Mexico, Nevada, Oregon, Utah, Washington, and Wyoming, an area of 3.1 million km^2 (Figure 2.1). This region is more arid than the eastern U.S. with exceptions in the Pacific Northwest and regions of northern California. Annual precipitation in the study area ranges from a minimum of approximately 60 mm $year^{-1}$ in southeast California to over 3000 mm $year^{-1}$ in the Cascade Mountains of Washington. Evaporative demand ranges from approximately 500 mm $year^{-1}$ in the Cascade Mountains of Washington to over 2600 mm $year^{-1}$ in southern Nevada. The Southwest U.S. is dominated by summer monsoonal precipitation, while the northern and Pacific zones receive the majority of precipitation in the winter, much of it in the form of snow. In general, the climate transitions from Pacific coastal and Mediterranean to continental, from west to east.

2.3.3 Landsat and Aerial Imagery

We extracted 132 parameters to use as input data to the model exclusively from datasets with continuous coverage of the entire study region and study period. The 30 m resolution Landsat data used in this work provides six optical bands collected from the Landsat TM, Landsat 7 ETM+, OLI sensors: red, green, blue, near infrared, and two shortwave infrared bands. We used the Landsat Collection 2 Surface Reflectance product, the highest level of processing currently available. Landsat 5 TM and Landsat 7 +ETM surface reflectance data have been corrected for atmospheric conditions and viewing angle geometry using the Landsat Ecosystem Disturbance Adaptive Processing System (LEDAPS [63]) algorithm. Landsat 8 OLI surface reflectance data were processed using the Land Surface Reflectance Code (LaSRC [64]). For each year, we calculated the mean surface reflectance for each of

the six optical bands for four periods: March 1–May 1; May 1– July 1; July 1–September 1; and September 1–November 1. We also calculated the maximum, minimum, and mean per-pixel Normalized Difference Vegetation Index (NDVI) for each year. We did not attempt to perform a radiometric cross-calibration between Landsat instruments; differences between processed surface reflectance images exist but are small [65].

Our study area consists of 186 Landsat path-row scenes (Figure 2.1), each of which was revisited every 16 days by each Landsat mission during the study period. Simultaneous operation of Landsat 5 and 7 from 1999 to 2012 and Landsat 7 and 8 from 2013 yields an 8-day revisit time during 20 years of our 33-year study period, a total of 269,241 available scenes. In May 2003, Landsat 7 suffered a scan line corrector hardware failure (SLC-off) resulting in data gaps in image captures covering about 20% of the image area. While the multiple concurrent Landsat operations during most of our study period allowed for data collection everywhere, during the 2012 collection period, only Landsat 7 SLC-off data were available.

We used images from the U.S. Farm Service Agency National Aerial Imaging Program (NAIP) to verify agricultural field boundary accuracy [66]. NAIP provides 3- and 4-channel (i.e., Red–Blue–Green and Red–Blue–Green–Near Infrared) imagery at various resolutions (0.6, 1, and 2 m) from 2003 to present, offered on a state-by-state basis for multiple years. We used the latest available imagery for each state in our data development process, see [67].

2.3.4 Meteorology and Climate Data

The University of Idaho Climatology Lab produced daily surface Gridded Meteorology (gridMet) at 4-km resolution for the conterminous U.S. from 1979 to present [68]. We extracted mean temperature and total precipitation from gridMet for the duration of the four growing season periods and for the preceding water year (i.e., October 1–September 30) to the termination of each of the growing season periods, for each year covered in our training data (28 years). We also extracted the 10th, 50th, and 90th percentile annual minimum

and maximum temperature, the annual total precipitation, and the annual total potential evapotranspiration from gridMET. We extracted minimum, maximum, and average monthly temperatures and monthly average precipitation for each month of the calendar year from WorldClim, a 1 km resolution worldwide gridded climate product providing 30-year climate normals based on the period 1970–2000 [69].

2.3.5 Terrain and Land Use Data

We extracted elevation, slope, and aspect from the USGS National Elevation Dataset $\frac{1}{3}$ arc-second resolution digital elevation model (DEM). Using the DEM we calculated the Topographic Position Index at 150, 250, and 1250 m [70]. We used the USDA Crop Data Layer [71] and the the USGS National Landcover Dataset [72] to generate binary crop mask and land cover layers.

2.3.6 Training Data

The training and validation datasets for IrrMapper were derived from polygon vector data covering partial areas of each state, obtained from federal and state agencies, and research institutions (Table 2.1). All data were stripped of attribution and joined into a database; only geometries were used. Four land classes were represented in the training data: irrigated agricultural fields (Figure 2.2), dryland agricultural fields, uncultivated lands, and wetlands (Figure 2.3).

We assumed the dryland agriculture, wetlands, and uncultivated lands were constant throughout our study period of 1986–2018. We attributed irrigation to irrigation-equipped fields during specific years to account for the possibility that irrigation-equipped fields were fallowed during some years (Table 2.1).

Irrigation-equipped polygon datasets that had been developed for specific time periods were verified for those years. Irrigation-equipped polygon datasets without temporal information were generally developed for 4–6 years. These years were chosen to represent a range of climatic variability within the study period found using the Climate at a Glance

tool [73], with at least one year of below normal water year precipitation, at least one year of above normal water year precipitation, and at least one year of near-normal water year precipitation (Figure 2.4).

Irrigation training data development consisted of two steps: (1) filtering the polygons by NDVI, a common satellite-detected proxy for vegetation density and vigor; and (2) visual inspection. Our filter kept the polygons containing pixels where the lower 15th percentile NDVI of pixels had maximum NDVI greater than 0.5 during either the early or the late summer, May to July and July to October, respectively. Polygons that did not meet the criteria of the filter were ignored. We inspected all polygons resulting from the filtering process using NAIP aerial imagery and Landsat 5, 7, or 8, early, late, and overall summer maximum NDVI. We compared the NDVI with the surrounding natural vegetation and removed any polygons with only partially irrigated extent or where the field boundaries were inaccurate. Our verified irrigation dataset consists of 101,875 features, each corresponding to the year for which it was filtered and then inspected, of which 53,367 are unique agricultural field boundaries covering 14,659 km^2 (1.9% of total training data area). The 48,508 duplicates are fields that were found to be irrigated for more than one year during the years we selected for data development in the state. To our knowledge, this represents an unprecedented collection of verified irrigated areas.

The dryland agriculture training data is almost entirely within the major wheat-growing regions of CO, MT, and WA, with a small amount in the Upper Colorado River Basin in WY, UT, AZ, and CO. The features represent cultivated lands lacking irrigation infrastructure. The dryland data consists of 38,259 fields covering 63,406 km^2 (10.4% of total training data area). These data were inspected for general accuracy using NAIP imagery at several locations but were not systematically verified on a field-by-field basis. The wetlands training data were collected from the U.S. Fish and Wildlife National Wetlands Inventory [74]. We chose 99,697 features at random from the 'Freshwater Emergent Wetland', 'Freshwater Forested/Shrub Wetland', and 'Riverine' classes, covering 2343 km^2 (0.4% of total training

data area). The uncultivated class was composed of the USDA Forest Service Roadless Areas Inventory [75], the National Wilderness Preservation System wilderness inventory (comprised of wilderness areas managed by the Bureau of Land Management, Fish and Wildlife Service, Forest Service and National Park Service) [76], and sources of forestry and rangeland data gleaned from states. The uncultivated dataset consists of 39,409 features covering 534,442 km^2 (87.4% of total training data area). As with the dryland data, the wetlands and uncultivated lands data were inspected to ensure general accuracy, but not systematically verified. We used all the appropriate training data we were able to obtain. The four classes of training data together cover 611,514 km^2, about 20% of the study region.

2.3.7 Model Training and Classification

IrrMapper is trained using the Random Forest (RF) algorithm, a non-parametric ensemble decision tree classification and regression algorithm. RF chooses random subsets of training samples to train many decision trees and makes a classification based on the mode of the set of trees. In the IrrMapper RF, model hyperparameters were tested using the Scikit-Learn Python implementation of the RF algorithm on our training dataset [77]. We set the number of Rifle decision trees to 100, the number of variables per split to 11, the minimum size of the terminal node to 1, and deactivated the out-of-bag mode in favor of testing accuracy using cross-validation (see below). We then used our hyperparameters to run the GEE implementation of RF.

To extract training data for IrrMapper, pixel sampling locations for 30,000 points within the irrigated areas and 10,000 points within each unirrigated class were placed randomly within a 20-m interior buffered extent of the vector coverage for each land class over the study area (Figure 2.5). The points within the irrigated coverage were attributed with the year for which that field polygon had been verified as irrigated, while the other classes were randomly assigned a year from the 28 years we had irrigation training data. We used GEE to then create a composite image of both static (i.e., land cover, terrain, and climate) and dynamic (i.e., Landsat, Landsat-derived indices, and meteorology) gridded data. Each pixel

value was extracted for each sample point and returned in a table for use in training the RF algorithm. We trained the RF algorithm within GEE and predicted land class using the 132-layer stack of input rasters over the entire study area each year 1986–2018. While IrrMapper is trained and predicts using four land cover classes, in a final processing step, the three unirrigated land classes are grouped into a general 'unirrigated' class, to give a binary irrigated/unirrigated classification result over the study region. To assess variable importance, we ran the Scikit-Learn implementation of the RF model using our IrrMapper hyperparameters over ten iterations to extract the average feature importance of our model parameters.

2.3.8 Model Cross Validation

To validate our GEE-based IrrMapper RF model, we extracted a sample set of 60,000 points using the same procedure as described above for training points extraction. Points located within a 60-m buffer of the original training dataset were removed. A random subset of 10,000 points from each class was then used to extract results from GEE and calculate a confusion matrix. Additionally, a random subset of points, the number of which for each class was weighted according to the relative area of each of the training classes, was selected for use in further assessment as discussed below. This provided a dataset for a spatially independent cross-validation and allowed us to use the maximum quantity of data in GEE to train the RF without holdouts.

2.3.9 Comparison with National Agricultural Statistics Service Data

For comparison purposes, we compiled Census of Agriculture data for 1987–2017 to find semi-decadal, county-level irrigated area. We aggregated data for years 1987, 1992, and 1997 from [78] and years 2002, 2012, and 2017 from Quick Stats [2]. To remove outliers in our comparison of NASS data with IrrMapper, we masked any pixel location where irrigation was detected for less than five years over the 33-year study period.

2.3.10 Calculation of Irrigated Area Change

To capture change in irrigated area over the course of the study period, we processed 'early' and 'late' irrigation-equipped masks. These masks represent areas where irrigation was detected during at least two of the five-year periods at the beginning and the end of the study period. We resampled these rasters to a 4-km resolution grid and calculated the change in irrigated area per 16 km^2 pixel.

2.4 Results

IrrMapper consists of 33 annual, 30-m resolution maps of the binary classification of irrigation status of the western 11 states, 1986–2018. We used GEE to train the RF and predict over the entire study region annually, producing a GEE Image Collection of 33 maps at 30 m resolution. Computation time for training and prediction was about 60 h (Figure 2.6).

2.4.1 Model Accuracy

Using 40,000 points for cross validation, we found an overall binary classification accuracy of 97.8% for classification of irrigated vs. unirrigated lands at the validation point locations. False positive prediction of unirrigated land as irrigated by IrrMapper dominated the model error, accounting for 88% of false classifications. IrrMapper has some limitations in discriminating between non-agricultural classes and shows a high level of confusion between the wetland and uncultivated lands classes in the validation data (Table 2.2). We found an overall accuracy of wetland vs. uncultivated classification by IrrMapper of 88.2%. Wetlands classification in terms of producer's accuracy was the lowest of the four classes at 77.1%. IrrMapper discriminates with a high level of accuracy between irrigated and dryland classes, however, and has an overall irrigated vs. dryland classification accuracy of 99.1%. IrrMapper had producer's accuracy of 98.9% and 96.6% for irrigated and dryland classes, respectively.

The limitations of the IrrMapper training data caused by the limited geographic extent of irrigated areas in our training data become apparent when the cross validation data are grouped into binary classes (i.e., irrigated and unirrigated) and weighted for the relative area of each training dataset (Table 2.3). While the overall accuracy of the weighted cross validation dataset is 98.6%, a small number of false positive classifications of unirrigated lands led to a low producer's accuracy of 57% for the irrigated class.

2.4.2 Variable Importance

Of the 132 parameters used in the study, the ten most important, in descending order, are CDL classification, NLCD classification, late summer near infrared, mid-summer near infrared, calendar year maximum NDVI, previous year maximum NDVI, latitude, terrain slope, two year's previous maximum NDVI, and mid-summer red (Figure 2.7).

2.4.3 Comparison with NASS Data

IrrMapper shows good agreement with the NASS agricultural statistics (Quick Stats) at the state scale and for counties with high irrigated area (Figures 2.8 and 2.9). Counties with low NASS-reported irrigated area have large relative differences with IrrMapper. Statewide estimates of irrigation matched well with NASS reported statistics over the seven years of available data from NASS ($r^2 = 0.94$). The county NASS data and IrrMapper had a lower level of agreement ($r^2 = 0.90$). IrrMapper and NASS show general agreement on the study area trends over the study period; both show relatively low irrigated area at the beginning of the study, a peak in the late 1990s, and increasing irrigation toward the end of the study (Figure 2.9).

IrrMapper tends to make lower estimates of irrigated area along the Pacific coast and in semi-arid areas where irrigation density is low (Figure 2.10). IrrMapper tends to make higher estimates of irrigated area in counties with urban centers and counties on the eastern plains. The best overall agreement between IrrMapper and NASS was found in the states of Idaho and Utah.

2.4.4 Trends in Irrigation

IrrMapper detected a general increase in total irrigated area over the course of the study period of 15.4%, from 97,100 km^2 in 1986 to 112,100 km^2 in 2018, with the maximum irrigated area reaching 116,100 km^2 in 1998, and the minimum irrigated area of 91,900 km^2 in 1992 (Figure 2.9). State-by-state trends of normalized irrigated area show that Colorado and Montana had the largest fluctuations in irrigated area with standard deviation of 2465 and 1494 km^2, respectively (Figure 2.11). IrrMapper detected a decrease in irrigated area among all states in the study region in 2012, potentially as a result of using Landsat 7 SLC-off data.

IrrMapper shows a general increase in irrigated area in the major arid and semi-arid agricultural regions around the west, including the eastern Columbia River Basin, the Snake River Plain, eastern Colorado and New Mexico, and southern Arizona (Figure 2.12). Notable decreases in detected irrigation were found in the Treasure Valley of Idaho, the southern Central Valley in California, and the western slope of the Columbia River Basin.

2.5 Discussion

Results of this study show IrrMapper classifies irrigated areas with a high degree of accuracy when tested on a spatially independent validation dataset (Table 2.2). Overall accuracy of IrrMapper in terms of irrigated vs. unirrigated classification (97.8%) is higher than comparable maps (MIrAD-US, 92%; LANID, 94%; and HPA, 91.4%). The skill of IrrMapper classification suggests the selected input data has a strong correlation with each of the target classes, and demonstrates the suitability of most predictive variables, i.e., land cover, Landsat satellite data, geographic location, and terrain (Figure 2.7). Further, IrrMapper validation results (Table 2.2) suggest the inclusion of training data from a vast representation of geographic locations, climate conditions, and meteorological scenarios enables high-accuracy classification over the extremely varied spatiotemporal domain of our study.

When weighted by relative area of training data, validation results suggest over-prediction of irrigation by IrrMapper (Table 2.3). The relative contribution of each unirrigated class to over-prediction can be inferred from Table 2.2, where misclassification of unirrigated land as irrigated (i.e., false positive) is much more common than the misclassification of irrigated as unirrigated (i.e., false negative). This is likely a result of both the unbalanced area of training data from each class and the unclear differentiation between irrigated areas and wetlands in the wetland training data. Over 97% of the total training data area is composed of the uncultivated and dryland classes. As these land uses represent the majority of both our training data and the study area as a whole, a low rate of false positives likely leads to a small but significant contribution to total irrigated area from unirrigated lands. This is evident in results over known uncultivated and dryland areas, where false positive classification of single or small groups of pixels is noted. This problem may be mitigated by using a noise removal technique in post-processing, as done by Deines [51]. While wetlands data represent a small fraction of the training area, during model development we found the inclusion of those data to be critical to IrrMapper's discriminative power in riparian areas where adjacent wetlands and irrigation are common and share a similar appearance. However, inspection of our wetland data reveals areas where irrigation likely occurs as evidenced by simple diversions and ditch networks. It is often unclear in NAIP imagery where areas supplied with irrigation water end and wetlands begin. In our training data and in nature, the existence of wetlands and irrigation in the same place is possible, and therefore both semantic and physical distinction between irrigated areas and wetlands is blurred. This problem may be overcome by restricting the wetlands training data to areas where irrigation does not occur.

Comparison of county-level NASS irrigation survey data and IrrMapper results shows general agreement ($r^2 = 0.90$) with the best agreement in areas with more irrigation and less agreement in counties with low rates of irrigation (Figure 2.8). Large relative differences are expected in counties where both estimates are a small fraction of total area (e.g.,

the northern counties of Arizona). In urban areas with limited irrigated area, IrrMapper generally estimates greater irrigated area relative to NASS. This can be explained in part by Census of Agriculture classification of farms, where only farms expected to produce and sell more than $1000 of agricultural products are surveyed. This approach omits irrigation by golf courses, hobby farms, and playing fields, areas which are detected by IrrMapper and may represent a large portion of total irrigation in urban and desert landscapes. The bias toward false positive classification of irrigation in IrrMapper likely also contributes to larger estimates by IrrMapper in counties with extensive dryland and uncultivated lands. In areas of extensive irrigation, results are in better agreement, likely due to higher contribution to irrigation from farms included in the Census of Agriculture survey, and less unirrigated area in which IrrMapper may misclassify land type.

IrrMapper tends to make county-level estimates of irrigated area lower than NASS estimates along the Pacific coast and in arid and semi-arid counties with low density of irrigation (Figure 2.10). In the Pacific Northwest, the high relative contribution to crop water requirements from precipitation may allow low irrigation intensity and thus low contrast in satellite images between irrigated and unirrigated areas, and under-classification of irrigation by IrrMapper. Along the coast of Oregon and California, underestimates may be attributable to lower density of IrrMapper training data and under-classification as a result. The most notable region of generally higher IrrMapper estimates are the easternmost counties of the study area in Colorado and New Mexico. These areas likely have significant rates of false positive classification of dryland agriculture as irrigated. This may be caused by sub-annual cropping of dryland agriculture in areas where soil moisture is conserved through the use of herbicides during fallow periods and where subsequent croppings result in a high NDVI relative to adjacent, unirrigated land. Despite disagreement between the two methods, when aggregated over the study area, IrrMapper and NASS show rough agreement on trends in the extent of irrigation; both identify a peak in irrigated area in the mid-1990s, followed by a decline through the 2000s, and a rise toward the end of the study period (Figure 2.9).

This suggests that, in addition to its capacity to accurately map irrigation at the local scale, IrrMapper also has the capacity to detect regional trends in irrigation at higher temporal resolution relative to NASS.

Spatial trends in irrigation detected by IrrMapper are complex and are likely driven by many factors, including changes in land use, timing of crop planting, crop type, water resource limitations, and changes in irrigation efficiency, and also limitations in the IrrMapper approach (Figure 2.12). While analysis of the drivers of changes in irrigation is outside the scope of this paper, we hypothesize several factors that deserve further investigation. We suspect the areas around Phoenix, AZ; Denver, CO; Portland, OR; Ellensburg and Yakima, WA; and Boise, ID have undergone suburban development that has replaced formerly irrigated areas. We suspect demand for fresh winter agricultural produce has driven a change in cropping time from summer to winter in southern California, a period for which IrrMapper is not designed to detect irrigation (see below). We suspect demand for orchard and vineyard crops has led to an increase in their extent. IrrMapper may not detect them due to bias in the training data development toward selection of irrigated fields with high maximum summer NDVI (see below), and that irrigation of vineyards and orchards may drive a weaker NDVI response due to crop spacing. We suspect formerly irrigated areas in Nevada, Colorado, and New Mexico have been retired due to legal and physical limits on water availability. Widespread increases in irrigated area may be due to irrigation development, and use of more efficient irrigation application equipment and thus expansion of irrigated area despite constant rates of water extraction. Deines et al. [50] studied changes in irrigation over the High Plains Aquifer; previous-year commodity price was found to be positively correlated to irrigated area, while irrigation volume and depth were negatively correlated with precipitation. Such studies of the drivers and patterns of irrigation and water use in the Western U.S. may be enabled in the future by IrrMapper.

IrrMapper limitations are likely due to its simple model parameterization and bias in the training data development process. A central assumption of IrrMapper is that the irri-

gation occurs during the March–November time period. The assumption that the growing season occurs between March 1 and November 31 may contribute to under-classification of irrigation in areas with a winter growing season. This is apparent in areas such as the southern Central Valley and Imperial Valley in California and Yuma, AZ, which have seen decreases in irrigated area according to IrrMapper (Figure 2.12). We ran a sub-model 'IrrMapper LCRB' for the Lower Colorado River Basin, and found that when the growing season is extended to the entire year, IrrMapper detects more irrigated fields. This suggests IrrMapper may benefit from customized parameterization within specific regions. Further, IrrMapper does not explicitly model the temporal dynamics of the Landsat spectral signal. IrrMapper uses the mean surface reflectance for each growing season period and thus information on the spectral dynamics of each location within that period is lost. Including temporal data associated with specific image captures may improve IrrMapper's ability to discriminate between land classes that experience distinct temporal dynamics in spectral response through the year, but have similar spectral means.

While the geometry of the fields was created by experts, the filtering process depended only on a set of NDVI statistics. This approach may systematically exclude areas that are sparsely irrigated and show a weak NDVI response, adding bias to the model. An effort was made to represent various land types, including those with weaker NDVI signal (e.g., vineyards and widely spaced orchards), but, in some cases, irrigated fields were removed from the data because the field included areas that were not reached by the irrigation equipment. The training data are thus biased toward intense irrigation, and likely fail to detect irrigation in areas with infrequent or low-intensity irrigation. The assumption of static land cover in the unirrigated classes (i.e., dryland, wetland, uncultivated) may also introduce error in the training data where land class has changed during the study period. The assumption is probably best for the uncultivated class (e.g., national forest, roadless areas), and weakest for the dryland class, where conversion to irrigation may occur. We suspect the locations where dryland was converted to irrigated are likely limited in our

training data because the geospatial data development occurred recently.

IrrMapper is an improvement over previous mapping efforts in the Western U.S. given the large geographic and temporal extent of both training data and our predictions. Further, our predictions depend only on our independently verified training data, compared to many previous efforts where irrigation models have depended on agricultural census data to parameterize models using spectral thresholds (e.g., LANID, MIrAD-US). While these models effectively leverage the predictive power of irrigated areas' spectral signature, they rely on agricultural statistics and therefore incorporate both the error in the survey and irrigated areas excluded from the tabulation according to the criteria of the agricultural survey. Further, they may not be suited to generalization in time, as the conditions during census years may not be representative of regional climatic variability. Models that 'tune' to the agricultural statistics during only one or several growing seasons may mistake irrigation status when the model is applied to the same place under different climate or economic scenarios [79, 4]. As the training data used in IrrMapper represent the wide range of climatic, spatial, and temporal variability we observe in the West, the model can be relied on to make good predictions for years without training data. Further, IrrMapper uses existing land use classification models (i.e., NLCD and CDL) as input parameters, rather than as training data or as a mask for areas not considered agricultural land by those model products (AIM-HPA, LANID, and MIrAD-US). This allows the model to determine the relative importance of these parameters, rather than using them as a mask and thus incorporating the error inherent in the land use data into the map. IrrMapper is created independently of the NASS agricultural statistics, and can thus be used as an independent comparison to examine both existing irrigation maps and historic agricultural census data.

2.6 Conclusions

Water resources management in the Western U.S. requires accurate, timely, and high resolution irrigation maps. These maps are a critical resource in assessing the impact of irrigation on human and ecological systems and quantifying irrigated water consumption.

Despite the critical importance of irrigation, the high spatial and temporal resolution mapping of its occurrence is currently lacking. IrrMapper introduces the high resolution mapping of irrigation annually, 1986–2018, over the Western U.S. Using IrrMapper, we found that irrigated area in our study region has ranged from 91,900 km^2 in 1992 to 116,100 km^2 in 1998. Irrigation increased by about 15% over the study period, from 97,100 km^2 in 1986 to 112,100 km^2 in 2018. We found that IrrMapper compares favorably with NASS agricultural census data, especially in areas of high irrigation density. IrrMapper differs most from NASS census data along the Pacific Coast, the eastern margin of the study area in Colorado and New Mexico. IrrMapper demonstrates the ability of a RF-based method to accurately map irrigation at a sub-continental scale. Future work should use a temporal parameterization and investigate the underlying drivers of change in irrigated area in the Western U.S.

REFERENCES

[1] C. A. Dieter, *Water availability and use science program: Estimated use of water in the United States in 2015*. Geological Survey, 2018.

[2] U. N. A. S. Service, "Nass - quick stats," 2017. Available online: `https://data.nal.usda.gov/dataset/nass-quick-stats` accessed 20-March-2019.

[3] X. Li and T. Troy, "Changes in rainfed and irrigated crop yield response to climate in the western us," *Environmental Research Letters*, vol. 13, no. 6, p. 064031, 2018.

[4] P. Wurster, M. Maneta, S. Beguería, K. Cobourn, B. Maxwell, N. Silverman, S. Ewing, K. Jensco, P. Gardner, J. Kimball, *et al.*, "Characterizing the impact of climatic and price anomalies on agrosystems in the northwest united states," *Agricultural and Forest Meteorology*, vol. 280, p. 107778, 2020.

[5] T. J. Troy, C. Kipgen, and I. Pal, "The impact of climate extremes and irrigation on us crop yields," *Environmental Research Letters*, vol. 10, no. 5, p. 054013, 2015.

[6] B. Schauberger, S. Archontoulis, A. Arneth, J. Balkovic, P. Ciais, D. Deryng, J. Elliott, C. Folberth, N. Khabarov, C. Müller, *et al.*, "Consistent negative response of us crops to high temperatures in observations and crop models," *Nature communications*, vol. 8, no. 1, pp. 1–9, 2017.

[7] W. J. Sacks, B. I. Cook, N. Buenning, S. Levis, and J. H. Helkowski, "Effects of global irrigation on the near-surface climate," *Climate Dynamics*, vol. 33, no. 2-3, pp. 159–175, 2009.

[8] B. Yang, Y. Zhang, Y. Qian, J. Tang, and D. Liu, "Climatic effects of irrigation over the huang-huai-hai plain in china simulated by the weather research and forecasting model," *Journal of Geophysical Research: Atmospheres*, vol. 121, no. 5, pp. 2246–2264, 2016.

[9] Z. Yang, F. Dominguez, X. Zeng, H. Hu, H. Gupta, and B. Yang, "Impact of irrigation over the california central valley on regional climate," *Journal of Hydrometeorology*, vol. 18, no. 5, pp. 1341–1357, 2017.

[10] Z. Yang, Y. Qian, Y. Liu, L. K. Berg, H. Hu, F. Dominguez, B. Yang, Z. Feng, W. I. Gustafson Jr, M. Huang, *et al.*, "Irrigation impact on water and energy cycle during dry years over the united states using convection-permitting wrf and a dynamical recycling model," *Journal of Geophysical Research: Atmospheres*, vol. 124, no. 21, pp. 11220–11241, 2019.

[11] S. M. Sterling, A. Ducharne, and J. Polcher, "The impact of global land-cover change on the terrestrial water cycle," *Nature Climate Change*, vol. 3, no. 4, pp. 385–390, 2013.

[12] M. Reisner, *Cadillac desert: The American West and its disappearing water*. Penguin, 1993.

[13] D. E. Peck and J. R. Lovvorn, "The importance of flood irrigation in water supply to wetlands in the laramie basin, wyoming, usa," *Wetlands*, vol. 21, no. 3, pp. 370–378, 2001.

[14] D. J. Stanley and A. G. Warne, "Nile delta: recent geological evolution and human impact," *Science*, vol. 260, no. 5108, pp. 628–634, 1993.

[15] M. G. Pitman and A. Läuchli, "Global impact of salinity and agricultural ecosystems," in *Salinity: environment-plants-molecules*, pp. 3–20, Springer, 2002.

[16] H. I. Essaid and R. R. Caldwell, "Evaluating the impact of irrigation on surface water–groundwater interaction and stream temperature in an agricultural watershed," *Science of the total environment*, vol. 599, pp. 581–596, 2017.

[17] E. M. Haacker, A. D. Kendall, and D. W. Hyndman, "Water level declines in the high plains aquifer: Predevelopment to resource senescence," *Groundwater*, vol. 54, no. 2, pp. 231–242, 2016.

[18] H. Ritzema, T. Satyanarayana, S. Raman, and J. Boonstra, "Subsurface drainage to combat waterlogging and salinity in irrigated lands in india: Lessons learned in farmers' fields," *agricultural water management*, vol. 95, no. 3, pp. 179–189, 2008.

[19] B. R. Scanlon, I. Jolly, M. Sophocleous, and L. Zhang, "Global impacts of conversions from natural to agricultural ecosystems on water resources: Quantity versus quality," *Water resources research*, vol. 43, no. 3, 2007.

[20] R. W. Skaggs, M. Breve, and J. Gilliam, "Hydrologic and water quality impacts of agricultural drainage," *Critical reviews in environmental science and technology*, vol. 24, no. 1, pp. 1–32, 1994.

[21] E. Kendy and J. D. Bredehoeft, "Transient effects of groundwater pumping and surface-water-irrigation returns on streamflow," *Water Resources Research*, vol. 42, no. 8, 2006.

[22] USDA, "Census of agriculture," *US Department of Agriculture, National Agricultural Statistics Service, Washington, DC*, vol. 1, 2007.

[23] L. J. Young, A. C. Lamas, and D. A. Abreu, "The 2012 census of agriculture: a capture–recapture analysis," *Journal of Agricultural, Biological and Environmental Statistics*, vol. 22, no. 4, pp. 523–539, 2017.

[24] J.-F. Exbrayat, A. A. Bloom, N. Carvalhais, R. Fischer, A. Huth, N. MacBean, and M. Williams, "Understanding the land carbon cycle with space data: current status and prospects," *Surveys in Geophysics*, vol. 40, no. 4, pp. 735–755, 2019.

[25] J. Sheffield, E. F. Wood, M. Pan, H. Beck, G. Coccia, A. Serrat-Capdevila, and K. Verbist, "Satellite remote sensing for water resources management: Potential for supporting sustainable development in data-poor regions," *Water Resources Research*, vol. 54, no. 12, pp. 9724–9758, 2018.

[26] N. Pettorelli, H. Schulte to Bühne, A. Tulloch, G. Dubois, C. Macinnis-Ng, A. M. Queirós, D. A. Keith, M. Wegmann, F. Schrodt, M. Stellmes, *et al.*, "Satellite remote

sensing of ecosystem functions: opportunities, challenges and way forward," *Remote Sensing in Ecology and Conservation*, vol. 4, no. 2, pp. 71–93, 2018.

[27] E. Babaeian, M. Sadeghi, S. B. Jones, C. Montzka, H. Vereecken, and M. Tuller, "Ground, proximal, and satellite remote sensing of soil moisture," *Reviews of Geophysics*, vol. 57, no. 2, pp. 530–616, 2019.

[28] K. Shi, Y. Zhang, B. Qin, and B. Zhou, "Remote sensing of cyanobacterial blooms in inland waters: present knowledge and future challenges," *Science Bulletin*, 2019.

[29] C. Dong, "Remote sensing, hydrological modeling and in situ observations in snow cover research: A review," *Journal of Hydrology*, vol. 561, pp. 573–583, 2018.

[30] Q. Zeng, Y. Wang, L. Chen, Z. Wang, H. Zhu, and B. Li, "Inter-comparison and evaluation of remote sensing precipitation products over china from 2005 to 2013," *Remote Sensing*, vol. 10, no. 2, p. 168, 2018.

[31] W. Bastiaanssen, E. Noordman, H. Pelgrum, G. Davids, B. Thoreson, and R. Allen, "Sebal model with remotely sensed data to improve water-resources management under actual field conditions," *Journal of irrigation and drainage engineering*, vol. 131, no. 1, pp. 85–93, 2005.

[32] R. G. Allen, M. Tasumi, and R. Trezza, "Satellite-based energy balance for mapping evapotranspiration with internalized calibration (metric)—model," *Journal of irrigation and drainage engineering*, vol. 133, no. 4, pp. 380–394, 2007.

[33] Q. Mu, M. Zhao, and S. W. Running, "Modis global terrestrial evapotranspiration (et) product (nasa mod16a2/a3)," *Algorithm Theoretical Basis Document, Collection*, vol. 5, 2013.

[34] G. B. Senay, M. Budde, J. P. Verdin, and A. M. Melesse, "A coupled remote sensing and simplified surface energy balance approach to estimate actual evapotranspiration from irrigated fields," *Sensors*, vol. 7, no. 6, pp. 979–1000, 2007.

[35] M. C. Anderson, R. G. Allen, A. Morse, and W. P. Kustas, "Use of landsat thermal imagery in monitoring evapotranspiration and managing water resources," *Remote Sensing of Environment*, vol. 122, pp. 50–65, 2012.

[36] D. P. Roy, M. A. Wulder, T. R. Loveland, C. Woodcock, R. G. Allen, M. C. Anderson, D. Helder, J. R. Irons, D. M. Johnson, R. Kennedy, *et al.*, "Landsat-8: Science and product vision for terrestrial global change research," *Remote sensing of Environment*, vol. 145, pp. 154–172, 2014.

[37] Z. Zhu, M. A. Wulder, D. P. Roy, C. E. Woodcock, M. C. Hansen, V. C. Radeloff, S. P. Healey, C. Schaaf, P. Hostert, P. Strobl, *et al.*, "Benefits of the free and open landsat data policy," *Remote Sensing of Environment*, vol. 224, pp. 382–385, 2019.

[38] M. Claverie, J. Ju, J. G. Masek, J. L. Dungan, E. F. Vermote, J.-C. Roger, S. V. Skakun, and C. Justice, "The harmonized landsat and sentinel-2 surface reflectance data set," *Remote sensing of environment*, vol. 219, pp. 145–161, 2018.

[39] M. A. Wulder, T. R. Loveland, D. P. Roy, C. J. Crawford, J. G. Masek, C. E. Woodcock, R. G. Allen, M. C. Anderson, A. S. Belward, W. B. Cohen, *et al.*, "Current status of landsat program, science, and applications," *Remote sensing of environment*, vol. 225, pp. 127–147, 2019.

[40] P. Döll, S. Siebert, *et al.*, "A digital global map of irrigated areas," *Icid Journal*, vol. 49, no. 2, pp. 55–66, 2000.

[41] S. Siebert, V. Henrich, K. Frenken, and J. Burke, "Update of the digital global map of irrigation areas to version 5," *Rheinische Friedrich-Wilhelms-Universität, Bonn, Germany and Food and Agriculture Organization of the United Nations, Rome, Italy*, 2013.

[42] P. S. Thenkabail, C. M. Biradar, P. Noojipady, V. Dheeravath, Y. Li, M. Velpuri, M. Gumma, O. R. P. Gangalakunta, H. Turral, X. Cai, *et al.*, "Global irrigated area

map (giam), derived from remote sensing, for the end of the last millennium," *International Journal of Remote Sensing*, vol. 30, no. 14, pp. 3679–3733, 2009.

[43] Y. Xie, T. J. Lark, J. F. Brown, and H. K. Gibbs, "Mapping irrigated cropland extent across the conterminous united states at 30 m resolution using a semi-automatic training approach on google earth engine," *ISPRS Journal of Photogrammetry and Remote Sensing*, vol. 155, pp. 136–149, 2019.

[44] J. F. Brown and M. S. Pervez, "Merging remote sensing data and national agricultural statistics to model change in irrigated agriculture," *Agricultural Systems*, vol. 127, pp. 28–40, 2014.

[45] M. S. Pervez and J. F. Brown, "Mapping irrigated lands at 250-m scale by merging modis data and national agricultural statistics," *Remote Sensing*, vol. 2, no. 10, pp. 2388–2412, 2010.

[46] M. Ozdogan, C. E. Woodcock, G. D. Salvucci, and H. Demir, "Changes in summer irrigated crop area and water use in southeastern turkey from 1993 to 2002: Implications for current and future water resources," *Water resources management*, vol. 20, no. 3, pp. 467–488, 2006.

[47] J. L. Peña-Arancibia, T. R. McVicar, Z. Paydar, L. Li, J. P. Guerschman, R. J. Donohue, D. Dutta, G. M. Podger, A. I. van Dijk, and F. H. Chiew, "Dynamic identification of summer cropping irrigated areas in a large basin experiencing extreme climatic variability," *Remote sensing of environment*, vol. 154, pp. 139–152, 2014.

[48] M. S. Pervez, M. Budde, and J. Rowland, "Mapping irrigated areas in afghanistan over the past decade using modis ndvi," *Remote sensing of environment*, vol. 149, pp. 155–165, 2014.

[49] P. Teluguntla, P. S. Thenkabail, J. Xiong, M. K. Gumma, R. G. Congalton, A. Oliphant, J. Poehnelt, K. Yadav, M. Rao, and R. Massey, "Spectral matching tech-

niques (smts) and automated cropland classification algorithms (accas) for mapping croplands of australia using modis 250-m time-series (2000–2015) data," *International journal of digital earth*, vol. 10, no. 9, pp. 944–977, 2017.

[50] J. M. Deines, A. D. Kendall, and D. W. Hyndman, "Annual irrigation dynamics in the us northern high plains derived from landsat satellite data," *Geophysical Research Letters*, vol. 44, no. 18, pp. 9350–9360, 2017.

[51] J. M. Deines, A. D. Kendall, M. A. Crowley, J. Rapp, J. A. Cardille, and D. W. Hyndman, "Mapping three decades of annual irrigation across the us high plains aquifer using landsat and google earth engine," *Remote Sensing of Environment*, vol. 233, p. 111400, 2019.

[52] L. Breiman, "Random forests," *Machine learning*, vol. 45, no. 1, pp. 5–32, 2001.

[53] M. O. Jones, B. W. Allred, D. E. Naugle, J. D. Maestas, P. Donnelly, L. J. Metz, J. Karl, R. Smith, B. Bestelmeyer, C. Boyd, *et al.*, "Innovation in rangeland monitoring: annual, 30 m, plant functional type percent cover maps for us rangelands, 1984–2017," *Ecosphere*, vol. 9, no. 9, p. e02430, 2018.

[54] R. R. Colditz, "An evaluation of different training sample allocation schemes for discrete and continuous land cover classification using decision tree-based algorithms," *Remote Sensing*, vol. 7, no. 8, pp. 9655–9681, 2015.

[55] N. Tsutsumida and A. J. Comber, "Measures of spatio-temporal accuracy for time series land cover data," *International Journal of Applied Earth Observation and Geoinformation*, vol. 41, pp. 46–55, 2015.

[56] V. Lebourgeois, S. Dupuy, É. Vintrou, M. Ameline, S. Butler, and A. Bégué, "A combined random forest and obia classification scheme for mapping smallholder agriculture at different nomenclature levels using multisource data (simulated sentinel-2 time series, vhrs and dem)," *Remote Sensing*, vol. 9, no. 3, p. 259, 2017.

[57] K. Tatsumi, Y. Yamashiki, M. A. C. Torres, and C. L. R. Taipe, "Crop classification of upland fields using random forest of time-series landsat 7 etm+ data," *Computers and Electronics in Agriculture*, vol. 115, pp. 171–179, 2015.

[58] J. A. Long, R. L. Lawrence, M. C. Greenwood, L. Marshall, and P. R. Miller, "Object-oriented crop classification using multitemporal etm+ slc-off imagery and random forest," *GIScience & Remote Sensing*, vol. 50, no. 4, pp. 418–436, 2013.

[59] D. C. Duro, S. E. Franklin, and M. G. Dubé, "A comparison of pixel-based and object-based image analysis with selected machine learning algorithms for the classification of agricultural landscapes using spot-5 hrg imagery," *Remote sensing of environment*, vol. 118, pp. 259–272, 2012.

[60] A. O. Ok, O. Akar, and O. Gungor, "Evaluation of random forest method for agricultural crop classification," *European Journal of Remote Sensing*, vol. 45, no. 1, pp. 421–432, 2012.

[61] M. Belgiu and L. Drăguţ, "Random forest in remote sensing: A review of applications and future directions," *ISPRS Journal of Photogrammetry and Remote Sensing*, vol. 114, pp. 24–31, 2016.

[62] N. Gorelick, M. Hancher, M. Dixon, S. Ilyushchenko, D. Thau, and R. Moore, "Google earth engine: Planetary-scale geospatial analysis for everyone," *Remote sensing of Environment*, vol. 202, pp. 18–27, 2017.

[63] J. G. Masek, E. F. Vermote, N. E. Saleous, R. Wolfe, F. G. Hall, K. F. Huemmrich, F. Gao, J. Kutler, and T.-K. Lim, "A landsat surface reflectance dataset for north america, 1990-2000," *IEEE Geoscience and Remote Sensing Letters*, vol. 3, no. 1, pp. 68–72, 2006.

[64] E. Vermote, C. Justice, M. Claverie, and B. Franch, "Preliminary analysis of the per-

formance of the landsat 8/oli land surface reflectance product," *Remote Sensing of Environment*, vol. 185, pp. 46–56, 2016.

[65] N. Mishra, M. O. Haque, L. Leigh, D. Aaron, D. Helder, and B. Markham, "Radiometric cross calibration of landsat 8 operational land imager (oli) and landsat 7 enhanced thematic mapper plus (etm+)," *Remote sensing*, vol. 6, no. 12, pp. 12619–12638, 2014.

[66] A. P. F. O. USDA-FSA-APFO *et al.*, "National geospatial data asset (ngda) naip imagery," 2018.

[67] A. P. F. O. USDA-FSA-APFO *et al.*, "National geospatial data asset (ngda) naip imagery," 2018. Available online: `https://www.fsa.usda.gov/Assets/USDA-FSA-Public/usdafiles/APFO/status-maps/pdfs/naipcov_2018.pdf` accessed 1-May-2019.

[68] J. T. Abatzoglou, "Development of gridded surface meteorological data for ecological applications and modelling," *International Journal of Climatology*, vol. 33, no. 1, pp. 121–131, 2013.

[69] S. E. Fick and R. J. Hijmans, "Worldclim 2: new 1-km spatial resolution climate surfaces for global land areas," *International journal of climatology*, vol. 37, no. 12, pp. 4302–4315, 2017.

[70] A. Weiss, "Topographic position and landforms analysis," in *Poster presentation, ESRI user conference, San Diego, CA*, vol. 200, 2001.

[71] U. NASS, "Usda-national agricultural statistics service, cropland data layer," *United States Department of Agriculture, National Agricultural Statistics Service, Marketing and Information Services Office, Washington, DC [Available at http//nassgeodata. gmu. edu/Crop-Scape, Last accessed 16-July-2019.]*, 2017.

[72] C. Homer, J. Dewitz, L. Yang, S. Jin, P. Danielson, G. Xian, J. Coulston, N. Herold, J. Wickham, and K. Megown, "Completion of the 2011 national land cover database

for the conterminous united states–representing a decade of land cover change information," *Photogrammetric Engineering & Remote Sensing*, vol. 81, no. 5, pp. 345–354, 2015.

[73] N. N. C. for Environmental information, "Climate at a glance: Global mapping," 2020. Available online: `https://www.ncdc.noaa.gov/cag/` accessed 25-August-2019.

[74] B. O. Wilen and M. Bates, "The us fish and wildlife service's national wetlands inventory project," in *Classification and inventory of the world's wetlands*, pp. 153–169, Springer, 1995.

[75] G. S. USDA Forest Service and T. Center, "Roadless areas: 2001 roadless rule," 2001. Available online: `http://data.fs.usda.gov/geodata/edw/datasets.php` accessed 29-October-2018.

[76] W. Connect, "wilderness system shapefile," 2018. Available online: `https://wilderness.net/visit-wilderness/gis-gps.php` accessed 30-October-2018.

[77] G. Varoquaux, L. Buitinck, G. Louppe, O. Grisel, F. Pedregosa, and A. Mueller, "Scikit-learn: Machine learning without learning the machinery," *GetMobile: Mobile Computing and Communications*, vol. 19, no. 1, pp. 29–33, 2015.

[78] M. Haines, P. Fishback, and P. Rhode, "United states agriculture data, 1840–2012," *Study No. ICPSR35206-v3, Inter-university Consortium for Political and Social Research*, pp. 06–29, 2016.

[79] P. M. Wurster, M. P. Maneta, S. M. Vicente-Serrano, S. Beguería, N. L. Silverman, and Z. Holden, "Farmer response to climatic and agricultural market drivers: characteristic time scales and sensitivities," *AGUFM*, vol. 2017, pp. H21S–08, 2017.

[80] S. G. Buto, B. L. Gold, and K. A. Jones, "Development of a regionally consistent geospatial dataset of agricultural lands in the upper colorado river basin, 2007–10," *US Geological Survey Scientific Investigations Report*, vol. 5039, p. 20, 2014.

[81] C. A. Commissioners and S. Association, "Field boundaries." personal communication, 2016.

[82] D. R. Institute, "Field boundaries." personal communication, 2018.

[83] C. W. C. B. Colorado Department of Water Resources, "Colorado decision support system - irrigated lands," 2017. Available online: `https://www.colorado.gov/pacific/cdss` accessed 25-October-2018.

[84] U. F. S. Agency, "Common land unit," 2008. `http://www.fsa.usda.gov//`.

[85] I. D. of Water Resources, "Irrigated lands," 2018. Available online: `https://data-idwr.opendata.arcgis.com/pages/gis-data` accessed 13-July-2018.

[86] M. D. of Natural Resources and Conservation, "Field boundaries." personal communication, 2017.

[87] R. Sabie, A. Fernald, and M. Gay, "Estimating land cover for three acequia-irrigated valleys in new mexico using historical aerial imagery between 1935 and 2014," *The Southwestern Geographer*, vol. 21, pp. 36–56, 2018.

[88] O. D. of Water Resources, "Harney field boundaries." personal communication, 2016.

[89] U. D. of Water Resources, "Water related land use," 2016. Available online: `https://gis.utah.gov/data/planning/water-related-land/` accessed 11-July-2018.

[90] W. S. D. of Agriculture, "Agricultural land use," 2017. Available online: `https://agr.wa.gov/departments/land-and-water/natural-resources/agricultural-land-use` accessed 18-October-2018.

[91] W. W. D. Office, "Statewide irrigated lands," 2007. Available online: `http://waterplan.state.wy.us/plan/statewide/gis/irriglands.html` accessed 25-October-2018.

Table 2.1: Summary of geospatial training data by state.

State	Source	Years	Coverage	Irr.	Dry.	Uncult.[a,b]	Wet.[c]
AZ	USGS[d]	5	Features	133	1843	437	4,711
			Area (km^2)	49.949	49	29,301	289
CA	CACASA[e]	6	Features	6022	0	5812	20,822
	DRI[f]		Area (km^2)	3676	0	5876	472
CO	CO DWR[g]	5	Features	23,919	3793	414	9012
	USGS[d]		Area (km^2)	4009	7468	29,204	200
	CLU[h]						
ID	ID DWR[i]	8	Features	4196	82	8168	5004
	CLU[h]		Area (km^2)	2355	73	105,838	82
MT	MT DNRC[j]	6	Features	4112	15,120	10,401	10,611
			Area (km^2)	628	47,656	85,573	64
NM	USGS[d]	11	Features	3563	615	455	6004
	NM WRRI[k]		Area (km^2)	353	28	24,636	42
NV	DRI[e]	8	Features	2346	0	1769	9496
			Area (km^2)	518	0	122,591	442
OR	OR DWR[l]	6	Features	1009	0	612	9923
	CLU[h]		Area (km^2)	333	0	34,348	393
UT	UT DWR[m]	5	Features	2323	5327	726	5399
			Area (km^2)	518	1175	47,196	147
WA	WSDA[n]	6	Features	4828	16,960	10,067	9764
			Area (km^2)	1833	14,225	15,239	167
WY	WY WDO[o]	5	Features	916	77	529	9553
			Area (km^2)	387	21	38,331	139

a, United States Forest Service; [75]; b, United States National Wilderness Preservation System; [76]; c, United States Fish and Wildlife Service; [74]; d, United States Geological Survey; [80]; e, California Agricultural Commissioners and Sealers Association; [81]; f, Desert Research Institute; [82]; g, Colorado Department of Water Resources, Colorado Water Conservation Board; [83]; h, United States Department of Agriculture, Common Land Unit; [84]; i, Idaho Department of Water Resources; [85]; j, Montana Department of Natural Resources and Conservation; [86]; k, New Mexico Water Resources Research Institute; [87]; l, Oregon Department of Water Resources; [88]; m, Utah Division of Water Resources; [89]; n, Washington State Department of Agriculture; [90]; o, Wyoming Water Development Office; [91].

Table 2.2: Confusion matrix of the four-class cross validation dataset, comparing the spatially independent, randomly sampled cross validation dataset of training data (i.e., 'Actual') and IrrMapper inference (i.e., 'Predicted').

		Predicted			
		Irrigated	**Dryland**	**Uncultivated**	**Wetland**
Actual	**Irrigated**	9893	24	15	68
	Dryland	149	9660	68	123
	Uncultivated	76	131	9058	733
	Wetland	555	432	1304	7708

Table 2.3: Confusion matrix of the binary cross validation dataset weighted according to areal extent of the training data. The points are a spatially independent, randomly sampled cross validation dataset of training data (i.e., 'Actual') and IrrMapper inference (i.e., 'Predicted').

		Predicted	
		Irrigated	**Unirrigated**
Actual	**Irrigated**	183	2
	Unirrigated	136	9679

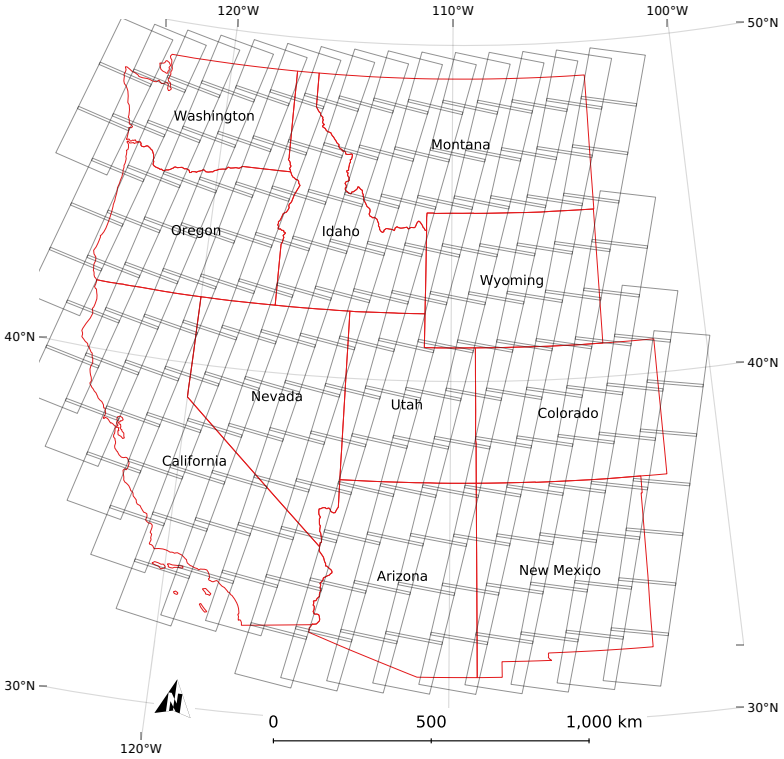

Figure 2.1: The 11 states of the Western U.S. included in our study area displayed with the 186 Landsat scene footprints from which imagery was used.

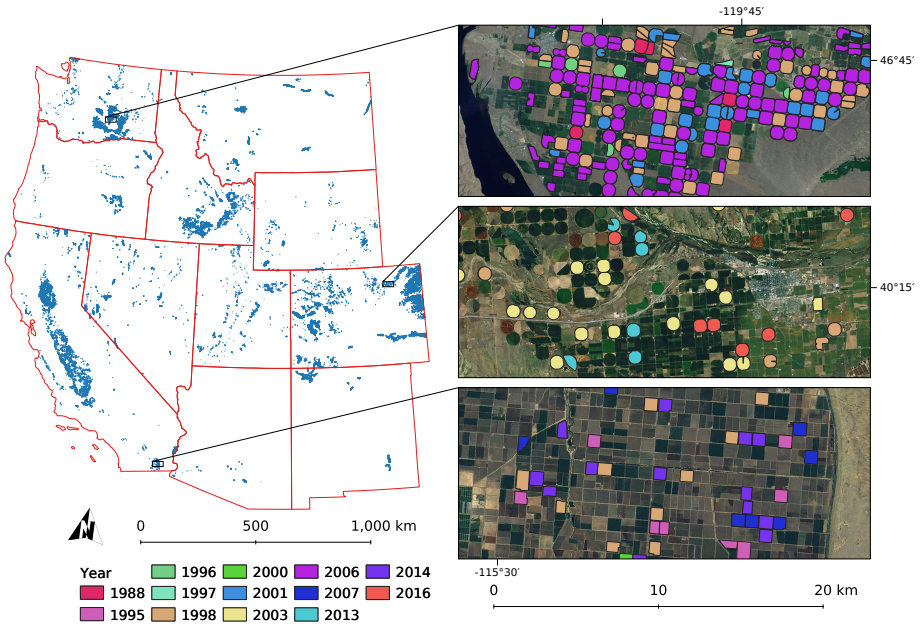

Figure 2.2: Training data from the irrigated class used to train IrrMapper. Table 2.1 shows the number of polygons and total irrigated training area from each class in each of the 11 Western States.

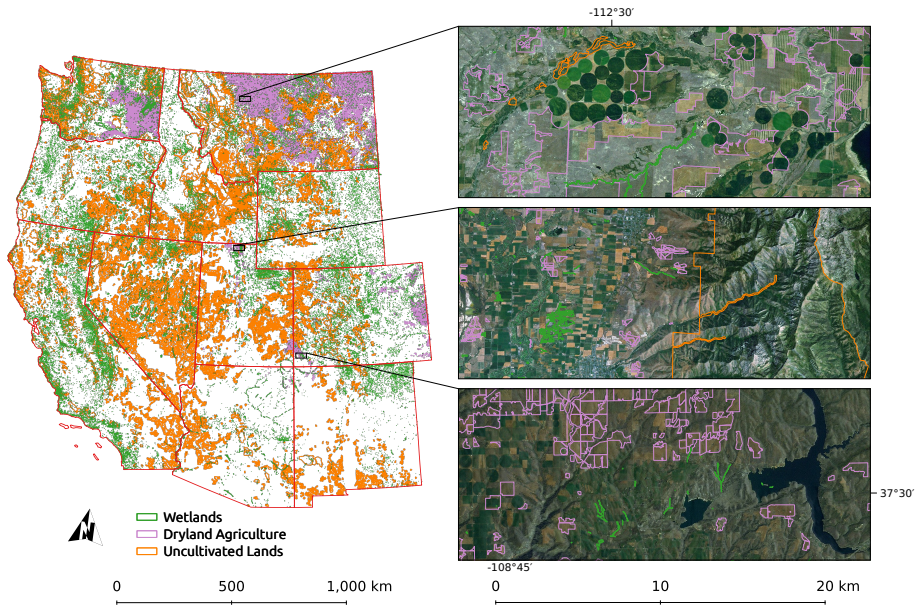

Figure 2.3: Training data from the unirrigated classes used to train IrrMapper (i.e., wetlands, dryland agriculture, and uncultivated lands). Table 2.1 shows the number of polygons and total training area from each class in each of the 11 Western States.

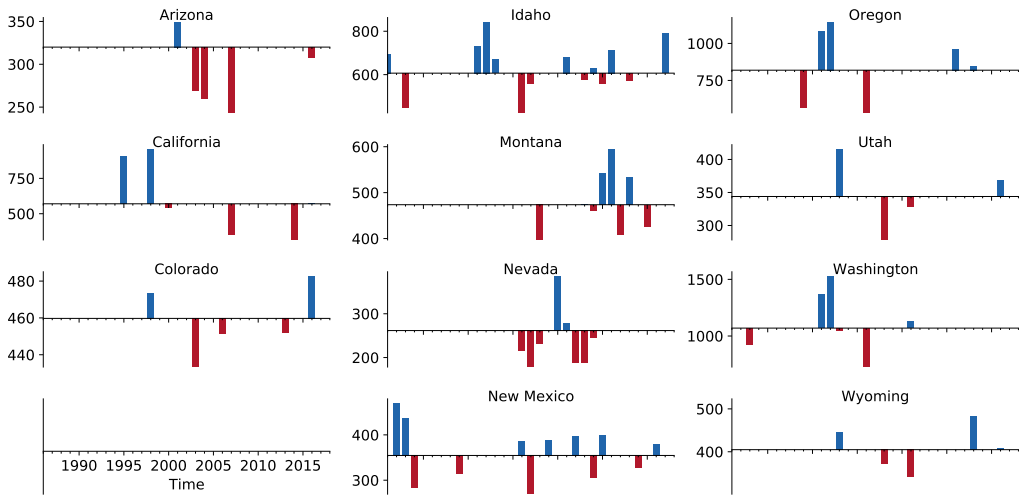

Figure 2.4: Precipitation during the years irrigation was verified for IrrMapper in millimeters; the bar height shows difference from mean statewide precipitation (i.e., the horizontal axis). Precipitation normals are the 100-year statewide average precipitation (1901–2000) during the 12 months ending in September of the year specified. All subplots range 1986–2018, as shown in lower left.

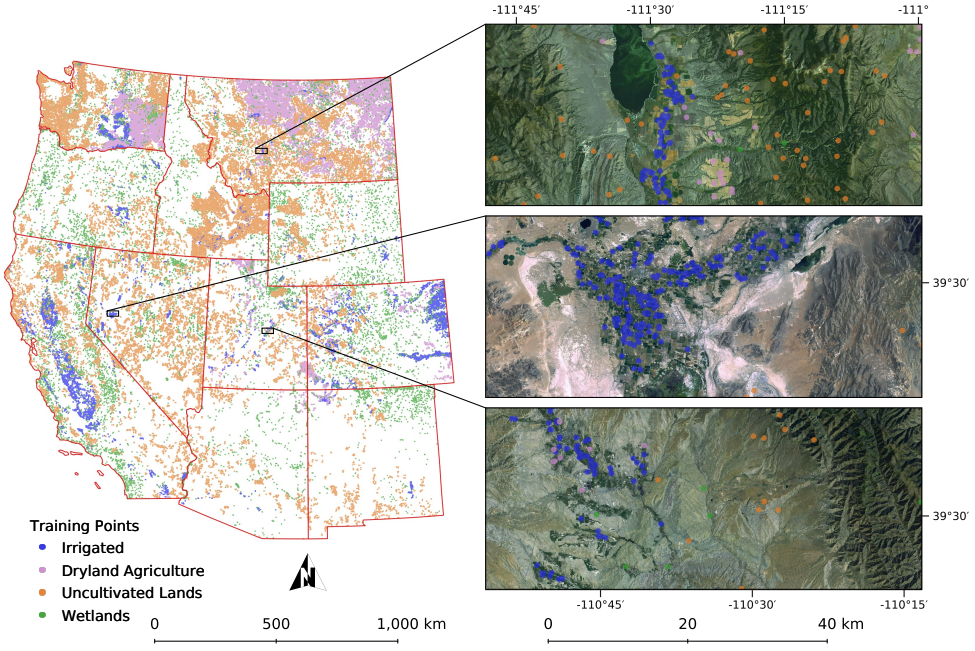

Figure 2.5: Training data sample points from the four classes used to train IrrMapper (i.e., irrigated, wetland, dryland agriculture, and uncultivated). Points were randomly sampled from within a 20-m interior buffer of the training data GIS polygons.

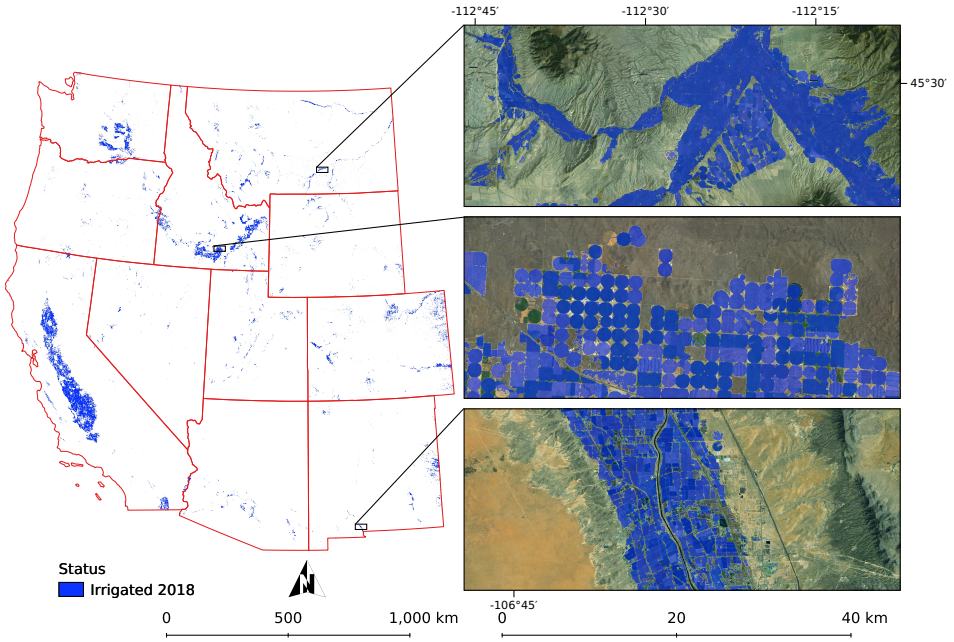

Figure 2.6: Irrigation status as predicted for the year 2018 by IrrMapper, at 30-m resolution.

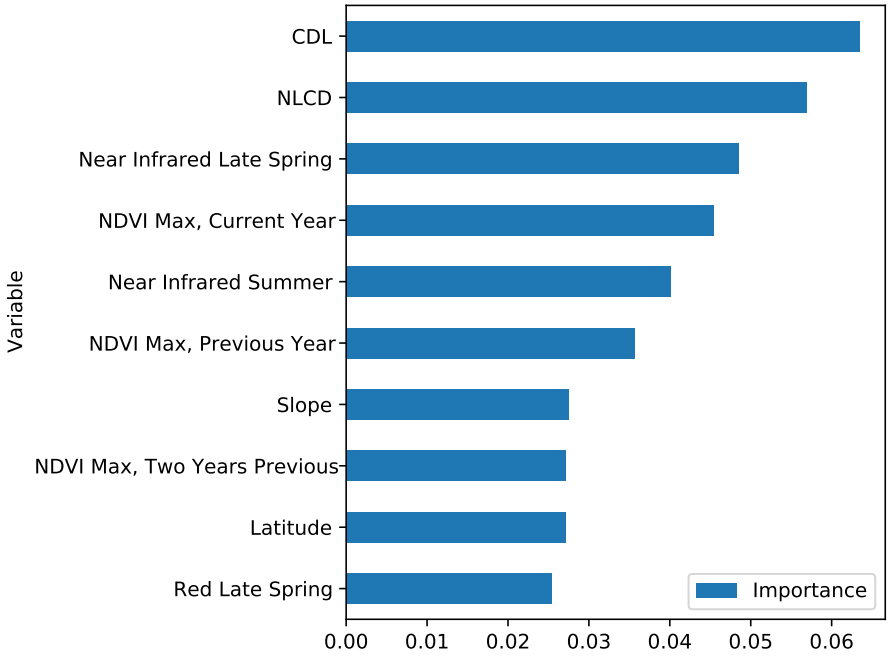

Figure 2.7: The fractional importance of the top 10 variables from the IrrMapper Random Forest model (0.40 accuracy contribution). Variable importance was calculated over ten iterations of model training using a total of 132 data inputs.

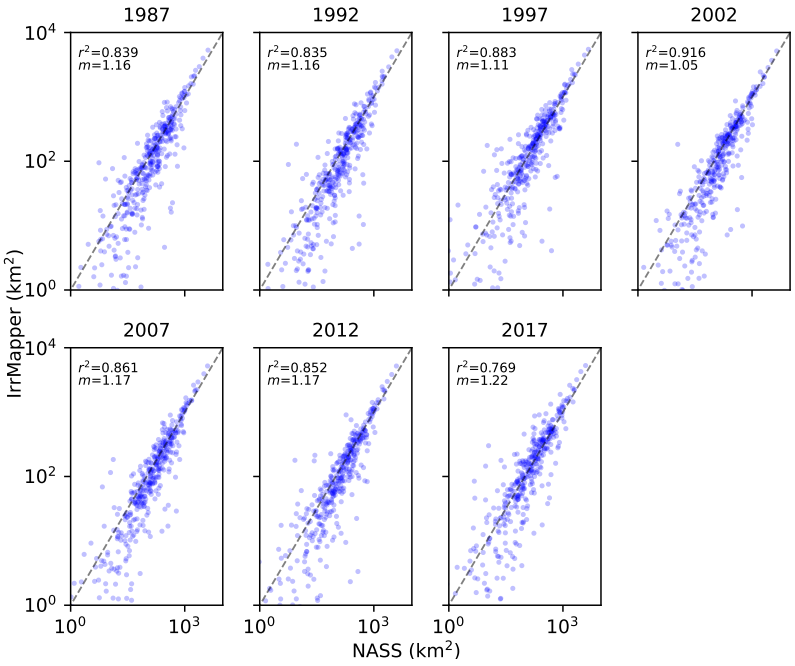

Figure 2.8: Comparison of NASS Census of Agriculture and IrrMapper estimates of county-level irrigated area. Comparison is over the 412 counties within the study region.

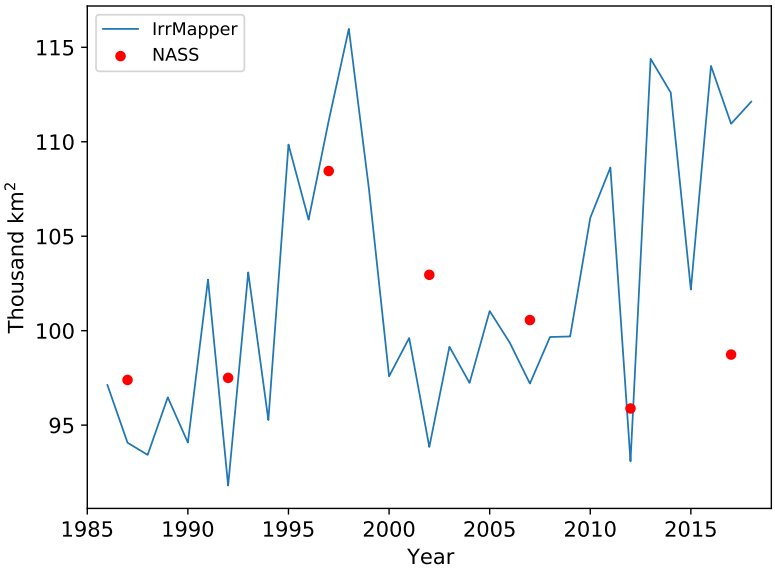

Figure 2.9: Comparison of NASS Census of Agriculture and IrrMapper estimates of irrigated area over the study domain. IrrMapper roughly follows the same pattern in irrigated area as the semi-decadal NASS estimates of total irrigated area.

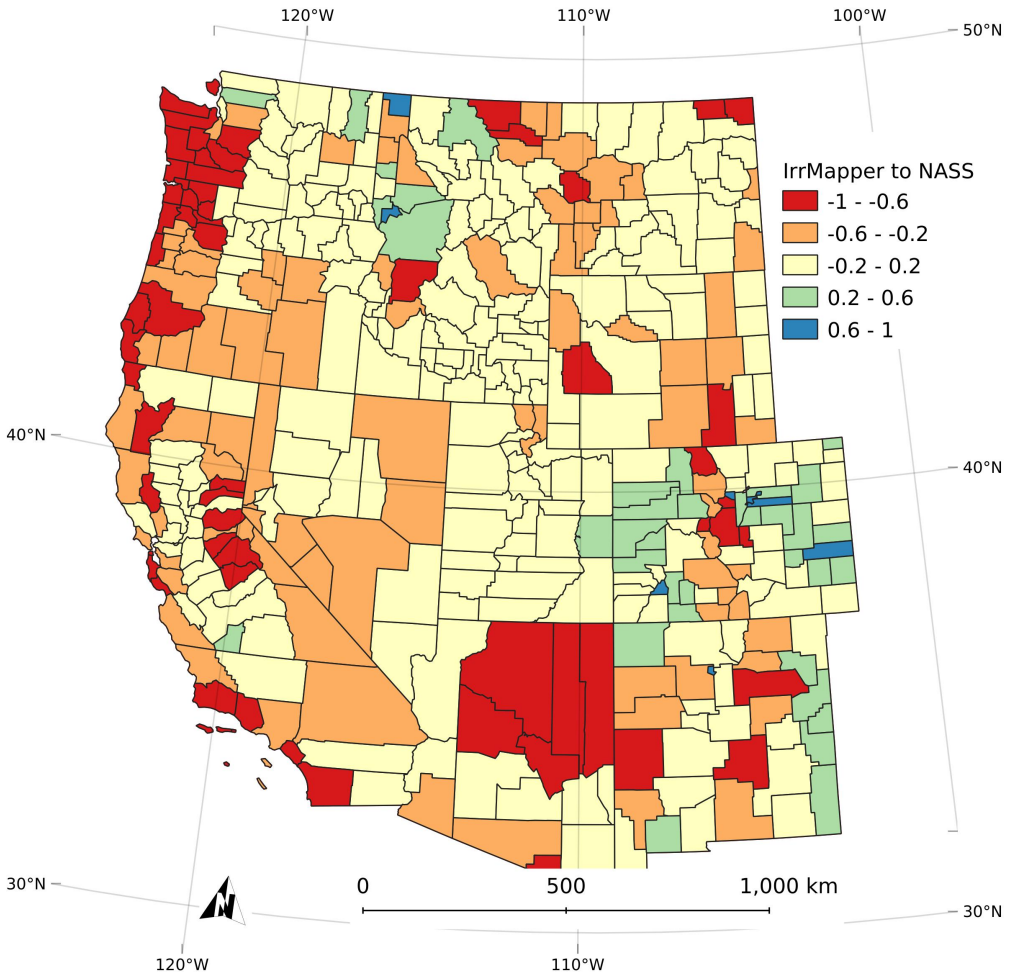

Figure 2.10: The normalized difference of IrrMapper and NASS county-wide Census of Agriculture mean irrigated area estimates over the years of available NASS data (i.e., 1987, 1992, 1997, 2002, 2007, 2012, and 2017). Positive values indicate where IrrMapper made larger estimates than NASS.

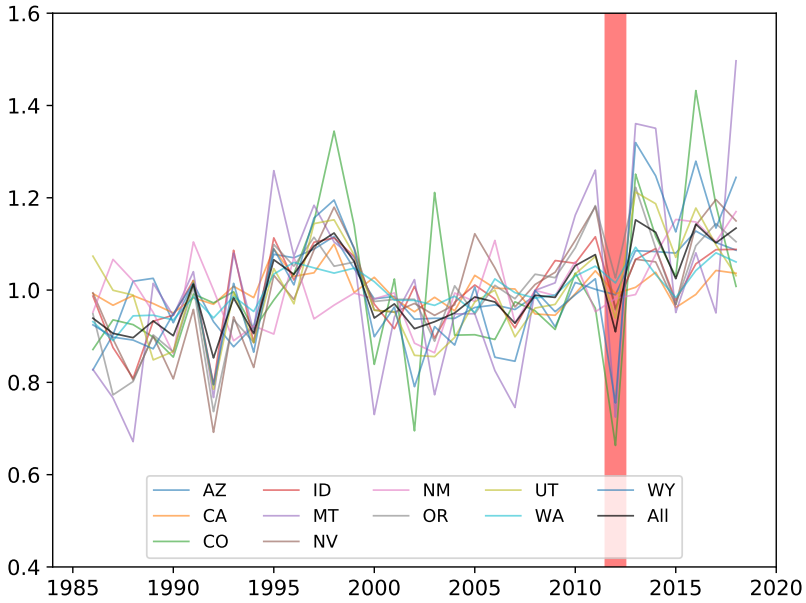

Figure 2.11: The statewide and study area sum of irrigated area predicted by IrrMapper over the 33-year study period, normalized to one. Highlighted is the year 2012, the only year in which the only available USGS atmospherically corrected Landsat surface reflectance data were impacted by the scan line corrector hardware failure on the Landsat 7 ETM+ mission.

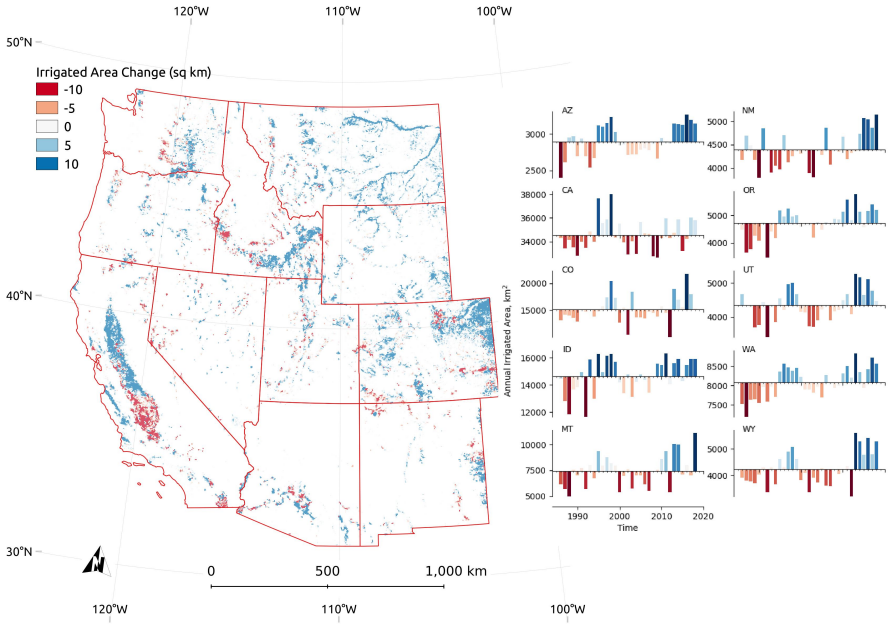

Figure 2.12: Change in 'irrigation equipped' area over the course of the study period, where locations with two or more years of detected irrigation in the periods 1986–1990 and 2014–2018 are considered equipped.

Chapter 3

SUSTAINABILITY OF IRRIGATION AND STREAMFLOW IN THE WESTERN UNITED STATES

3.1 Abstract

Quantifying the interconnected impacts of climate change and irrigation on surface water flows is critical for the proactive management of our water resources and the ecosystem services they provide. Changes in streamflow across the Western U.S. have generally been attributed to an aridifying climate, but in many basins flows can also be highly impacted by irrigation. We developed a 35-year dataset consisting of streamflow, climate, irrigated area, and crop water use to quantify the effects of both climate change and irrigation water use on streamflow across 221 basins in the Colorado, Columbia, and Missouri River systems. We demonstrate that flows have been altered beyond observed climate-related changes and that many of these changes are attributable to irrigation. Further, our results indicate that increases in irrigation water use have occurred over much of the study area, a finding that contradicts government-reported irrigation statistics. Increases in crop consumption have enhanced fall and winter flows in some portions of the Upper Missouri and northern Columbia River basins, and have exacerbated climate change-induced flow declines in parts of the Colorado basin. We classify each basin's water resources sustainability in terms of flow and irrigation trends and link irrigation-induced flow changes to irrigation infrastructure modernization and differences in basin physiographic setting. These results provide a basis for determining where modern irrigation systems benefit basin water supply, and where less efficient systems contribute to return flows and relieve ecological stress.

3.2 Introduction

Irrigation is a critical component of large-scale agriculture and allows for food and fiber production in areas where insufficient precipitation would otherwise inhibit crop growth. About 86 km^3 yr^{-1} of water is applied to irrigated crops annually in the Western U.S., representing nearly 90% of total human water consumption in the region [1]. This practice in turn supports over 75% of commodity sales on less than 25% of harvested land [2]. The waters of the Colorado, Columbia, and Upper Missouri river systems are perhaps the most important natural resources in the region, supporting a population of 20 million people and an economy of nearly a trillion dollars annually; over 75% of irrigation water in this region is drawn from surface water sources [3, 4, 5].

Many irrigated regions across the west continue to expand in area and intensify irrigation water use despite ongoing and projected threats to water supply by humans and a changing climate. Further, ecological impacts (e.g., fish mortality) have been linked to irrigation withdrawal for food production in the region, implying a human-ecological use tradeoff in water scarce systems [6]. Overall, the quantity of irrigation water applied has declined over the past 40 years as more efficient (i.e. greater fraction of applied water used by plants) and advanced irrigation systems have been adopted [7]. However, in a 'paradox of irrigation efficiency', reduced irrigation withdrawal and application requirements have led to higher consumptive irrigation water use (IWU; i.e., irrigation-derived water lost irretrievably to the atmosphere through crop evapotranspiration). This results in reductions in downstream water supply as crop irrigation is optimized for production [8, 9, 10].

The consequences of the efficiency paradox are exacerbated by climate change-induced increases in crop water requirements which may lead to increased evapotranspiration (ET) and reduced runoff at the basin scale [11, 12]. Further, climate change has altered important natural hydrological processes that affect streamflow: precipitation, evaporative demand, evapotranspiration, formation and melting of snowpack, and groundwater recharge [13, 14, 15, 16, 17, 18, 19]. While the implications of climate-induced changes to surface water

supply are widely recognized in the scientific literature, a systematic and spatiotemporally resolved examination of irrigation – our society's greatest hydrological intervention – has not been undertaken in the context of changing surface water availability in the region. Studies demonstrating irrigation impacts on streamflow across the Western U.S. are few and limited to relatively short periods at the basin scale [20, 21, 22], hindered by coarse spatiotemporal information, or dependent on proxies for crop water use [23, 24, 6, 7, 25]. Advances in scalable evapotranspiration and irrigation detection algorithms using long-period, high resolution satellite remote sensing now enable the systematic estimate of crop water use at continental scales [26, 27].

In this study we developed a 35-year dataset consisting of high resolution climate, irrigation, and evapotranspiration data alongside streamflow, interbasin transfer, and reservoir storage records for 221 subbasins in the Colorado, Columbia, and Missouri river systems. We determined the characteristic climate response period of monthly streamflow and show that climate change is impacting streamflow in regionally organized patterns and across basin scales. Our analysis suggests that crop irrigation can mediate or exacerbate climate-induced changes to flow and may contribute to streamflow change in the absence of climate change effects. We summarize our results by providing an estimate of sustainability that is sensitive to water supply, use, and climate change. Ultimately, our results map the basin-specific consequences of the irrigation efficiency paradox, characterize the trajectory of surface water sustainability, and provide a means to evaluate the likely impacts of irrigation management decisions on streamflow.

3.3 Input Data

3.3.1 Streamflow and Reservoir Data

We extracted daily mean discharge data from 221 USGS stream gages draining basins with at least 10 sq km of mean irrigated area (1987-2021) in the Colorado, Columbia, and Upper Missouri river systems [28]. We used the ResOpsUS database to identify gages

draining areas with significant storage reservoirs and to track monthly changes in basin reservoir storage [29] and the United State Bureau of Reclamation's Hydromet data service to extract interbasin transfer volumes at diversions documented by [30]. At gages draining basins with significant storage (i.e., included in ResOpsUS), or where diversions export water via interbasin transfers, the increase in storage or export was added to the gage hydrograph as 'virtual' water that we assume would have flowed past the gage had storage or diversion not occurred. Monthly discharge was calculated for only the months with complete daily records. Discharge observations were matched with topographically delineated contributing basins [31]. The basins range in area from 1,000 sq km to over 243,000 sq km. Gages below Lake Powell and Fort Peck Reservoir, on the Colorado and Missouri rivers, respectively, and where major tributaries enter from Canada were manually excluded. We assumed that standard deviation in stream discharge estimates was 8%, including imprecision in measurement and rating curve model error, after [32, 33, 34, 35].

3.3.2 Gridded Meteorology Data

To calculate the climatic water balance (CWB, i.e., reference evapotranspiration minus precipitation), we obtained precipitation and reference evapotranspiration (ETr) estimates from gridMET, a 4 km resolution gridded daily meteorological dataset [36]. We validated gridMET precipitation at 4,237 stations in the Global Historical Climate Network (GHCN) within the study region and calculated an annual root-mean squared error in each system. We removed any station with an anomalously high precipitation non-detection rate, where greater than 10% of days with nonzero precipitation in gridMET had zero precipitation in the GHCN record. We also removed any station's annual data with less than 250 daily records. We found a mean, study-wide root-mean squared error (RMSE) of 12.7% (Table 3.1). We estimated a single, study-wide ETr RMSE using data from 51 non-agricultural weather stations within the study area with observations suitable for estimating ETr (RMSE 57 mm, 15.3%; [37]. Bias-corrected GridMET is also an input into the remote sensing-based ET estimates in SSEBop whose uncertainty is included in our irrigation water use (IWU)

error estimate. We aggregated CWB data over each basin, giving a monthly 1982-2021 basin-specific time series of CWB.

3.3.3 Irrigation Data

To map the spatiotemporal extent of irrigation, we used IrrMapper [38], a gridded, annual 30 m resolution map of irrigated areas covering the 11 western states of the conterminous U.S. We built an updated version of IrrMapper, training new models and predicting irrigation status state-by-state for the years 1987 - 2021 and using additional predictors of vegetation density (i.e., enhanced vegetation index and greenness index) from the Landsat satellite mission. We further refined the IrrMapper training database through extensive manual remote sensing-based editing and automated filtering of both agricultural and uncultivated training data using land cover models, Landsat satellite images, and National Agricultural Imagery Program aerial photography. We validated our new version of IrrMapper using randomly selected spatial holdouts from a grid of 2,092 23 km x 23 km cells intersecting our irrigated training data. We withheld training data from 413 cells, covering 20% of the irrigated training data. Performance was assessed by comparing IrrMapper predictions to training data in the hold-out grid. To estimate error in our irrigated area estimates, we calculated the system-specific F1 score (i.e., harmonic mean of precision and recall) as a proxy for standard deviation in Bayesian analysis (Table 3.1).

3.3.4 Effective Precipitation

Here we refer to the part of crop ET ultimately derived from in-place natural precipitation as 'effective precipitation'. We sought to model an idealized flat, unforested, uncultivated surface in order to determine the potential for natural ET in the locations now occupied by irrigated agriculture by emulating the ET process in the surrounding areas representing such a surface. We used the OpenET fields geodatabase to form a spatial sampling regime around irrigated areas by selecting fields with greater than 19 years of irrigation in the study period (1987 - 2021; 1.2M fields, 423k irrigated fields). Irrigated fields

were buffered by 1 km and polygon edge overlaps dissolved, producing irrigated region polygon coverages. A 1-km buffer region was produced surrounding the irrigated regions, and a sample of 300k points randomly distributed within the buffer region. The points were filtered by land use type using the National Landcover Dataset and Cropland Data Layers [39, 40], and with IrrMapper, discarding any points that were found to be on cultivated, forested, developed, or wetland areas. At each sample point we extracted 60 predictors and seven target features per year, consisting of climate, soils, and terrain data, and of ET for each of the growing season months we analyzed (April - October, 1987 - 2021).

We estimated effective precipitation using a deep neural network regression model. Our feed forward model is based on multilayer perceptrons (9 hidden layers), one-dimensional convolutions at the input and output of the model, randomized node dropout between the first five hidden layers, batch normalization of inputs, and adaptive learning using the Adam algorithm [41]. We trained a model for each of the seven growing season months in the study. Prior to training, sample points where growing season ET was exceeded by the previous year's precipitation were excluded, giving a mean annual training data set size of 109k samples. We assessed the accuracy of our models by holding out from training 20% of the data for validation. We found an overall, study basin growing season sample root mean squared error of 168 mm, about 25% of the study-wide estimated field-scale mean irrigated crop ET of 681 mm.

3.3.5 Irrigation Water Use Data

To produce monthly ET estimates for the study domain, we applied the Operational Simplified Surface Energy Balance Model (SSEBop; [42]) to 86,812 Landsat Collection 1 images. SSEBop uses psychrometric principles to obtain estimates of 'dry bulb' and 'wet bulb' temperature proxies using land surface temperature estimates from thermal satellite imagery. SSEBop maps the estimated ratio of actual ET to ETr (ETf) over the Landsat image by scaling the difference between wet and dry reference pixels to 0-1. SSEBop ETf values estimated from Landsat images are used as a reference in time, between which

daily ETf is linearly interpolated at each pixel location. The SSEBop time-integrated ET estimate is the product of daily ETf and a gridMET-based daily ETr. ETr was obtained from the grass reference estimate in GridMET and corrected for monthly bias in agricultural regions by an interpolated surface using hundreds of quality-controlled agricultural weather station records [27]. We applied SSEBop, time integration, and ETr development procedures following the methodology outlined in [27] and [43]. We subtracted modeled monthly effective ET estimates from SSEBop [44, 45] . We masked each monthly IWU estimate to the annual IrrMapper irrigated extent, and applied system-specific water balance ET error estimates from [43] and from our own error estimates of IrrMapper and effective precipitation to our IWU estimates (Table 3.1). We further developed IWU for the perennially-irrigated domain, where IrrMapper indicated all years 1987-2021 were irrigated, and repeated the above steps. All gridded data was projected to the USGS CONUS Albers Equal Area projection to make volumetric IWU estimates.

3.3.6 Snake River and Upper Missouri Basin Physiography and Irrigation Management Data

To examine the differences found in the Snake and Missouri River basins in the context of their respective physiography and management patterns, we extracted geographic information using irrigated lands mapping data from Idaho and Montana [46, 47, 48]. In both areas, we extracted geologic unit information and distance from the irrigated field centroid to the nearest, minimum fourth order stream for each of the irrigated fields using statewide geology maps and hydrographic data [49, 50, 51]. We estimated center pivot irrigation area directly from Montana's 2019 field attributes, and used a simple arc-finding algorithm to estimate the fraction of irrigated area under center pivot irrigation in the Snake River Plain in 1985 and 2015.

3.4 Regression Modeling

3.4.1 The Climate-Flow Relationship

We performed an initial grid search of time, monthly streamflow, and CWB to identify the month- and basin-specific climate period that best predicted flow at each study gage. We modeled streamflow using simple linear regression of CWB and monthly flow, choosing the climate period by testing models over an iteratively expanding time window from 1 to 60 months preceding the end of the flow month. We found the most highly correlated climate period (i.e., the 'climate-flow period') for each month of each basin's streamflow, and used that period in subsequent analysis to account for climate covariance with flow. These 160,560 regression tests yielded 2,676 monthly, basin-specific climate-flow periods for use in our Bayesian analysis (Table 3.2). The models showed that climate explains over 50% of monthly variance in flow volume ($r^2 > 0.5$) at an average of 191 of the 221 irrigated basins for each of the 12 months of flow, and was significant ($p < 0.05$) in over 97% of the irrigated basin-months analyzed. Basin response times averaged 10.4 months; the shortest were for June discharge (mean 7.3 months) and longest for December and January flows (13.8 months each). The climate-flow period is systemic; rivers have similar climate-flow periods at each gage along their length.

3.4.2 The Irrigation-Flow Relationship

We performed a further grid search through time, using monthly streamflow, CWB, and IWU to identify basins where IWU was a potentially significant predictor of streamflow variability. To control for climate-induced interannual variance in flow, we used simple linear regression on the residuals of the climate-flow relationship (the dependent variable), and IWU as the predictor. For flow in the growing season months (i.e., April - October), we tested the relationship in all possible consecutive monthly growing season time periods preceding the end of the flow period. For example, we tested if June residual flows (as determined from the climate-flow analysis, above) were significantly explained by IWU in

April, May, June, April and May, May and June, and April through June. For flow after the growing season (i.e., November - March), we tested the previous growing season's IWU time windows. In such a manner, we assume that natural flows depend on the (potentially longer-term) climate-flow relationship, and that true flows are subject further to irrigation during the growing season preceding the flow period. These 42,240 regression tests of possible IWU-flow relationships were filtered by p-value ($p < 0.05$) and yielded 776 significant relationships to be further tested and corroborated in our subsequent Bayesian analysis (Table 3.2).

3.4.3 Bayesian Analysis of Trends and Irrigation-Flow Response

We constructed Bayesian linear models to test the significance of time trends and the IWU-flow response over our study area basins. These models allow us to incorporate our estimates of uncertainty and provide probability distributions describing model parameters. We use Bayes' theorem:

$$P(\boldsymbol{\alpha}|\hat{x}) \propto P(\hat{x}|\boldsymbol{\alpha})P(\boldsymbol{\alpha}) \tag{3.1}$$

where $\hat{x}$ is a vector of observations, and $\boldsymbol{\alpha}$ is a vector of unobserved model parameters. Our aim is to estimate the posterior $P(\boldsymbol{\alpha}|x)$ using the likelihood $P(x|\boldsymbol{\alpha})$ (or, the probability of the data given the parameters) and the the prior $P(\boldsymbol{\alpha})$ assumption of the distribution of model parameters. From these posterior probability distributions, we draw conclusions on the significance and direction of trends and IWU-flow response. In the case of time trends we assume the response is a random variable, dependent on time:

$$Y \sim \mathcal{N}(\boldsymbol{t}\beta + \alpha, \sigma_Y^2) \tag{3.2}$$

where $\boldsymbol{t}$ is the month, α and β are the intercept and slope coefficients, respectively, and Y is a random variable with mean $\boldsymbol{t\beta} + \alpha$ and variance σ_Y^2, derived from error estimates discussed below. Y represents a series of observations of monthly CWB, irrigated area, IWU, or streamflow in a given basin. The length of Y is equal to that of $\boldsymbol{t}$, which may reach

35, but is less in the case where incomplete monthly flow records exist, as described above. In this and in the following cases, we assume an uninformative, normally distributed prior distribution of the parameters with a mean of zero and a variance much higher than the range of the data (which is scaled to the range 0 - 1):

$$\alpha \sim \mathcal{N}(0, 20) \tag{3.3}$$

$$\beta \sim \mathcal{N}(0, 20) \tag{3.4}$$

In the case of time trend analysis for climate-normalized IWU and streamflow, we use a bivariate, time- and climate-dependent model:

$$\mathrm{I}_{CN,i,\mathrm{obs}} \sim \mathcal{N}(C_{m,i,\mathrm{true}}\beta_0 + \boldsymbol{t}\beta_1 + \alpha, \sigma^2_{\mathrm{IWU-CNBasin}}) \tag{3.5}$$

$$\mathrm{C}m, i, \mathrm{obs} \sim \mathcal{N}(C_{m,i,\mathrm{true}}, \sigma_{C\mathrm{Basin2}}) \tag{3.6}$$

$$\mathrm{Q}_{CN,i,\mathrm{obs}} \sim \mathcal{N}(C_{CP,i,\mathrm{true}}\beta_2 + \boldsymbol{t}\beta_3 + \alpha, \sigma^2_{\mathrm{Q-CNBasin}}) \tag{3.7}$$

$$\mathrm{C}_{CP,i,\mathrm{obs}} \sim \mathcal{N}(C_{p,i,\mathrm{true}}, \sigma_{C\mathrm{Basin2}}) \tag{3.8}$$

where I_{CN} is climate-normalized monthly IWU estimate, Q_{CN} is climate-normalized monthly streamflow, C_{CP} is CWB aggregated over the climate-flow period, C_m is CWB over the concurrent month of IWU observation, and each of α and β is drawn from the distributions given in (3.3) and (3.4), respectively. $\sigma_{I,CN,Basin}$ and $\sigma_{Q,CN,Basin}$ are system-specific estimates of uncertainty in the dependent (i.e., I_{CN}, Q_{CN}) variables, and $\sigma_{C,Basin}$ is a system-specific estimate of uncertainty in the climate data.

Finally, in the case of the IWU-streamflow response, we also use a bivariate model:

$$\mathrm{Q}_{m,i,\mathrm{obs}} \sim \mathcal{N}(C_{CP,i,\mathrm{true}}\boldsymbol{\beta_4}, I_{p,i,\mathrm{true}}\boldsymbol{\beta_5} + \alpha, \sigma^2_{\mathrm{QBasin}}) \tag{3.9}$$

$$\mathrm{I}_{p,i,\mathrm{obs}} \sim \mathcal{N}(I_{p,i,\mathrm{true}}, \sigma^2_{IWU\mathrm{Basin}}) \tag{3.10}$$

where Q_m is observed volumetric monthly streamflow on the i-th observation in the series, I_p is monthly IWU summed over the preceding growing season irrigation period, σ_{QBasin} is a system-specific estimate of uncertainty in flow, and $\sigma_{IWUBasin}$ is a system-specific estimate of uncertainty in IWU.

Here, σ represents the uncertainty associated with input data modeling systems (i.e., Gridmet, IrrMapper, USGS streamflow rating curves, and SSEBop), and includes measurement error in the observations upon which the models depend. We further assume σ is proportional to our estimates of long-term fractional error in each of our input datasets, that the error is independent and identically distributed, constant through the study period and over sub-annual time scales and basin geographies. In the case of CWB, we propagate uncertainty through addition in quadrature:

$$\sigma_{CWB\mathrm{Basin}} = (PPT^2_{\mathrm{Basin}} + ETr^2_{\mathrm{Overall}})^{1/2} \tag{3.11}$$

$$\sigma_{IWU\mathrm{Basin}} = (SSEBop^2_{\mathrm{Basin}} + EffPpt^2_{\mathrm{Overall}} + IrrMapper^2_{\mathrm{Basin}})^{1/2} \tag{3.12}$$

where $\sigma_{IWUBasin}$ is system-specific error in IWU, and $\sigma_{SSEBopBasin}$, $\sigma_{IrrMapperBasin}$, and $\sigma_{EffPptOverall}$ are errors in system-specific ET and irrigated area, and study-wide effective precipitation estimates, respectively. SSEBop ET was corrected for system-specific bias before Bayesian analysis, but was not corrected for our estimate of basin-scale volumetric IWU.

We used the PyMC Python package to perform Markov Chain Monte Carlo sampling and generate a sequence of posterior samples from which we could discern a distribution of linear model parameters describing our observations [52]. Sample step proposals were

generated using the No U-Turn sampler for 5000 tuning and 1000 posterior sample draws. We quantified convergence using the Arviz package to calculate the Gelman-Rubin statistic, $\hat{r}$, and discarded models where $\hat{r} > 1.1$ [53, 54]. We used the posterior distribution of slopes to find the highest credible interval (CI; 2.5% to 97.5%); cases where the CI was above or below zero were considered significant and the mean slope of the CI selected for interpretation (Table 3.2).

3.5 Results

The objective of this analysis is to understand the sustainability of water resources across the Western U.S. We define sustainability as the trajectory (directionality of change) of surface water flows and irrigation water use, the principal water supply and use in the region, while accounting for climate change. Below, we describe our hierarchical approach to evaluating sustainability, ultimately resulting in spatial information that can inform future water management across the west.

3.5.1 Climate and Streamflow Relationships in Irrigated Basins

We quantified climatic drivers of streamflow using linear regression of the climatic water balance (CWB; reference evapotranspiration [ETr] minus precipitation) and monthly flow over the basin-specific climatic aggregation period (Figure 3.4). Unsurprisingly, basin-specific models of CWB and streamflow indicate they are inversely related; 96.8% of significant relationships exhibited a negative slope demonstrating that drier climatic aggregation periods yield lesser volumetric flow. The flow-CWB relationship explains the majority of monthly flow variance ($r^2 > 0.5$) for at least one month of the year at 97% of the irrigated basins in our study. Model explanatory power was lowest in February flows (median r^2:0.41, interquartile range [IQR] 0.23) and was highest in June (median r^2: 0.69, IQR 0.19).

3.5.2 Streamflow Trends

Temporal trend analysis using Bayesian linear regression (i.e., the change in flow over time, Eqn. 3.2) revealed that monthly flow volumes have experienced significant changes during the study period; nearly all irrigated basins experienced monthly discharge changes during at least one month across our study area (Figure 3.5). The Colorado basin experienced the most widespread and seasonally persistent declines in flow, especially along the major tributaries of the west slope (e.g., main stem Colorado and San Juan rivers). Major drainages within the Missouri (e.g. Yellowstone, Missouri rivers) experienced increases in flow in the spring and summer.

Temporal trends in climate-normalized flows (i.e., the time component of the bivariate Bayesian linear regression of flow as a function of climate and time, (Eqn. 3.7) revealed significant changes in flow unrelated to climate, mostly in the northern latitude systems of the study area. Widespread flow increases were observed in the upper reaches of the Missouri and around the Columbia, except in the Snake River basin. Of the 30 gages with negative median trends in monthly climate-normalized flow, the Snake River showed the most seasonally persistent and systemic response, with negative trends found along the lower length of the river, generally during the winter and spring.

3.5.3 Irrigation Water Use Trends

Volumetric IWU has represented a large fraction of total available surface water in the most heavily irrigated basins since the beginning of our study period in 1987 (Figure 3.1). The mean annual ratio of April - October IWU to annual flows at the outlets of major basins range from 0.02 on the Pend Oreille River to over 0.6 on the Snake River. In other words, the volume of water used for IWU represents an impressive 60 percent of the water flowing through the Snake River at the Weiser, ID gage annually. Increases in IWU were widespread in terms of all metrics we tested; total IWU, IWU within the perennially-irrigated domain (irrigated all years 1987-2021), and climate-normalized IWU (i.e., the time

component of the bivariate Bayesian linear regression of IWU as a function of climate and time, (Eqn. 3.5) all showed generally positive trends (Figure 3.6). Increases in total IWU were experienced across the Missouri and Colorado systems, but mixed in the Columbia, where decreases occurred in the Cascades. In nearly all cases, IWU increases are associated with the expansion of irrigated area (Figure 3.7); of the 15 largest irrigated basins in the study, 12 experienced significant increases in irrigated area. Increases in IWU are further associated with increasing aridity in the Northern Rockies and the Colorado River Basin (i.e., aridification, Figure 3.8).

3.5.4 Stream Response to Irrigation Water Use

We found IWU was a significant predictor of climate-normalized flows for at least one month at 90% of analyzed basins (Figure 3.2). Our analysis identified bidirectional regional and seasonal patterns; increased flows were associated with increased IWU in the Upper Colorado and Missouri basins in the winter, while increased summer flows were less common in large basins, but were detected at smaller basin scales in the headwaters of each system. The largest basins generally experienced flow decreases associated with increased IWU in the summer, while many smaller basins had mixed flow responses to IWU. Over 60 of the study basins experienced IWU-associated impacts in opposite directions from summer to winter. For example, the two largest basins with this response were the Pend Oreille and the Yellowstone Rivers, both of which see reduced flows in the summer and greater flows in the winter subsequent to increased IWU.

3.6 Discussion

Our results show that in many basins, irrigation is causing changes to streamflow, sometimes in opposition to climate change (i.e., trends in aridification). This response varies from basin to basin, and may increase or decrease flows during different times of the year. Our results indicate that in some basins, water returns to rivers from irrigated lands after some delay, while in others, the water is effectively removed from the basin and 'lost' to ET. We

suggest that these responses provide information that could allow for targeted irrigation expansion of infrastructure type, timing, and intensity with an understanding of potential surface water consequences. In areas where applied water is lost to further in-basin uses (e.g., lost to ET), irrigation infrastructure should be made as efficient as possible with the intent of minimizing avoidable non-beneficial consumptive uses (e.g., excessive spray and canopy interception losses; [55]). Conversely, in areas where flows are enhanced by irrigation systems, intensification of inefficient irrigation systems (e.g. flood irrigation) may benefit streams in the late summer when return flows of groundwater buffer low flow and high temperatures [56]. No two basins are the same and decisions to mitigate declines in water resources must be based upon the interplay of a basin's unique hydrological properties, irrigation systems, climate change trajectory, and multiple and often competing uses of water.

3.6.1 Disentangling Climate Change and Irrigation Impacts on Streamflow

As expected, the annual streamflow variability in irrigated basins across the Western U.S. is primarily driven by climatic variability [57]). The significant declines in flow around the Colorado River basin and in the northern Rocky Mountains, and increases in flow in the lower Missouri basin coincide with the regions' respective drying and wetting climates (Figures 3.5, 3.4). Interestingly, streamflow has changed in opposition to an obvious climate change signal in 83 basins, indicating the influence of additional forcings.

There has been an intensive (depth) and extensive (area) increase of irrigation over our study period; it is now more intense, more temporally persistent, covers more of each field, and has expanded into the margins of existing irrigated regions across the west (Figures 3.6, 3.7). This finding contradicts commonly cited county-based irrigated area estimates by the U.S. Department of Agriculture (USDA), which documented only a modest 2% expansion of irrigated area from 1987 - 2017 in the study area, and a decline in irrigation water application [1, 58]. The limited areal expansion of irrigation reported in survey statistics was concurrent with a nearly two-fold increase in the area under pressurized irrigation systems

(e.g. center pivot systems) in the 17 Western states, while gravity-fed systems (e.g. flood) saw a decrease in area of nearly 50% [7]. While systematic and methodologically consistent, USDA reporting of irrigated area and applied irrigation volumes are a poor proxy for IWU, and it appears the widespread reliance upon such data has led to the operation of the efficiency paradox at scale going unobserved. The increasing intensity of IWU, concurrent with the remarkable expansion of modern irrigation systems across the region, and with regional increases in CWB appear to have outweighed any retraction in irrigated area due to suburban development or water conservation efforts. Trends in climate-normalized IWU and IWU in perennially irrigated areas further support the notion of the counterintuitive increase in water use accompanying increases in irrigation efficiency, despite reductions in irrigation water applications, and are consistent with previous work at smaller scales [10, 59].

Climate-normalized flow responses to IWU show that streams are sensitive to the expansion and intensification of irrigation operations (Figure 3.2). Our results indicate that the most widespread negative impacts of increased IWU on flow occur during the summer, which may imply strong ecological implications [60]. Impacts on winter flows have distinct systemic patterns, where unidirectional, multi-gage impacts are noted along the Pend Oreille, Snake, and Upper Missouri rivers (negative responses), while the Yellowstone and Green also show organized responses at multiple gages (positive responses). In both seasons, response directions and timing are highly variable from basin to basin, and while we emphasize system-wide patterns here, the larger basins are likely integrating bi-directional influences and noise resulting from our simplified modeling approach.

Trends in climate-normalized flows indicate that concurrent trends in irrigation are contributing to streamflow changes in many of the study basins. The widespread positive trends observed in this study are focused around October and November flows, suggesting that irrigation during the summer can increase flows later in the season. The positive influence on flows later in the season in some basins suggests that IWU may augment flows when they are at their lowest, providing valuable ecosystem services during times

of stress for aquatic and adjacent terrestrial ecosystems [61]. Positive impacts were not ubiquitous across the region; negative trends on the San Juan river suggest water diversions do not increase late season flows and imply IWU is exacerbating the negative impacts of an aridifying climate in the region, further diminishing instream flows. On the Snake River, flow trends in the lower basin are opposite than what we would expect given the slight wetting of the climate and increases in flows in upper tributaries. It appears IWU in the Snake River basin has overcome increased water availability and caused flows to decline over the study period.

3.6.2 Why do basins respond differently?

The Missouri and Snake river basins are illustrative of IWU impacts on contrasting streamflow trends. The Snake appears to have undergone a more clear wetting trend relative to the Missouri Basin, while both have seen increases in IWU (Figures 3.8, 3.6). In spite of these climate and IWU trends, the Missouri has mostly experienced increases in flow while the Snake has seen decreases (Figure 3.5); due to physiographic and management differences. For example, in the Eastern Snake River Plain, there has been a rapid conversion of irrigation infrastructure to more efficient center pivot systems, representing a transition from about 35% in 1986 to about 75% 2015 [46, 47]). Snake River basin irrigation systems are located on average 8km from the nearest stream in areas hydrologically connected to the river via regional aquifer flow paths that operate on long time scales [62]. Further, 50% of irrigated area overlays less permeable basalt formations with thick unsaturated zones [49]. In summation, Snake river irrigation is more efficient, is less likely to recharge the subsurface, and the subsurface aquifer is less hydrologically connected to the river than the Upper Missouri system [62, 63]. This causes a diminished and long-term delay in return flows, potentially explaining the lack of a lagged, positive streamflow response to increases in irrigation during the time scales assessed in this study (up to 60 months). In contrast, the Upper Missouri Basin in Montana saw mixed streamflow impacts, with more frequent detection of lagged increases in streamflow due to irrigation on short time scales (Missouri

Basin median lag: 5.2 months), especially along the Yellowstone River. Here, only 40% of the basin's irrigated lands utilized center pivot in 2019, over 50% of irrigation overlies unconsolidated alluvial and periglacial aquifers, and irrigated fields average only 2.7 km from the nearest stream [48, 50]. The Upper Missouri irrigation is less efficient due to the slower adoption of modern irrigation systems, likely resulting in more groundwater recharge during periods of intense irrigation. Finally, irrigated regions in the Missouri River basin overlay aquifers that are more immediately hydrologically connected to neighboring streams, likely leading to more robust return flows on sub-annual timescales [50].

3.6.3 Sustainability of Water Resources

Comparison of trends in flow and IWU indicate the trajectory of water resources across the region and provide a basis for classifying irrigated basins in terms of water resources sustainability (Figure 3.3). Declining flows and increasing IWU are found at 43 gages, focused in the Snake and Colorado river basins, and represent the least sustainable water resources trajectory identified in this study. Surprisingly the most numerous classification (60 gages) is found where IWU and flow trends are both increasing, most widely observed in the Missouri basin (an area with widespread flood irrigation) and scattered through the Columbia and Colorado basins. The most sustainable trajectory is focused in the western Columbia river basin, where water resource pressure is alleviated due to less IWU demand which subsequently increases streamflow (13 gages; Figure 3.3). There are only a few cases of declining flows and declining IWU (3 gages). The trends identified here therefore suggest that the Upper Missouri system follows a more sustainable trajectory, where increased water use is associated with generally increasing flows. This is in contrast to many of the major tributaries in the Colorado basin and the Snake River, where water use, starting from an already very high baseline, has increased despite diminishing supplies and ongoing efforts to make water use more sustainable [64]. In fact, it appears IWU and associated management actions on the Snake River have overcome a slight wetting trend in the fall and winter, which would otherwise be expected to increase flow. However, a generally aridifying climate

appears to play a primary role in the decline in flow throughout the Colorado River basin, though it appears that increasing IWU in the San Juan has exacerbated these impacts.

Much of our study area has experienced a deepening water crisis since the onset of drought two decades ago [65]. Under these conditions of non-stationarity, it is crucial to configure our irrigated agricultural systems in such a way that they become resilient to climate change and flexible in their intensity of water use [66]. Our results show that, given the unique response of basins to irrigation intensification and climate change, agricultural paradigms viewed as non-efficient, such as flood irrigation, may in fact be preferable in regions such as the Missouri basin. Further irrigation development in areas experiencing surface water supply declines should be considered in the context of basin physiography and likely streamflow impacts of irrigation expansion and intensification. This study advances that imperative through the spatiotemporal description of such basin-specific characteristics in the context of climate change and human water use.

REFERENCES

[1] United States Department of Agriculture, National Agricultural Statistics Service, "2017 census of agriculture," Tech. Rep. 1, United States Department of Agriculture, Apr. 2019.

[2] N. Gollehon and W. Quinby, "Irrigation in the american west: Area, water and economic activity," *Int. J. Water Resour. Dev.*, vol. 16, pp. 187–195, June 2000.

[3] U.S. Bureau of Economic Analysis, "Gross domestic product by county, 2020." `https://www.bea.gov/news/2021/gross-domestic-product-county-2020`, Dec. 2021. Accessed: 2022-11-1.

[4] T. James, A. Evans, E. Madly, and C. Kelly, "The economic importance of the colorado river to the basin region." `http://greatbasinwater.org/archives/doc/ptf_final-121814.pdf`, 2014. Accessed: 2022-11-19.

[5] United States Department of Agriculture, National Agricultural Statistics Service, "2018 irrigation and water management survey," Tech. Rep. 3, United States Department of Agriculture, Nov. 2019.

[6] B. D. Richter, D. Bartak, P. Caldwell, K. F. Davis, P. Debaere, A. Y. Hoekstra, T. Li, L. Marston, R. McManamay, M. M. Mekonnen, B. L. Ruddell, R. R. Rushforth, and T. J. Troy, "Water scarcity and fish imperilment driven by beef production," *Nature Sustainability*, vol. 3, pp. 319–328, Mar. 2020.

[7] A. Hrozencik and M. Aillery, "Trends in irrigated agriculture reveal sector's ability to adapt to evolving climatic, resource, and market conditions," *Amber Waves*, vol. 2022, no. 1490-2022-276, 2022.

[8] R. Q. Grafton, J. Williams, C. J. Perry, F. Molle, C. Ringler, P. Steduto, B. Udall, S. A. Wheeler, Y. Wang, D. Garrick, and R. G. Allen, "The paradox of irrigation efficiency," *Science*, vol. 361, pp. 748–750, Aug. 2018.

[9] C. A. Scott, S. Vicuña, I. Blanco-Gutiérrez, F. Meza, and C. Varela-Ortega, "Irrigation efficiency and water-policy implications for river basin resilience," *Hydrol. Earth Syst. Sci.*, vol. 18, pp. 1339–1348, Apr. 2014.

[10] F. A. Ward and M. Pulido-Velazquez, "Water conservation in irrigation can increase water use," *Proc. Natl. Acad. Sci. U. S. A.*, vol. 105, pp. 18215–18220, Nov. 2008.

[11] P. Vahmani, A. D. Jones, and D. Li, "Will anthropogenic warming increase evapotranspiration? examining irrigation water demand implications of climate change in california," *Earths Future*, vol. 10, Jan. 2022.

[12] J. T. Abatzoglou, S. Z. Dobrowski, and S. A. Parks, "Multivariate climate departures have outpaced univariate changes across global lands," *Sci. Rep.*, vol. 10, p. 3891, Mar. 2020.

[13] Z. A. Holden, A. Swanson, C. H. Luce, W. M. Jolly, M. Maneta, J. W. Oyler, D. A. Warren, R. Parsons, and D. Affleck, "Decreasing fire season precipitation increased recent western US forest wildfire activity," *Proc. Natl. Acad. Sci. U. S. A.*, vol. 115, pp. E8349–E8357, Sept. 2018.

[14] C. H. Luce, J. T. Abatzoglou, and Z. A. Holden, "The missing mountain water: slower westerlies decrease orographic enhancement in the pacific northwest USA," *Science*, vol. 342, pp. 1360–1364, Dec. 2013.

[15] L. E. Condon, A. L. Atchley, and R. M. Maxwell, "Evapotranspiration depletes groundwater under warming over the contiguous united states," *Nat. Commun.*, vol. 11, p. 873, Feb. 2020.

[16] P. C. D. Milly and K. A. Dunne, "Colorado river flow dwindles as warming-driven loss of reflective snow energizes evaporation," *Science*, vol. 367, pp. 1252–1255, Mar. 2020.

[17] D. A. Atawneh, N. Cartwright, and E. Bertone, "Climate change and its impact on the

projected values of groundwater recharge: A review," *J. Hydrol.*, vol. 601, p. 126602, Oct. 2021.

[18] T. Meixner, A. H. Manning, D. A. Stonestrom, D. M. Allen, H. Ajami, K. W. Blasch, A. E. Brookfield, C. L. Castro, J. F. Clark, D. J. Gochis, A. L. Flint, K. L. Neff, R. Niraula, M. Rodell, B. R. Scanlon, K. Singha, and M. A. Walvoord, "Implications of projected climate change for groundwater recharge in the western united states," *J. Hydrol.*, vol. 534, pp. 124–138, Mar. 2016.

[19] C. M. Albano, J. T. Abatzoglou, D. J. McEvoy, J. L. Huntington, C. G. Morton, M. D. Dettinger, and T. J. Ott, "A multidataset assessment of climatic drivers and uncertainties of recent trends in evaporative demand across the continental united states," *J. Hydrometeorol.*, vol. 23, pp. 505–519, Apr. 2022.

[20] H. I. Essaid and R. R. Caldwell, "Evaluating the impact of irrigation on surface water – groundwater interaction and stream temperature in an agricultural watershed," *Sci. Total Environ.*, vol. 599-600, pp. 581–596, Dec. 2017.

[21] F. Wen and X. Chen, "Evaluation of the impact of groundwater irrigation on streamflow in nebraska," *J. Hydrol.*, vol. 327, pp. 603–617, Aug. 2006.

[22] R. Zeng and X. Cai, "Analyzing streamflow changes: irrigation-enhanced interaction between aquifer and streamflow in the republican river basin," *Hydrol. Earth Syst. Sci. Discuss.*, vol. 10, pp. 7783–7807, June 2013.

[23] S. M. Vicente-Serrano, M. Peña-Gallardo, J. Hannaford, C. Murphy, J. Lorenzo-Lacruz, F. Dominguez-Castro, J. I. López-Moreno, S. Beguería, I. Noguera, S. Harrigan, and J.-P. Vidal, "Climate, irrigation, and land cover change explain streamflow trends in countries bordering the northeast atlantic," *Geophys. Res. Lett.*, vol. 46, pp. 10821–10833, Oct. 2019.

[24] Y. Wada, L. P. H. van Beek, N. Wanders, and M. F. P. Bierkens, "Human water

consumption intensifies hydrological drought worldwide," *Environ. Res. Lett.*, vol. 8, p. 034036, Sept. 2013.

[25] I. K. Mpanga and O. J. Idowu, "A decade of irrigation water use trends in southwestern USA: The role of irrigation technology, best management practices, and outreach education programs," *Agric. Water Manage.*, vol. 243, p. 106438, Jan. 2021.

[26] M. C. Anderson, R. G. Allen, A. Morse, and W. P. Kustas, "Use of landsat thermal imagery in monitoring evapotranspiration and managing water resources," *Remote Sens. Environ.*, vol. 122, pp. 50–65, July 2012.

[27] F. S. Melton, J. Huntington, R. Grimm, J. Herring, M. Hall, D. Rollison, T. Erickson, R. Allen, M. Anderson, J. B. Fisher, A. Kilic, G. B. Senay, J. Volk, C. Hain, L. Johnson, A. Ruhoff, P. Blankenau, M. Bromley, W. Carrara, B. Daudert, C. Doherty, C. Dunkerly, M. Friedrichs, A. Guzman, G. Halverson, J. Hansen, J. Harding, Y. Kang, D. Ketchum, B. Minor, C. Morton, S. Ortega-Salazar, T. Ott, M. Ozdogan, P. M. ReVelle, M. Schull, C. Wang, Y. Yang, and R. G. Anderson, "OpenET: Filling a critical data gap in water management for the western united states," *J. Am. Water Resour. Assoc.*, Nov. 2021.

[28] U.S. Geological Survey, "National water information system." `http://waterdata.usgs.gov/nwis/`, 2016. Accessed: 2022-10-26.

[29] J. C. Steyaert, L. E. Condon, S. W D Turner, and N. Voisin, "ResOpsUS, a dataset of historical reservoir operations in the contiguous united states," *Sci Data*, vol. 9, p. 34, Feb. 2022.

[30] M. A. B. Siddik, K. E. Dickson, J. Rising, B. L. Ruddell, and L. T. Marston, "Interbasin water transfers in the united states and canada," *Sci Data*, vol. 10, p. 27, Jan. 2023.

[31] United States Geological Survey, "USGS streamgage NHDPlus version 1 basins 2011," Aug. 2011.

[32] V. B. Sauer and R. W. Meyer, "Determination of error in individual discharge measurements," 1992.

[33] R. W. Herschy, "The uncertainty in a current meter measurement," *Flow Meas. Instrum.*, vol. 13, pp. 281–284, Dec. 2002.

[34] A. Domeneghetti, A. Castellarin, and A. Brath, "Assessing rating-curve uncertainty and its effects on hydraulic model calibration," *Hydrol. Earth Syst. Sci. Discuss.*, vol. 8, pp. 10501–10533, Dec. 2011.

[35] J. R. Dymond and R. Christian, "Accuracy of discharge determined from a rating curve," *Hydrol. Sci. J.*, vol. 27, pp. 493–504, Dec. 1982.

[36] J. T. Abatzoglou, "Development of gridded surface meteorological data for ecological applications and modelling," *Int. J. Climatol.*, vol. 33, pp. 121–131, Jan. 2013.

[37] J. Volk, A. K. Christian Dunkerly, C. Pearson, J. Huntington, F. Melton, R. Allen, M. Anderson, and B. Minor, "Mapping and correcting biases in gridded reference evapotranspiration over irrigated agricultural lands across the contiguous united states," *Manuscript In Preparation.*

[38] D. Ketchum, K. Jencso, M. P. Maneta, F. Melton, M. O. Jones, and J. Huntington, "IrrMapper: A machine learning approach for high resolution mapping of irrigated agriculture across the western U.S," *Remote Sensing*, vol. 12, p. 2328, July 2020.

[39] C. Boryan, Z. Yang, R. Mueller, and M. Craig, "Monitoring US agriculture: the US department of agriculture, national agricultural statistics service, cropland data layer program," *Geocarto Int.*, vol. 26, pp. 341–358, Aug. 2011.

[40] C. H. Homer, J. A. Fry, C. A. Barnes, and Others, "The national land cover database," *US geological survey fact sheet*, vol. 3020, no. 4, pp. 1–4, 2012.

[41] D. P. Kingma and J. Ba, "Adam: A method for stochastic optimization," *arXiv preprint arXiv:1412.6980*, 2014.

[42] G. B. Senay, "Satellite psychrometric formulation of the operational simplified surface energy balance (SSEBop) model for quantifying and mapping evapotranspiration," *Appl. Eng. Agric.*, vol. 34, no. 3, pp. 555–566, 2018.

[43] G. B. Senay, M. Friedrichs, C. Morton, G. E. L. Parrish, M. Schauer, K. Khand, S. Kagone, O. Boiko, and J. Huntington, "Mapping actual evapotranspiration using landsat for the conterminous united states: Google earth engine implementation and assessment of the SSEBop model," *Remote Sens. Environ.*, vol. 275, p. 113011, June 2022.

[44] J. T. Abatzoglou, S. Z. Dobrowski, S. A. Parks, and K. C. Hegewisch, "TerraClimate, a high-resolution global dataset of monthly climate and climatic water balance from 1958–2015," *Scientific Data*, vol. 5, pp. 1–12, Jan. 2018.

[45] N. M. Velpuri and G. B. Senay, "Partitioning evapotranspiration into green and blue water sources in the conterminous united states," *Sci. Rep.*, vol. 7, p. 6191, July 2017.

[46] IDWR GIS Section, Idaho Department of Water Resources, "1986 irrigated lands for the eastern snake plain aquifer," Feb. 2019.

[47] IDWR GIS Section, Idaho Department of Water Resources, "2015 irrigated lands for the eastern snake plain aquifer," June 2020.

[48] Montana Department of Revenue, "Revenue final land unit (FLU) classification, 2019," May 2019.

[49] Reed S. Lewis Paul K. Link Loudon R. Stanford Sean P. Long, "Geologic map of idaho," 2012.

[50] Montana Bureau of Mines and Geology, "Geologic map of montana," 1996.

[51] National Operational Hydrologic Remote Sensing Center, National Weather Service, "Rivers and streams of the U.S," Sept. 1999.

[52] A. Patil, D. Huard, and C. J. Fonnesbeck, "PyMC: Bayesian stochastic modelling in python," *J. Stat. Softw.*, vol. 35, pp. 1–81, July 2010.

[53] R. Kumar, C. Carroll, A. Hartikainen, and O. Martin, "ArviZ a unified library for exploratory analysis of bayesian models in python," *J. Open Source Softw.*, vol. 4, p. 1143, Jan. 2019.

[54] A. Gelman and D. B. Rubin, "Inference from iterative simulation using multiple sequences," *Stat. Sci.*, vol. 7, no. 4, pp. 457–472, 1992.

[55] C. M. Burt, A. J. Clemmens, T. S. Strelkoff, K. H. Solomon, R. D. Bliesner, L. A. Hardy, T. A. Howell, and D. E. Eisenhauer, "Irrigation performance measures: Efficiency and uniformity," *J. Irrig. Drain. Eng.*, vol. 123, no. 6, p. 423, 1997.

[56] R. G. Niswonger, E. D. Morway, E. Triana, and J. L. Huntington, "Managed aquifer recharge through off-season irrigation in agricultural regions," *Water Resour. Res.*, vol. 53, pp. 6970–6992, Aug. 2017.

[57] D. L. Ficklin, I. T. Stewart, and E. P. Maurer, "Climate change impacts on streamflow and subbasin-scale hydrology in the upper colorado river basin," *PLoS One*, vol. 8, p. e71297, Aug. 2013.

[58] M. Haines, P. Fishback, and P. Rhode, "United states agricultural data, 1840-2012 (ICPSR 35206)," 2019.

[59] G. F. Martinez Baquero, D. L. Jordan, A. T. Whittaker, and R. G. Allen, "Remote-Sensing-Based evaluation of relative consumptive use between flood- and Drip-Irrigated fields," vol. 2013, pp. H41A–1199, ui.adsabs.harvard.edu, Dec. 2013.

[60] G. C. Poole, J. Risley, and M. Hicks, "Issue paper 3 spatial and temporal patterns of stream temperature (revised)," *Environ. Prot.*, 2001.

[61] J. P. Donnelly, S. L. King, N. L. Silverman, D. P. Collins, E. M. Carrera-Gonzalez, A. Lafón-Terrazas, and J. N. Moore, "Climate and human water use diminish wetland

networks supporting continental waterbird migration," *Glob. Chang. Biol.*, vol. 26, pp. 2042–2059, Jan. 2020.

[62] D. J. Ackerman, G. W. Rattray, J. P. Rousseau, L. C. Davis, and B. R. Orr, "A conceptual model of ground-water flow in the eastern snake river plain aquifer at the idaho national laboratory and vicinity with implications for contaminant transport." `https://pubs.usgs.gov/sir/2006/5122/`, 2006. Accessed: 2022-11-19.

[63] D. J. Ackerman, *Analysis of Steady-state Flow and Advective Transport in the Eastern Snake River Plain Aquifer System, Idaho.* U.S. Department of the Interior, U.S. Geological Survey, 1995.

[64] I. W. R. Board, "Eastern snake plain aquifer comprehensive aquifer management plan," *Idaho Water Resource Board: Boise, ID, USA*, 2009.

[65] A. P. Williams, E. R. Cook, J. E. Smerdon, B. I. Cook, J. T. Abatzoglou, K. Bolles, S. H. Baek, A. M. Badger, and B. Livneh, "Large contribution from anthropogenic warming to an emerging north american megadrought," *Science*, vol. 368, pp. 314–318, Apr. 2020.

[66] S. Stevenson, S. Coats, D. Touma, J. Cole, F. Lehner, J. Fasullo, and B. Otto-Bliesner, "Twenty-first century hydroclimate: A continually changing baseline, with more frequent extremes," *Proc. Natl. Acad. Sci. U. S. A.*, vol. 119, p. e2108124119, Mar. 2022.

Parameter	**Basin**	**Error Calculation**	**Fractional Error**
Streamflow	All	RMSE	0.08
Irrigated Area	Columbia	1 - F1 SCORE	0.1168
	Upper Missouri	1 - F1 SCORE	0.1015
	Colorado	1 - F1 SCORE	0.1596
Evapotranspiration	Columbia	RMSE	0.210
	Upper Missouri	RMSE	0.130
	Colorado	RMSE	0.140
Effective Precipitation	All	RMSE	0.246
Precipitation	Columbia	RMSE	0.11
	Upper Missouri	RMSE	0.125
	Colorado	RMSE	0.146
Reference Evapotranspiration	All	RMSE	0.153
Time	All	None	0.0

Table 3.1: Error calculations for various parameters and basins

Relationship	Initial Tests	Significant ($p < 0.05$) OLS	Bayes (Sig. Negative Slope)	Bayes (Sig. Positive Slope)
Climate - Flow	160,560	2,676		
Time - IWU	1,494		24	181
Time - IWU (Perennially Irrigated)	1,535		17	67
Time - IWU (Climate-Normalized)	1,494		8	269
Time - Irrigated Area	221		6	176
Time - Flow	2,524		643	853
Time - Flow (Climate-Normalized)	2,524		35	192
IWU - Flow	42,240	1,878	341	424
Climate-Period CWB	1,587		30	276
Monthly CWB	2,382		146	365

Table 3.2: Regression Tests

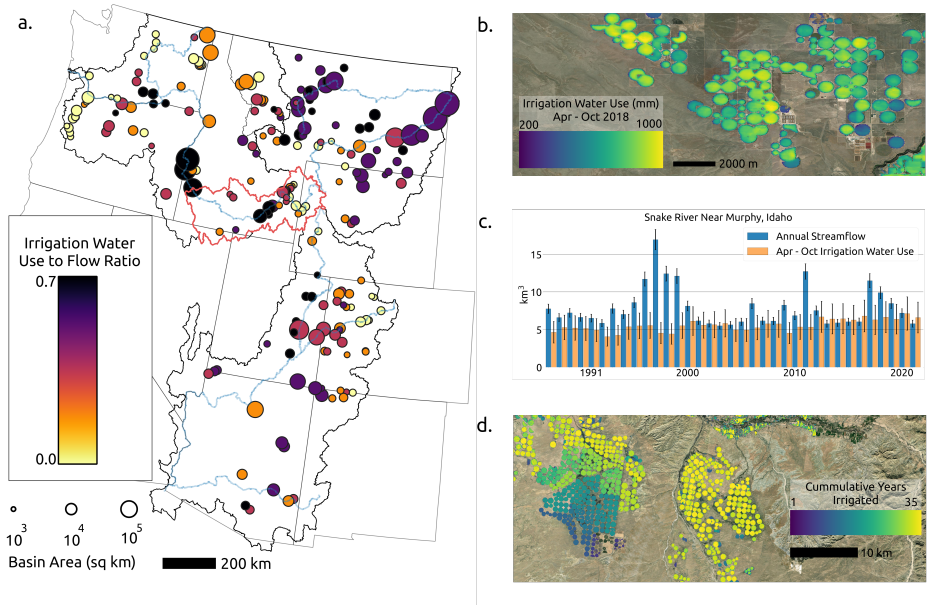

Figure 3.1: The 1987-2021 mean annual flow-to-irrigation water use ratio (dimensionless) at 221 gages draining irrigated basins is shown (a), with the region of the Snake River Basin drained at Murphy, Idaho highlighted in red (USGS Gage 13172500). Symbols are scaled to drainage area. Detail view of 30 m resolution Landsat satellite-based crop consumption estimates in the Snake River Plain of Southwestern Idaho is shown in (b). Annual volumetric discharge at Murphy, Idaho (c), with irrigation water use during the period April 1st to October 31st within the basin. An example of rapid expansion of irrigated area over the study period in northwest New Mexico is shown in (d).

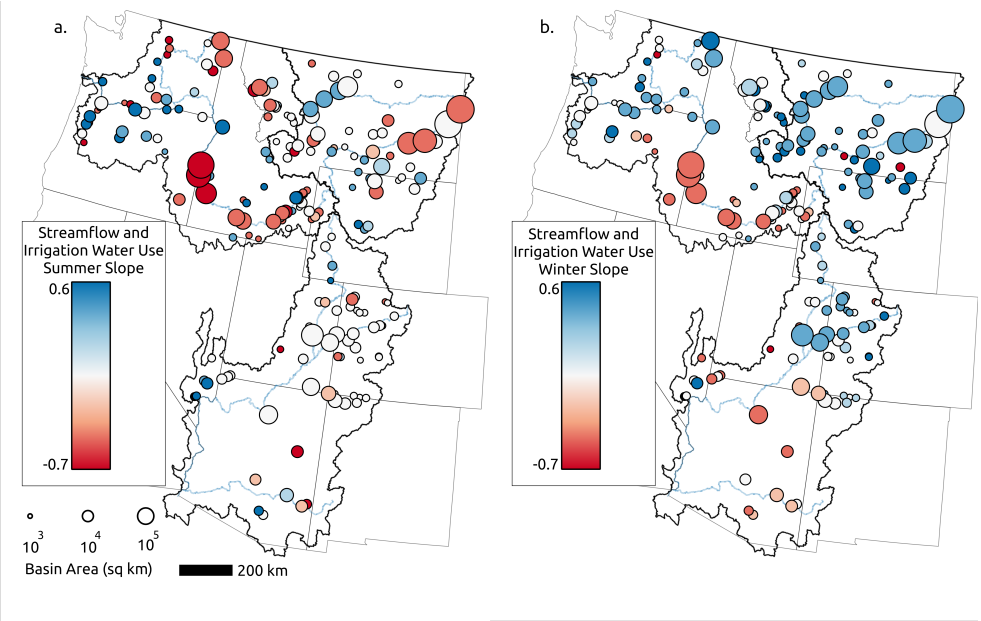

Figure 3.2: The summer (May through October; a.) and winter (November through March; b.) climate-normalized flow-irrigation water use relationship, where flow is a function of irrigation water use in preceding growing season months, and is displayed as the median of monthly significant relationships. significance is based on gage- and month-specific Bayesian linear univariate (a) and bivariate (b) models, where significance based on the highest credible interval of the posterior distribution of slopes; the relationship is significant where 95% of posterior slopes are of a single sign (i.e., positive or negative). Irrigation water use, climatic water balance, and flow were scaled from 0 to 1 prior to analysis (slopes are dimensionless). Symbols are scaled to drainage area.

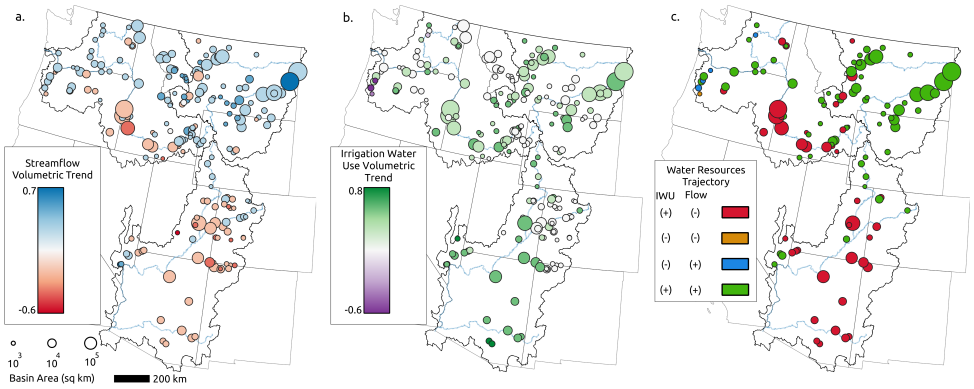

Figure 3.3: Trends in (a.) streamflow and (b.) irrigation water use (IWU) 1987 - 2021 at 221 gages draining irrigated basins. Trend significance is based on 95% of the highest credible interval of the posterior distribution of slopes in a. and b.; the relationship is significant where 95% of posterior slopes are of a single sign. Water resources trajectory in (c.) shows in which basins significant relationships in flow and irrigation water use were found, and classifies them according to the slope of each trend, indicating basin water use sustainability. Flow and irrigation water use were scaled from 0 to 1 prior to analysis (slopes are dimensionless). Symbols are scaled to drainage area.

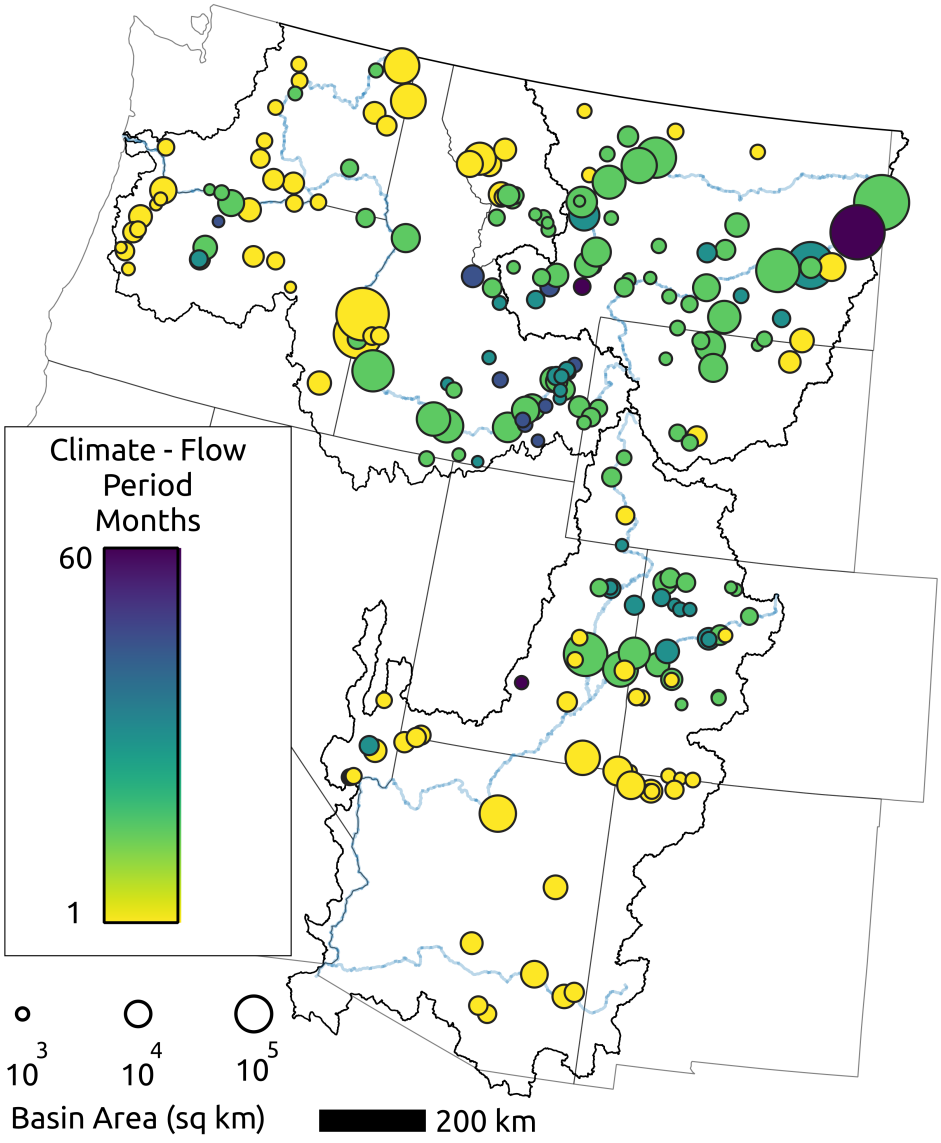

Figure 3.4: The mean monthly climate-flow response time, where each basin's monthly characteristic climate response time was the maximum correlation (Pearson's R-squared) between monthly flow and a 1- to 60-month window of mean climatic water balance (reference evapotranspiration minus precipitation). The climate period with highest correlation to a given month's flow was considered characteristic of the basin during that month. Symbols are scaled to drainage area.

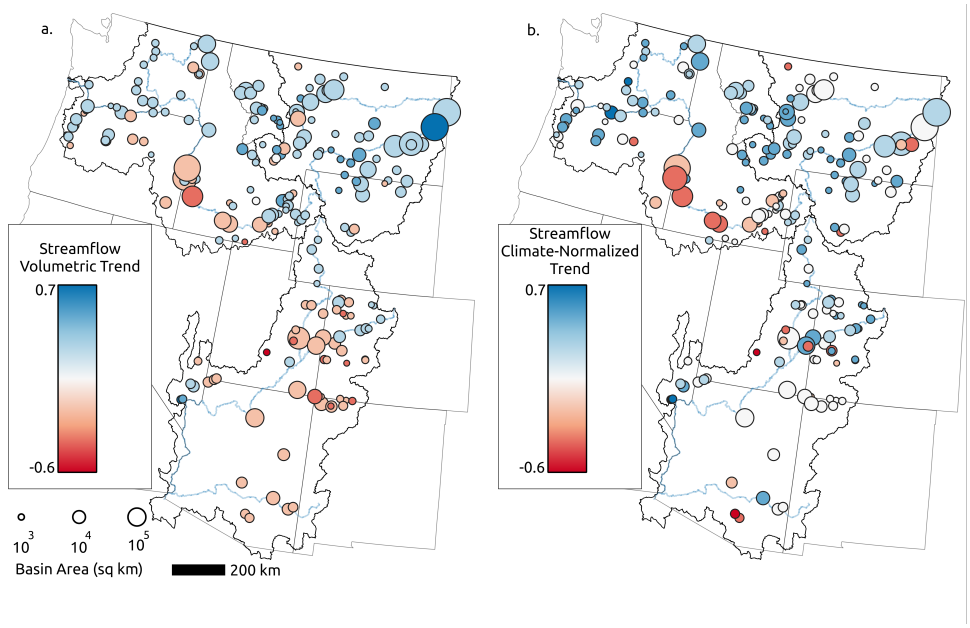

Figure 3.5: Trends in (a) volumetric and (b) climate-normalized streamflow from 1987 - 2021 at 221 stream gages draining irrigated basins. The trend is the median of any significant trends during each of 12 months, from records ranging from 20 to 35 years in length. Trend significance is calculated using gage- and month-specific Bayesian linear univariate (a) and bivariate (b) models, where significance is based on the highest credible interval of the posterior distribution of slopes; the relationship is significant where 95% of posterior slopes are of a single sign (i.e., positive or negative). Streamflow was scaled from 0 to 1 prior to analysis (slopes are dimensionless). Symbols are scaled to drainage area.

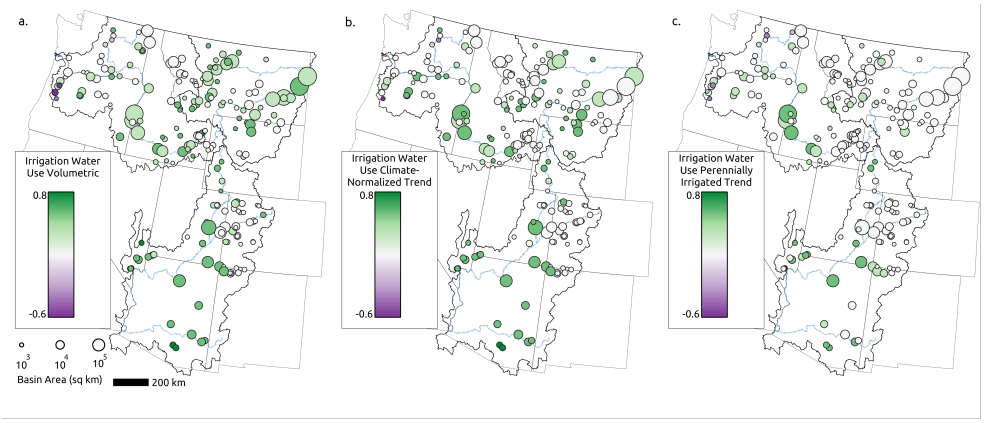

Figure 3.6: Irrigation water use trends, displayed as the median of significant trends for the months April through October. Trends are for a., volumetric irrigation water use within the annual irrigation extent; b., climate-normalized irrigation water use, in which the IWU concurrent month climatic water balance is included as a predictor; and c., volumetric irrigation water use in the perennially irrigated domain (i.e., irrigated every year, 1987-2021). Significance is based on 95% of the highest credible interval of the posterior distribution of slopes; the relationship is significant where 95% of posterior slopes are of a single sign. Irrigation water use was scaled from 0 to 1 prior to analysis (slopes are dimensionless). Symbols are scaled to drainage area.

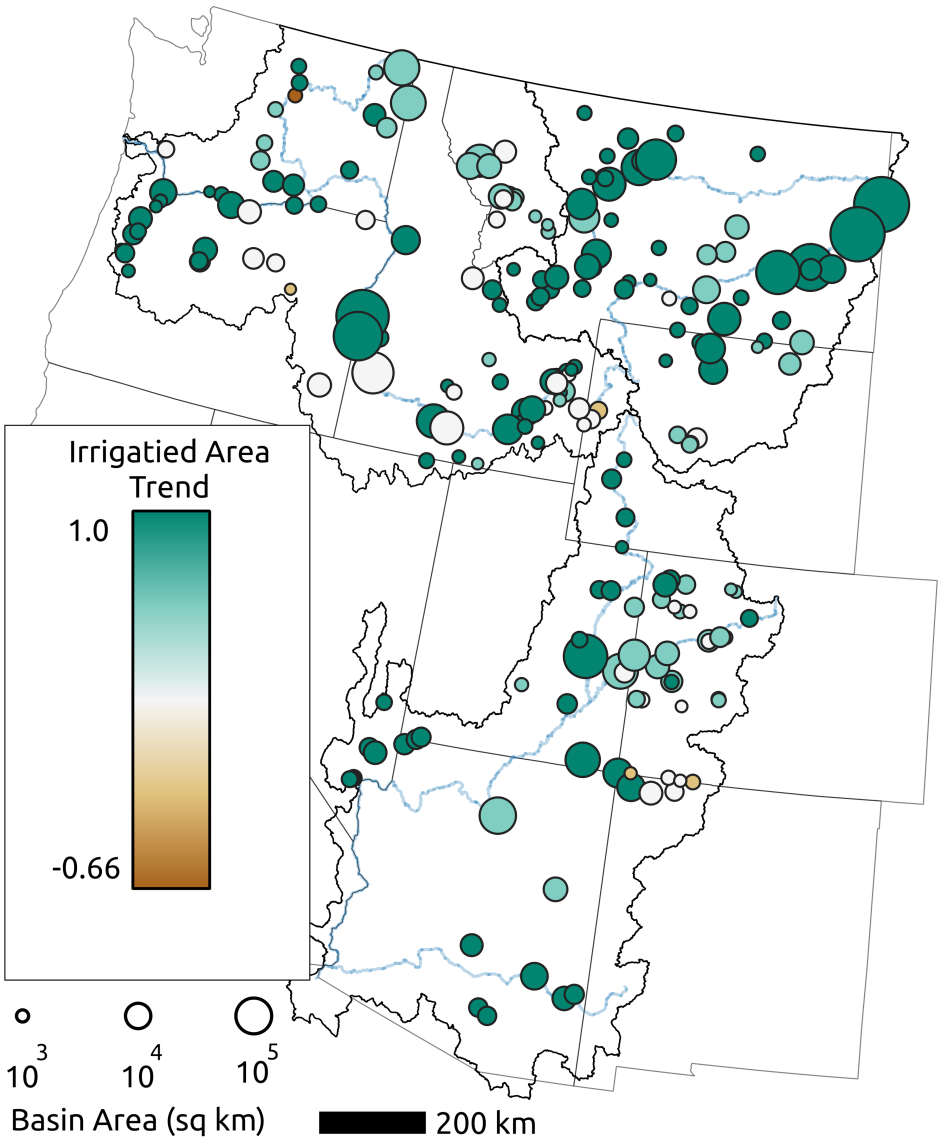

Figure 3.7: Irrigated area annual trends, 1987-2021. Significance is based on 95% of the highest credible interval of the posterior distribution of slopes; the relationship is significant where 95% of posterior slopes are of a single sign. Irrigated area was scaled from 0 to 1 prior to analysis (slopes are dimensionless). Symbols are scaled to drainage area.

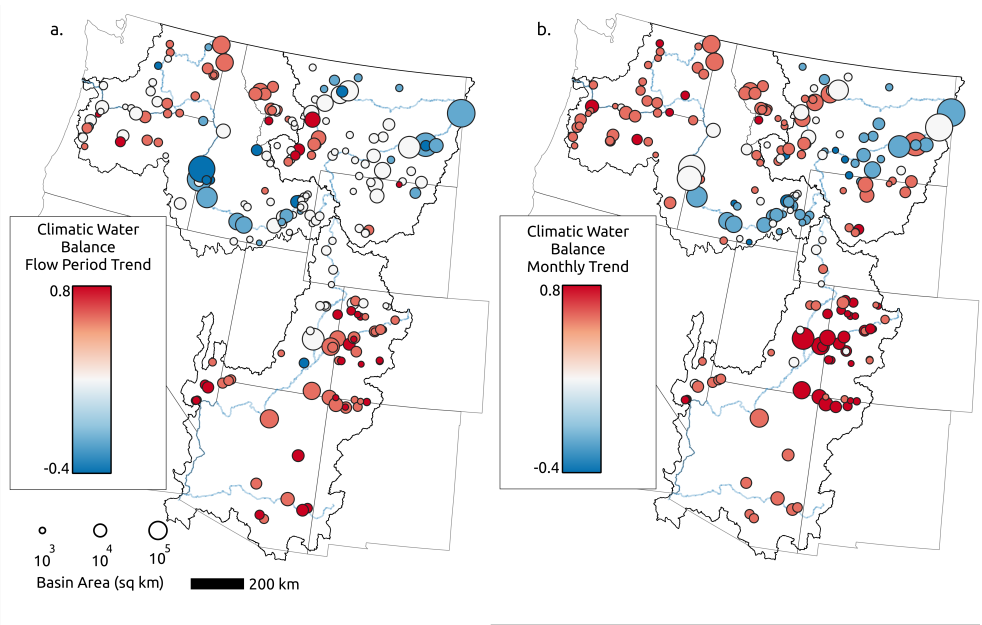

Figure 3.8: Climate trends in the irrigated basins drained by 221 USGS gages used in the study, where climatic water balance (CWB; reference evapotranspiration minus precipitation) is used as a proxy for climate. In a., trends are calculated over the basin-specific climatic aggregation period (i.e., climate period to which monthly flow is most responsive, ranging from 1 - 60 months), and displayed as the median of monthly significant trends. In b., trends are calculated by basin, for each month of the year, and displayed as the median of monthly significant trends. Climatic water balance was scaled from 0 to 1 prior to analysis (slopes are dimensionless). Symbols are scaled to drainage area.

Chapter 4

IRRIGATION RESPONSE TO DROUGHT IN THE WESTERN US, 1987 - 2021

4.1 Abstract

The Western United States heavily relies on surface water sources for both ecological services and for irrigation. However, the interannual variation in irrigation water use during drought and its ecological consequences are not well documented. Irrigation decision-making is complex and influenced by numerous human and environmental factors such as water deliveries, crop yields, input and crop prices, and climate variability. While few irrigation districts have plans in place to curtail water deliveries during drought, water rights, fallowing patterns, crop rotations, and profit expectations also influence irrigation management at the farm scale. This study uses high-resolution satellite-derived data to examine the response of irrigators to drought by developing a novel measure of irrigation management anomaly, the Standardized Irrigation Management Index (SIMI). We assess the state of drought at the field and basin scale in terms of precipitation and atmospheric demand and analyze the relative importance of variations in crop price and drought status on crop planting decision-making and associated irrigation water use. The study provides insights into irrigation management during drought, which is crucial for sustainable water supply in the face of the ongoing water supply crisis in the US Southwest.

4.2 Introduction

Water for irrigation is an indispensable natural resource in the Western US, where over 75% of irrigation comes from surface water sources. Despite contributing two-thirds of commodities revenue while only occupying one-quarter of the cultivated land in the west, the interannual variation in irrigation water use is not well documented. During drought, critical periods of surface water scarcity have led to negative ecological consequences, including

high temperatures, fish die-off, riparian system impacts, and shortages for human users [1, 2]. While the purpose of irrigation is to enable crop production in areas with insufficient precipitation, studies have indicated that the buffering function of irrigation may lead to human-ecological trade-offs during water-scarce times. While impacts on natural flows during drought have been studied, the degree to which irrigators respond to water scarcity has not been systematically addressed.

A key challenge to understanding irrigation decision making is accounting for the plethora of human and environmental factors that influence on-farm response. Factors that producers take into account include the consideration of water deliveries by government controlled and on farm infrastructure, potential crop yields, the price of inputs and crop products, and climate variability [3, 4, 5]. Most irrigated lands in the US that use off-farm water are served by large irrigation districts, and while drought may fundamentally alter the economic prospects of irrigation and cropping decisions, few irrigation districts in the US have plans in place to effect an organized response, such as curtailing water deliveries [6]. Water rights, fallowing patterns, crop rotation cycles, and long-term trends in crop profit expectations may further influence differences in irrigation management at farm scale during drought [7].

Irrigation management decisions have important implications for the sustainability of surface and groundwater supply; in the most heavily irrigated regions of the Snake and Colorado rivers, for example, irrigation water use represents greater than 50% of the total outflows of each system [8, 9]. Further, many natural and managed systems in the region have experienced (and are projected to further experience) declines in flow [10, 11]. Recent work demonstrated that changes in irrigation water use can have a subannual, bidirectional impact on streamflow and that increases in irrigation water use are exacerbating climate-driven streamflow changes, especially in the Colorado River basin [8]. The ongoing water supply crisis in the US Southwest has led to calls for alternative, adaptive management [12, 13, 14] and a recognition that simply improving on-farm water efficiency through infrastructure modernization might have the unintended consequence of increasing basin-scale

water use (i.e., the 'paradox of irrigation efficiency'; [15, 16]). While humans have control over water use in the river systems in the region, and could thus expect management actions to impact future water supply, creative and cooperative management is impossible without first characterizing the behavior of irrigation, the largest consumptive use by society.

Recent developments in satellite remote sensing have enabled systematic estimates of the occurrence and water use of irrigated crops over sub-continental to continental scales at high resolution [17, 18, 19]. Annual land cover maps reliably map the distribution of irrigated lands and crop type, and long period, gridded meteorological datasets provide tools to analyze water use, while detailed geospatial datasets provide for field-scale analysis of on-farm decision making at large scale [20]. In this study, we determine where and when irrigators respond to water shortage. We use a high-resolution satellite-derived dataset to systematically examine the response of irrigators to drought using a novel measure of irrigation management anomaly, the Standardized Irrigation Management Index (SIMI). We analyze drought response by relating SIMI to two common drought metrics at the field-scale to assess the state of drought at the field and basin scale in terms of precipitation and atmospheric demand (i.e., reference evapotranspiration, ETr). We examine whether climate and drought play a role in crop planting decision making, analyzing the relative importance of variations in crop price and drought status.

4.3 Materials and Methods

4.3.1 Study Area

Our study area focuses on the Colorado, Klamath, and the U.S. portions of the Upper Missouri (in Montana and Wyoming) and Columbia river basins (Figure 4.3). The study area encompasses a large portion of the intermountain and Pacific Northwest physiographic regions. The area experiences a wide range of climate, with precipitation amounts ranging from less than 150 mm yr^{-1} in southeast Utah to over 2000 mm yr^{-1} on the coast of Oregon. Irrigated regions in the study area tend to occupy low-lying valleys where precipitation is

insufficient for consistent agricultural production and depend on the transport of surface water by rivers and canals from mountainous areas. Groundwater represents less than 25% of total irrigation water withdrawals in the region [21].

4.3.2 Input Spatial Data

We developed data for our analysis at the hydrologic unit and agricultural field scales. At the basin scale we extracted 337 Watershed Boundary Unit level 8 polygons for processing aggregated data in an initial time scale analysis with complete spatial coverage of the study area (hereafter 'hydrologic units'; [22]). We used the OpenET fields database to represent field-scale agriculture in the region, to estimate the spatial coverage of irrigated regions, and to analyze field-scale response of irrigators to meteorological drought conditions [19]. The OpenET fields database consists of 12.3 million fields in the contiguous United States and we used this database to calculate the centroid of 1.9 million fields within the Columbia, Klamath, Upper Missouri, and Colorado River basins. The field centroids were used to find a sample frequency of irrigation; we extracted 492k fields which were irrigated at least ten years from 1987-2021 for further analysis.

We aggregated precipitation, ETr, and irrigation water use volumes (IWU, the component of irrigated crop evapotranspiration (ET) derived from applied irrigation water; [8]). Penman-Monteith ETr and precipitation data was extracted from gridMET, a 4 km^2 resolution, daily meteorological product [23]. Monthly, 30 m resolution SSEBop ET was extracted from within the annual irrigated extent estimated by IrrMapper, an annual Landsat-based irrigation mask [24, 18].

4.3.3 Irrigation Response Timescales

We estimated irrigation sensitivity to drought by calculating the relationship of drought severity and irrigation water use over the study area at all pixel locations where irrigation had been detected for at least 5 years of the 35-year study period. For our purposes, sensitivity is the degree to which the variance in irrigation intensity is explained by climate

using the squared Pearson correlation coefficient. We analyzed the response to drought by irrigators at the field scale in terms of meteorological drought with the Standardized Precipitation Index (SPI) and Standardized Precipitation and Evaporation Index (SPEI), both commonly applied multiscalar estimates of the deviation of meteorology from long-term normals [25, 26]. We assessed irrigator response to drought by creating the Standardized Irrigation Management Index. SIMI is an estimate of the anomaly of the crop coefficient (Kc; Allen, 2006), or the relative ET rate of a crop compared to the rate of ETr (the reference, 0.5 m healthy alfalfa crop). The purpose of using this indirect measure of water use (rather than ET) is to make an estimate of irrigation management that is less dependent on meteorological conditions than ET. Estimating SIMI from SSEBop ET data depends on Kc_m, and requires the removal of the monthly OpenET bias-corrected ETr signal (ETr_m) from the remotely sensed estimate of ET (ETr_m):

$$Kc_m = \frac{E_{Tm}}{E_{Tr_m}} \tag{4.1}$$

For all three index calculations (SPEI, SPI, SIMI), we fit the probability distribution of the time series using the two-parameter gamma distribution, then transformed to a standardized normal distribution using the Climate-Indices Python package [27]. We used the drought metrics (SPEI and SPI), which range from -3 to 3, to classify the climate state into wet, normal and dry years. We classified wet periods when SPEI or SPI over the specified time scale was greater than 0.0, normal when the index was between -1.3 and 0.0, and dry (drought) when the index was less than -1.3.

4.3.4 Timescale of Meteorological and Hydrological Controls on Irrigation

In order to estimate the responsiveness of irrigation, we first identify the time scale on which irrigation varies. We expect that in a typical spring (or fall), when surface and soil water are plentiful (or limited), irrigated lands would have a relatively uniform Kc signal, and thus a SIMI that varies little in relation to meteorology, as expressed by SPEI and

SPI. Therefore we analyze the variance of SIMI in relation to meteorology during single- and multi-month periods covering all windows of time during the April-October growing season and find when SIMI responds most to SPEI and SPI. We used Pearson's squared correlation to estimate this relationship at the hydrologic unit and field level, comparing irrigated area-weighted, mean hydrologic unit scale SIMI and field-scale SIMI at all growing season time periods. The growing season analyzed was from April through October, while the meteorological drought metrics were calculated at 1 through 12, 18, 24, 30, and 36-month time periods, ending at the end of each growing season month.

4.3.5 Controls on Irrigation Response to Drought: Federal Projects, Crop and Irrigation Type

We created a database of irrigated regions served by United States Bureau of Reclamation (Reclamation) infrastructure projects in the Klamath, Columbia, and Upper Missouri basins. We attributed our fields database to a status of Reclamation (115k fields) and non-federal-serviced irrigation infrastructure (331k fields; [28, 29, 30]). An irrigation type database was developed from fields drawn from state agency and federal sources over the areas intersecting the stud area in Colorado, Montana, Utah, and Washington [31, 32, 33, 34]. We aggregated and re-classified irrigation types found in state and federal sources to four general classes (drip, flood, pivot, and sprinkler irrigation). The Cropland Data Layer (CDL) was used to extract annual crop types at each field from 2008 - 2021 and summarize them by the majority count at each field. The crops were mapped to generalized crop type (forage, vegetable, grain, and orchard) for comparative analysis during drought states, and mapped to a more specific crop nomenclature. We used each of the federal project status, irrigation type, and crop categories to divide the population of fields into classes used to characterize potential drivers of differences in drought response. The CDL was also used to track the transitions of crops through the period of record at the field scale and calculate crop transition matrices over the period of study and during the three drought state classifications (i.e., wet, normal, and dry). We estimated the CDL classification accuracy

using an F1 score derived from area weighted, state-based, CDL validation reporting from 2015-2021 (n = 19.7M).

4.3.6 Impact of Price and Climate on Crop Planting Decisions

We extracted annual nominal price data for each major crop category using data from the United States Department of Agriculture's National Agricultural Statistics Service (NASS; [35]) and the Producer Price Index (PPI) developed and maintained by the Federal Reserve Bank of St. Louis (FRE; [36]). The most specific nominal and price index data with complete temporal coverage from 2008 - 2021 was used for each crop; less prevalent crops that fell into generalized NASS price categories or did not have an established price index were priced in our model using the grouped NASS price and the FRED's Farm Products PPI, respectively. Where available, the NASS crop price was found at state scales and the average for the states in our study area was used. PPI data is national. Price data was adjusted to January 2021 prices (i.e., 2021 = \$100):

$$P_{adj,t} = P_{nominal,t} \times \frac{PPI_t}{PPI_{2021}} \tag{4.2}$$

Where $P_{adj,t}$is the adjusted price at time t, $P_{nominal,t}$ is the nominal NASS price at time t, PPI_t is the price index of the crop time t, and PPI_{2021} is the price index of the crop in the base year (2021). Price data were then normalized using the same procedure as that for normalizing drought data. To estimate the time scale at which price best predicts cropping patterns, field data was aggregated to an annual time series of planted area for each crop and tested against each month in the 24 months leading to May of the year of interest. The lag in price that best explained the total cropping area for each crop (i.e., highest Pearson's r) was used for subsequent modeling of crop transitions. To account for the high spatiotemporal heterogeneity in drought status, we tested the correlation of SPEI with crop area time series at the hydrologic unit scale and at time scales ranging from one to 36 months, ending at the end of each of 12 month period (January through May

of the year of interest, and June through December of the previous year). We modeled price and climate dependence of crop transitions among the 13 most common crops in our domain by area and removed long-term orchard and vineyard crops (including hops) under the assumption that planting decisions for these crop types are independent of short-term climate and price conditions.

We used a Bayesian multinomial softmax regression approach to model the transition of crops and estimate the relative importance of crop price and climate on cropping decisions:

$$\boldsymbol{y_i} \sim Categorical(\boldsymbol{\theta}) \tag{4.3}$$

$$\boldsymbol{\theta} = \frac{e^{\boldsymbol{\alpha}+x_i\boldsymbol{\beta})}}{\sum_{j=1}^{K}(\boldsymbol{\alpha}+x_j\boldsymbol{\beta})} \tag{4.4}$$

$$\boldsymbol{\alpha} \sim \mathcal{N}(0, 20) \tag{4.5}$$

$$\boldsymbol{\beta} \sim \mathcal{N}(0, 20) \tag{4.6}$$

Where $\boldsymbol{y_{i,k}}$ is the vector of indicator variables that take the value of 1 if the $\boldsymbol{i}$-th observation belongs to crop $\boldsymbol{k}$, $\boldsymbol{x_{i,k}}$ is the vector of the field's previous crop's price, the price of the planted crop, and the drought index value, calculated at their respective time scales, $\boldsymbol{\alpha}$ and $\boldsymbol{\beta}$ are the vector of intercepts and coefficients for category $\boldsymbol{k}$, and K is the number of crops to which the modeled crop might transition.

We used the PyMC Python package to estimate the coefficients of each model using Markov Chain Monte Carlo sampling. We generated a sequence of samples from the posterior distribution by iteratively proposing new coefficient values, and accepting or rejecting them based on their posterior probabilities. Each sampler was tuned with 1000 steps and retained the final 1000 steps, from which we extracted the posterior distribution of coefficient values. We ran 4 sampling chains in parallel for each model, and used saved sampling

trace data to calculate the Gelman-Rubin statistic ($\hat{r}$), and determined convergence in cases where $\hat{r} > 1.1$ [37].

We used our standardized model coefficients to interpret the sensitivity of cropping patterns to price and climate variables. To ensure coefficient interaction or collinearity was not obfuscating the relative importance of our fitted coefficients, we calculated the change in deviance of each model when used to predict transitions using a single coefficient (i.e., from price, to price, or climate). This deviance was normalized using the complete and the null model, where deviance was based on the mean outcome in the observed data:

$$D_{model} = \frac{D_{coeff} - D_{full}}{D_{null}} \tag{4.7}$$

Where D_{model} is the normalized model deviance for a single-coefficient model, D_{coeff} is the deviance of the single-coefficient model, D_{full} is the model deviance for the model fit with all three variables, and D_{null} is the deviance calculated on the mean of the transitions.

4.4 Results

4.4.1 Basin Scale Sensitivity

Overall, climate variables explained a relatively small amount of variance in irrigation management (SIMI). We hereafter use SPEI as our main climatological variable because it explained slightly more variance in irrigation intensity across our study region (Figure 4.1). SPI and SPEI both showed increasing explanatory power through the early growing season, reaching a maximum in August, when they reached their peak correlation with SIMI (SPI $r^2 = 0.31$ and SPEI $r^2 = 0.36$, respectively) at a three month irrigation and four month meteorological timescale. That is, SIMI variance is best explained over the study area as a whole by both drought metrics when the SIMI is calculated from June through August, and SPEI or SPI calculated from May through August, hereafter referred to as the 'study-wide optimal time scale'. Response changes quickly over the growing season lookback period, falling steeply as SIMI departs from the optimal time scale into periods that include

the beginning and end of the growing season. In contrast, strong meteorological correlation extends into longer time scales while losing little explanatory power. For example, the SPEI - SIMI correlation falls only slightly as SPEI period lengthens from a four to an 11-month time scale (from r^2 of 0.36 to 0.30).

4.4.2 Field Scale Sensitivity

Field scale analysis of the response of irrigation to SPEI revealed that most fields respond to short-term SPEI over short-term SIMI time scales during the late summer and early fall, and like the basin-averaged response, respond most strongly in August (Figure 4.2). There are multiple modes of SPEI response beyond nine months, found at 12 and 36 months. The distribution of field response time scales is geographically coherent in terms of the study-wide response at the optimal time scale; at large scales, clusters of relatively less sensitive fields are noted around major waterways and in large irrigation districts equipped with large-scale reservoir and canal infrastructure (Figure 4.3a). In the Missouri River basin and on the western side of the Upper Colorado River basins, the response is generally stronger than in the Columbia River basin, especially along the Snake river and in central Washington. At local spatial scales, the distribution of irrigation response is highly varied, with individual fields of widely differing response time scales and sensitivities interspersed (Figure 4.3b - e).

4.4.3 Controls on Irrigation Response to Drought

We found that irrigation management during drought differs significantly, albeit modestly, among crop, irrigation type, and irrigation infrastructure management classes. Response during drought of three of the four irrigation types studied was significant ($p < 0.05$; Figure 4.4). The largest change was in flood irrigated fields, where the mean flood-irrigated SIMI over the study-wide optimal time scale falls from -0.21 to -0.55 during drought, compared to normal years (n=417,102 field-seasons). Pivot- and sprinkler-irrigated fields also experience significant but small reductions in SIMI of 0.07 and 0.09, respectively (n =

190,295 and 389,074 field-seasons). Changes in SIMI under drip irrigation systems between normal and dry years were insignificant (n = 46,592). All systems had relatively large increases in mean SIMI during wet years of 0.48, 0.20, 0.25, and 0.17 for flood, pivot, sprinkler, and drip systems when compared to normal years, respectively.

Federally-developed and operated irrigation infrastructure showed significant differences in SIMI response in all three climate states when compared to non-federal irrigation (Figure 4.5). Federal projects had a SIMI of 0.27 higher than non-federal irrigation during drought, a slightly higher (0.01) SIMI during normal years, and a SIMI 0.05 lower during wet years (federal n = 6,412,105; non-federal n = 9,203,950 field-seasons).

All four generalized crop classes had significant changes in mean SIMI during drought (Figure 4.6). Vegetable, forage, and grain crops all decreased SIMI, by -0.15, -0.39, and -0.34, respectively (n = 551,909, 2,793,224, and 1,448,268 field-seasons). Orchard crops (including vineyards) increased SIMI during drought by 0.2. All crop classes experienced significant increases in SIMI during wet years of 0.16, 0.44, 0.40, and 0.12 in vegetable, forage, grain, and orchard crops, respectively.

4.4.4 Crop Planting Decisions

Transition matrices illuminate the cropping patterns in our study area, the most salient of which is the autocorrelation of cropping; most crops are more likely to be replanted (or continue to grow, if perennial) than to transition to other crops (Figure 4.7). The opposite is true for crops involved in typical rotation patterns. For example, potatoes were highly unlikely to grow two years in a row in the same field, and are commonly planted in rotation with barley, wheat, and sugarbeets. The most common crop was alfalfa, which was grown over 1.8 M field-seasons from 2008 - 2021 in the study area. Crop transition probabilities undergo a subtle shift during drought. When comparing the difference between wet and dry growing seasons, the probability of overall crop shifts toward wheat increases. While the change in transition probabilities suggests a possible shift in SIMI and therefore water use, the shift is well within the bounds of uncertainty in the CDL and IWU data and thus

is not considered significant (Figure 4.8). We summarize crop-specific IWU, response, and harvest area in Table 4.1.

Our softmax regression transition models were generally fit with standardized coefficients of greater magnitude for prices than for climate. Deviance loss was least for most crops when the 'from price' coefficients were used (n=6), followed by 'to price' (n=4), and 'climate' (n=3). That is, the 'from price' coefficients were the most explanatory of the data in most models and climate was the least. This pattern is observed across the individual 'sub-model' components, where the model is fit with a set of coefficients for each possible transition (Figure 4.9). For example, in both spring wheat and alfalfa, model coefficient magnitudes are largest for the price terms, while climate coefficient magnitudes are relatively small. As expected, for most models and transition crops the 'from price' coefficient is negative and the 'to price' coefficient is positive. Coefficient magnitudes overall show a slightly different pattern as that found in the deviance analysis: the 'to price' is the largest magnitude coefficient in 45% of the cases, 'from price' is the largest in 38%, and 'climate' is the largest in only 17% of the standardized sets of coefficients (n=169).

4.5 Discussion

Overall, our results indicate that irrigation is driven by economic factors to a greater extent than interannual climate variability. This was especially the case in capital intensive regions where the federal government has invested in large-scale irrigation infrastructure, and producers have invested in long term crops such as orchards. Marginal irrigation, such as flood irrigation for forage crops in areas where the availability of water depends on local-scale hydrology and access to regional water sources is limited, appears to be much more responsive to interannual climate variability, as expressed by SPEI. Irrigation is designed to buffer against seasonal and interannual water shortage, and our results indicate it doing so in the most intensely irrigated regions.

Large scale analysis of response of irrigation to climate (as expressed by SIMI, SPEI and SPI) shows that, at the basin scale, irrigation responds on short time scales (Figure

4.1). This implies that the response is only partly impacted by management; during hot, dry growing seasons, crops with sufficient irrigation are expected to have higher crop coefficients and thus higher SIMI, while longer-term response to SPEI would indicate that water availability plays a role in irrigation management itself. For example, if irrigation decision making was based on multi-year water availability, there would be higher correlation with SPEI at long time scales, indicating that management of irrigated fields was impacted through less intense irrigation, decreased density of crops, or irrigating through a shorter period. While there is a correlation between long-term SPEI, and thus water availability, it is much less than that of short time scales, indicating that the occurrence of this type of irrigation management in the context of long-term climate is not prevalent in the region.

At the field scale, our results show that irrigation management patterns differ among the major river basins (Figure 4.3). The Columbia and Klamath basins are less responsive at the study-wide time scale ($r^2 = 0.14$ and 0.11, respectively) than are the Colorado and Missouri basins ($r^2 = 0.24$ and 0.27, respectively). The major differences in response to drought in these systems are likely explained by differences in irrigation infrastructure, federal management, and crop type. The Columbia and Klamath systems are dominated by federally-managed projects; 47% and 52% of fields are within federal projects in the Columbia and Klamath basins, respectively. Further, in the Columbia River basin in Washington, 67% of the 7,500 km^2 irrigated area is under pressurized (i.e., pivot or drip) irrigation, and the Columbia Basin as a whole hosts over 98% of the study area's 3,200 km^2 of orchards. In contrast, much of the irrigation in Montana and Wyoming is flood; for example, 56% of the irrigation in the Missouri River basin of Montana is flood. The dominance of forage in the Missouri Basin (72% of irrigated agriculture), and the less extensive development of federal irrigation projects (only 25% of irrigated fields in the parts of Montana and Wyoming in the Missouri Basin are in federal projects, explains further the relative responsiveness of irrigation during drought observed there.

Crop transition models suggest prices are a more significant driver of the behavior of

the regional agricultural system than climate conditions and explain, in part, the lack of irrigation response to drought. The transition matrix for the study region (2008-2021) changes only slightly during drought (Figures 4.7, 4.8) suggesting that drought status does not greatly impact cropping decisions. Further, the results of our crop transition modeling suggest price is most often the dominant factor in crop planting decisions when compared with climate. Most crop-specific price coefficients reflect the expected behavior of moving away from crops with declining prices (negative 'from price' coefficients) and toward higher prices (positive 'to price' coefficients). Alfalfa and potatoes stand out as notable exceptions in other crop's transition models, which suggests the perennial cultivation of alfalfa (often 3-6 years) and the need to rotate potatoes to avoid pest infestations obfuscates the price dependence of the crop planting patterns or operates on a longer time scale than what we considered in this study.

Our results suggest considerable inertia in the irrigated system; the most common crops are among the most intensely irrigated and least responsive to climate conditions. Of the 22 crops analyzed, alfalfa is harvested over nearly three times the area of the next most common crop and has the fifth highest mean study-wide annual IWU (0.605 ± 0.20 m yr^{-1} on $15{,}000 \pm 1{,}900$ km^2). Corn is the third most common crop and is also the third most intensely irrigated crop (0.645 ± 0.21 m yr^{-1} on $2{,}500 \pm 310$ km^2). Apples are the second most consumptive crop in terms of IWU (0.657 ± 0.22 m yr^{-1}), and as an orchard crop, are unsurprisingly unresponsive to drought, and are the 7th most prevalent by area among the 22 crops studied ($1{,}700 \pm 220$ km^2).

The results of this study suggest that there is limited response to climate by irrigators in the most heavily irrigated regions and among the most intensely irrigated crops in our study area, an unsurprising result, as the intent of irrigation is to buffer production from climate fluctuations. In previous work showing the streamflow impacts of irrigation, widespread increases in IWU were attributed to irrigation infrastructure, climate change, and increase in irrigated area [8]. Our results here suggest that advanced irrigation infrastructure (i.e., drip

and pivot systems) is associated with relatively higher irrigation intensity during drought, and thus could be expected to exacerbate surface water supply issues during times of water scarcity. This further supports the notion that increases in on-farm irrigation efficiency through irrigation modernization do not equate to decreases in overall water use, especially during drought [15]. While we do not address trends in this study, the trends identified in [8], combined with lack of reduction in SIMI during drought, and concurrency of the two studies, imply that aridification (i.e., higher recent SPEI) has not generally been met with reductions in SIMI. Given the human-ecological use trade-off under which the irrigated system operates in water-scarce regions, these findings indicate the potential for further surface water impacts due to irrigation infrastructure change and increasing aridity in parts of the study region. While our modeling of the role of price and climate is very simple and excludes myriad on-farm management factors affecting cropping decisions (e.g., input and labor costs, crop-specific expertise), they do imply the subordinate role played by climate in planting decisions on irrigated lands and thus the low probability of water use reductions (under an unchanged management and policy environment) in the case of water scarcity in the future.

4.6 Conclusion

In this study, we examined the response of irrigation management using SIMI to find the characteristic response time scales of irrigation at the hydrologic unit scale to two drought metrics: SPI and SPEI. We found the SPEI better explains the variance in SIMI. Time scale analysis indicated irrigation at the large scale is most responsive at short time scales: correlation between SIMI and SPEI was maximized over a three-month SIMI period and four-month SPEI period ending in August. We found that irrigation has a highly varied response to drought among individual fields; at large geographic scales, field-level drought response is higher in the Missouri River basin, where irrigated systems are smaller and associated with small-scale watersheds. In contrast, lower field-scale response was found in the large irrigated regions in the Columbia and Snake river basins. We found significant

differences between drought response, as observed in SIMI, between classes of management, irrigation type, and crop type, explaining, in part, the differences in field-scale response to drought over the study area. We examined the relative importance of climate and crop prices on crop planting decisions, finding crop type is explained more by price than climate conditions. While cropping decisions are likely driven by many farm-specific factors that we cannot observe at the study scale, the relatively high importance of price, coupled with the relative inflexibility of irrigation to climate in the most heavily irrigated regions in the study, indicate the system is inflexible and unlikely to respond to a great degree to further water scarcity in the future without different management incentives.

REFERENCES

[1] B. A. Sinokrot and J. S. Gulliver, "In-stream flow impact on river water temperatures," *J. Hydraul. Res.*, vol. 38, pp. 339–349, Sept. 2000.

[2] B. D. Richter, D. Bartak, P. Caldwell, K. F. Davis, P. Debaere, A. Y. Hoekstra, T. Li, L. Marston, R. McManamay, M. M. Mekonnen, B. L. Ruddell, R. R. Rushforth, and T. J. Troy, "Water scarcity and fish imperilment driven by beef production," *Nature Sustainability*, vol. 3, pp. 319–328, Mar. 2020.

[3] D. J. Molden, R. Sakthivadivel, C. J. Perry, and C. de Fraiture, *Indicators for Comparing Performance of Irrigated Agricultural Systems*. IWMI, 1998.

[4] J. D. Oster and D. Wichelns, "Economic and agronomic strategies to achieve sustainable irrigation," *Irrig. Sci.*, vol. 22, pp. 107–120, Nov. 2003.

[5] P. Wurster, M. Maneta, S. Beguería, K. Cobourn, B. Maxwell, N. Silverman, S. Ewing, K. Jensco, P. Gardner, J. Kimball, Z. Holden, X. Ji, and S. M. Vicente-Serrano, "Characterizing the impact of climatic and price anomalies on agrosystems in the northwest united states," *Agric. For. Meteorol.*, vol. 280, p. 107778, Jan. 2020.

[6] S. Wallander, A. Hrozencik, M. Aillery, S. Wallander, A. Hrozencik, and M. Aillery, "Irrigation organizations: Drought planning and response," Jan. 2022.

[7] C. L. Norton, M. P. Dannenberg, D. Yan, C. S. A. Wallace, J. R. Rodriguez, S. M. Munson, W. J. D. van Leeuwen, and W. K. Smith, "Climate and socioeconomic factors drive irrigated agriculture dynamics in the lower colorado river basin," *Remote Sensing*, vol. 13, p. 1659, Apr. 2021.

[8] D. Ketchum, Z. Hoylman, D. Brinkerhoff, J. Huntington, and K. Jencso, "The sustainability of irrigation and streamflow in the western united states,"

[9] United States Bureau of Reclamation and Interior Region 7: Upper Colorado River Basin, "Upper colorado river basin consumptive uses and losses, 2016 - 2020," tech. rep.

[10] B. Udall and J. Overpeck, "The twenty-first century colorado river hot drought and implications for the future," *Water Resour. Res.*, vol. 53, pp. 2404–2418, Mar. 2017.

[11] P. C. D. Milly and K. A. Dunne, "Colorado river flow dwindles as warming-driven loss of reflective snow energizes evaporation," *Science*, vol. 367, pp. 1252–1255, Mar. 2020.

[12] S. Blumstein and J. D. Petersen-Perlman, "When the water runs dry: supporting adaptive governance in transboundary river basins," *Water Int.*, vol. 46, pp. 306–324, Apr. 2021.

[13] K. Wheeler, E. Kuhn, L. Bruckerhoff, B. Udall, J. Wang, L. Gilbert, S. Goeking, A. Kasprak, B. Mihalevich, B. Neilson, H. Salehabadi, and J. C. Schmidt, "Alternative management paradigms for the future of the colorado and green rivers." `https://www.fs.usda.gov/rm/pubs_journals/2021/rmrs_2021_wheeler_k001.pdf`, 2021. Accessed: 2023-4-13.

[14] K. G. Wheeler, B. Udall, J. Wang, E. Kuhn, H. Salehabadi, and J. C. Schmidt, "What will it take to stabilize the colorado river?," *Science*, vol. 377, pp. 373–375, July 2022.

[15] R. Q. Grafton, J. Williams, C. J. Perry, F. Molle, C. Ringler, P. Steduto, B. Udall, S. A. Wheeler, Y. Wang, D. Garrick, and R. G. Allen, "The paradox of irrigation efficiency," *Science*, vol. 361, pp. 748–750, Aug. 2018.

[16] C. A. Scott, S. Vicuña, I. Blanco-Gutiérrez, F. Meza, and C. Varela-Ortega, "Irrigation efficiency and water-policy implications for river basin resilience," *Hydrol. Earth Syst. Sci.*, vol. 18, pp. 1339–1348, Apr. 2014.

[17] M. C. Anderson, R. G. Allen, A. Morse, and W. P. Kustas, "Use of landsat thermal

imagery in monitoring evapotranspiration and managing water resources," *Remote Sens. Environ.*, vol. 122, pp. 50–65, July 2012.

[18] D. Ketchum, K. Jencso, M. P. Maneta, F. Melton, M. O. Jones, and J. Huntington, "IrrMapper: A machine learning approach for high resolution mapping of irrigated agriculture across the western U.S," *Remote Sensing*, vol. 12, p. 2328, July 2020.

[19] F. S. Melton, J. Huntington, R. Grimm, J. Herring, M. Hall, D. Rollison, T. Erickson, R. Allen, M. Anderson, J. B. Fisher, A. Kilic, G. B. Senay, J. Volk, C. Hain, L. Johnson, A. Ruhoff, P. Blankenau, M. Bromley, W. Carrara, B. Daudert, C. Doherty, C. Dunkerly, M. Friedrichs, A. Guzman, G. Halverson, J. Hansen, J. Harding, Y. Kang, D. Ketchum, B. Minor, C. Morton, S. Ortega-Salazar, T. Ott, M. Ozdogan, P. M. ReVelle, M. Schull, C. Wang, Y. Yang, and R. G. Anderson, "OpenET: Filling a critical data gap in water management for the western united states," *J. Am. Water Resour. Assoc.*, Nov. 2021.

[20] C. Boryan, Z. Yang, R. Mueller, and M. Craig, "Monitoring US agriculture: the US department of agriculture, national agricultural statistics service, cropland data layer program," *Geocarto Int.*, vol. 26, pp. 341–358, Aug. 2011.

[21] United States Department of Agriculture, National Agricultural Statistics Service, "2018 irrigation and water management survey," Tech. Rep. 3, United States Department of Agriculture, Nov. 2019.

[22] P. R. Seaber, F. Paul Kapinos, and G. L. Knapp, "WSP 2294." `https://pubs.usgs.gov/wsp/wsp2294/`, 1987. Accessed: 2023-4-14.

[23] J. T. Abatzoglou, "Development of gridded surface meteorological data for ecological applications and modelling," *Int. J. Climatol.*, vol. 33, pp. 121–131, Jan. 2013.

[24] G. B. Senay, "Satellite psychrometric formulation of the operational simplified surface

energy balance (SSEBop) model for quantifying and mapping evapotranspiration," *Appl. Eng. Agric.*, vol. 34, no. 3, pp. 555–566, 2018.

[25] T. B. Mc Kee, N. J. Doesken, and J. Kleist, "The relationship of drought frequency and duration to time scales." `https://climate.colostate.edu/pdfs/relationshipofdroughtfrequency.pdf`, 1993. Accessed: 2023-4-14.

[26] S. M. Vicente-Serrano, S. Beguería, and J. I. López-Moreno, "A multiscalar drought index sensitive to global warming: The standardized precipitation evapotranspiration index," *J. Clim.*, vol. 23, pp. 1696–1718, Apr. 2010.

[27] J. Adams, "climate_indices, an open source python library providing reference implementations of commonly used climate indices," 2017.

[28] R. Frasure. personal communication, Jan. 2023.

[29] B. Kirschenheiter. personal communication, Jan. 2023.

[30] E. Bell, "per." personal communication, Jan. 2023.

[31] Montana Department of Revenue, "Revenue final land unit (FLU) classification, 2019," May 2019.

[32] U. D. of Water Resources, "Water related land use," 2016.

[33] S. G. Buto, B. L. Gold, and K. A. Jones, "Development of a regionally consistent geospatial dataset of agricultural lands in the upper colorado river basin, 2007–10," *US Geological Survey Scientific Investigations Report.*

[34] W. S. D. of Agriculture, "Agricultural land use," 2017.

[35] "Quick stats: United states department of agriculture national agricultural statistics service," 2020.

[36] U.S. Bureau of Labor Statistics, "Producer price index by commodity: Farm products." Title of the publication associated with this dataset: Producer Price Index by Commodity: Farm Products.

[37] A. Gelman and D. B. Rubin, "Inference from iterative simulation using multiple sequences," *Stat. Sci.*, vol. 7, no. 4, pp. 457–472, 1992.

Table 4.1: Summary of crops: drought response, area, and irrigation water use

CDL Crop Code	Crop	Area [sq km^2]	Response	IWU Rank	Area Rank	IWU Rank
1	Corn	2453	0.322	3	3	3
12	Sweet Corn	149	0.368	18	19	18
21	Barley	2388	0.348	11	4	11
23	Spring Wheat	1791	0.399	13	6	13
24	Winter Wheat	1881	0.290	9	5	9
28	Oats	126	0.493	17	20	17
36	Alfalfa	15246	0.354	5	1	5
37	Other Hay	3796	0.342	12	2	12
41	Sugarbeets	694	0.309	1	10	1
42	Dry Beans	619	0.336	14	11	14
43	Potatoes	1152	0.398	6	8	6
49	Onions	178	0.331	10	16	10
53	Peas	150	0.279	16	18	16
56	Hops	173	0.283	19	17	19
57	Herbs	109	0.283	7	21	7
58	Clover	107	0.191	22	22	22
59	Sod/Grass	998	0.319	21	9	21
66	Cherries	379	0.281	4	13	4
68	Apples	1731	0.261	2	7	2
69	Grapes	512	0.274	15	12	15
71	Tree Crops	234	0.298	20	15	20
77	Pears	246	0.247	8	14	8

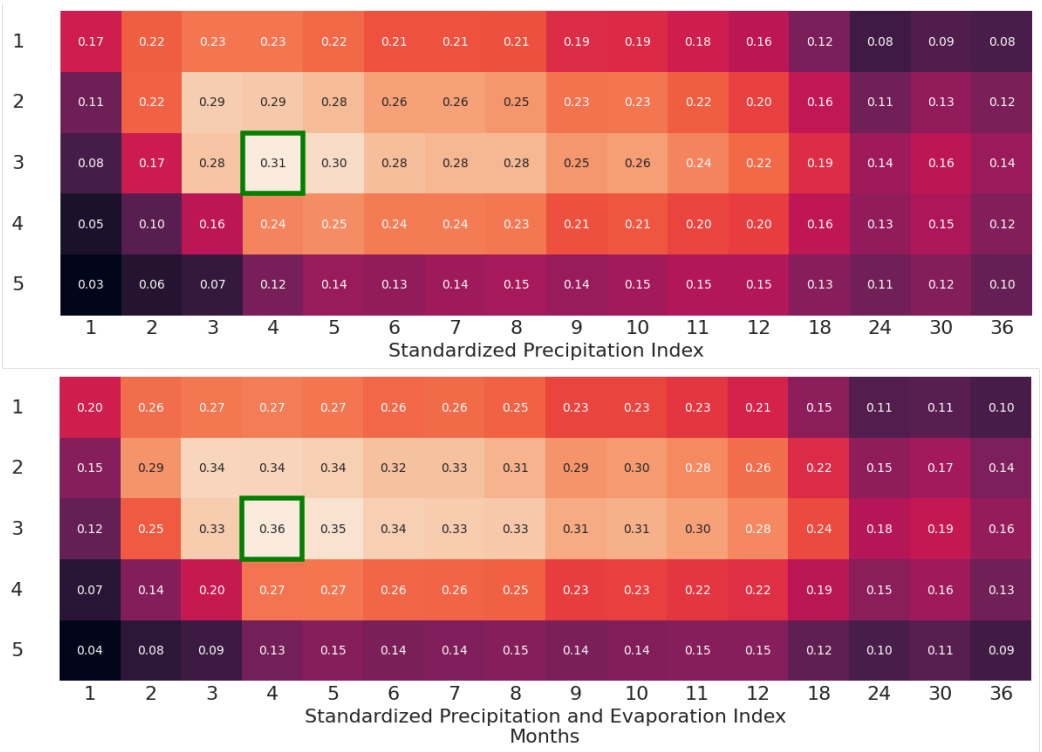

Figure 4.1: August correlations between Standardized Precipitation and Evaporation Index and Standardized Precipitation Index, and Standardized Irrigation Management Index calculated by hydrologic unit (HUC-8) over the study area and weighted by hydrologic unit mean irrigated area, 1987-2021. Months are the length of the period over which remote sensing-based crop coefficient (i.e., base data for SIMI) and gridded precipitation and reference evapotranspiration (i.e., base data for SPEI) are aggregated over the irrigated extent of each basin. Correlations (Pearson's r^2) were calculated for each month (April - October), the highest values of which were found for both SPEI and SPI in August, and are outlined in green.

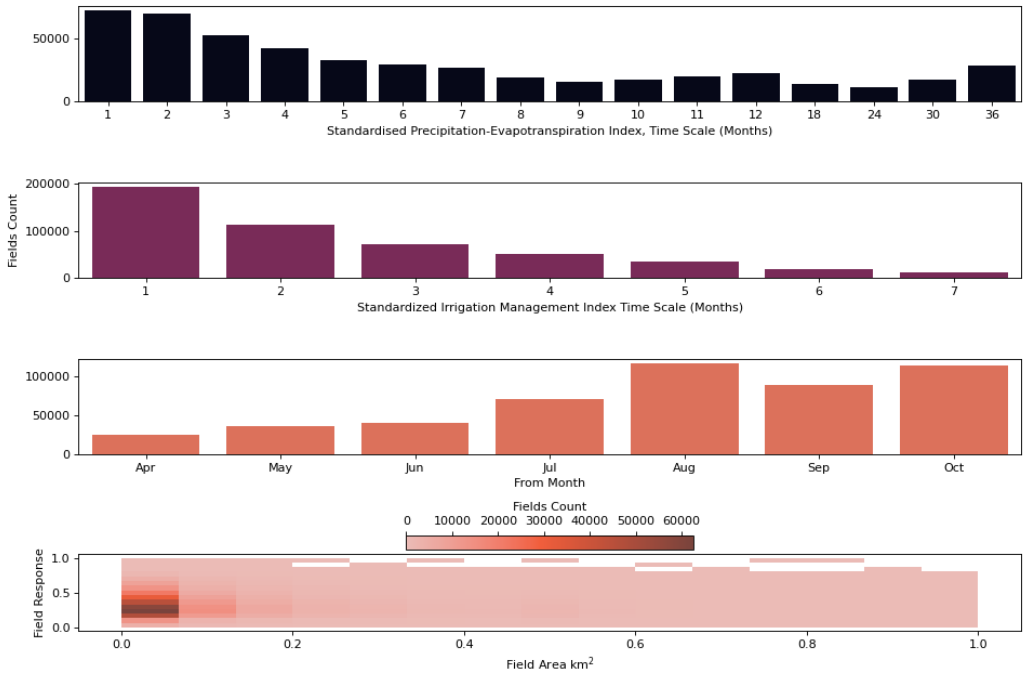

Figure 4.2: Histogram of fields' maximum correlation between Standardized Precipitation and Evaporation Index and Standardized Irrigation Management Index during the period 1987-2021 (n=495,700 fields). The third panel shows the 'lookback month' from which the highest correlation (Pearson's r^2) was found at the optimal SPEI and SIMI time scales.

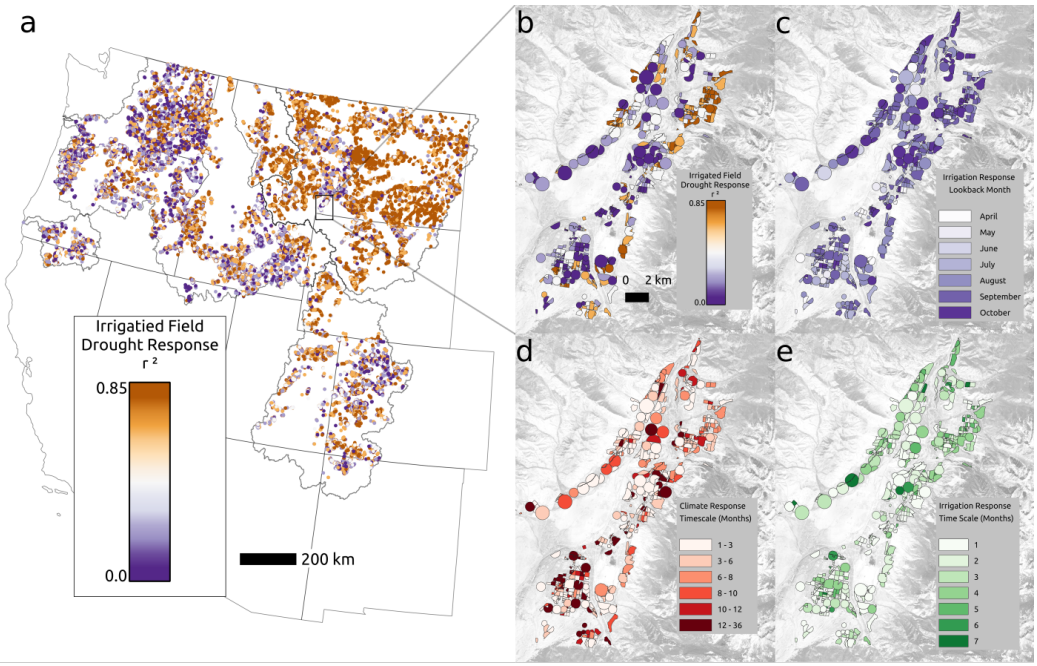

Figure 4.3: Map of the study area correlation (Pearson's r^2) between Standardized Precipitation and Evaporation Index and Standardized Irrigation Management Index during the study-wide optimal time scale (3 months SIMI, 4 months SPEI, from the end of August; n=388,600 fields). Stronger correlations are interpreted as higher response, i.e., fields that reduce irrigation during dry periods. Detail map is of Park County, Montana along the Yellowstone River, where fields are displayed (b.) according to the study-wide optimal time scales, as in (a.). In (c., d., and e.), the field-specific optimal time period of greatest SPEI-SIMI correlation is displayed, where a pattern of highly heterogeneous time scales for the lookback month (from which SIMI and SPEI are calculated), and the most responsive SPEI (climate response) and SIMI (irrigation response) is typical of the region.

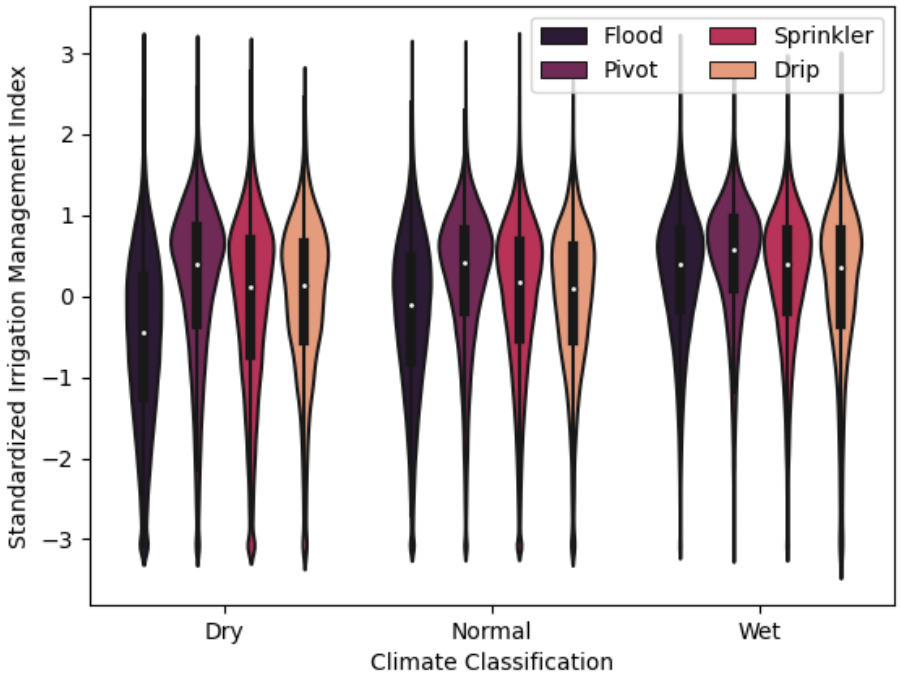

Figure 4.4: Violin diagrams show the response of individual fields categorized by irrigation type during the growing seasons 2015-2021 (n=149,000 fields). The Standardized Irrigation Management Index at each field for each growing season at the study-wide optimal time scales was sorted according to that field's Standardized Precipitation and Evaporation Index (SPEI), where SPEI less than -1.3 was classified as dry, from -1.3 to 0.0 as normal, and SPEI greater than 0.0 as wet. Fields are from the areas intersecting the study area from Colorado, Montana, New Mexico, Utah, Washington, and Wyoming, where available. Sample sizes are of 46,600 drip-, 417,100 flood-, 190,300 pivot-, and 389,100 sprinkler-irrigated field-seasons.

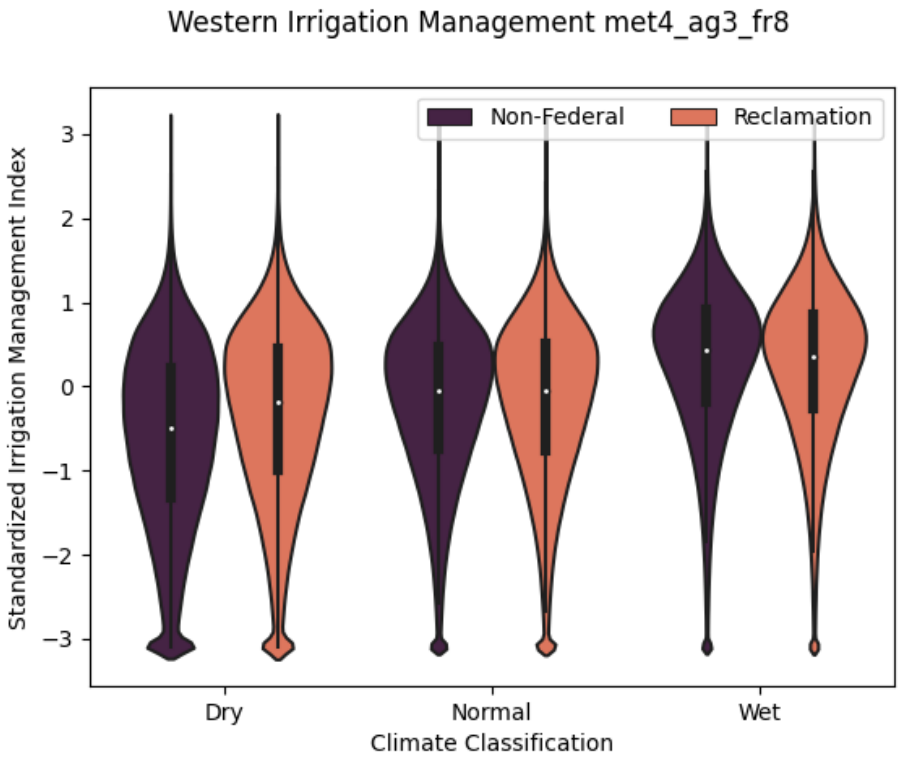

Figure 4.5: Violin diagrams show the response of individual fields categorized by federal management during the growing seasons 1987-2021 (n=115,400 fields in United State Bureau of Reclamation 'Areas Benefited' places of irrigation water use, and 330,700 fields not associated with federal infrastructure). The Standardized Irrigation Management Index at each field for each growing season at the study-wide optimal time scales was sorted according to that field's Standardized Precipitation and Evaporation Index (SPEI), where SPEI less than -1.3 was classified as dry, from -1.3 to 0.0 as normal, and SPEI greater than 0.0 as wet.

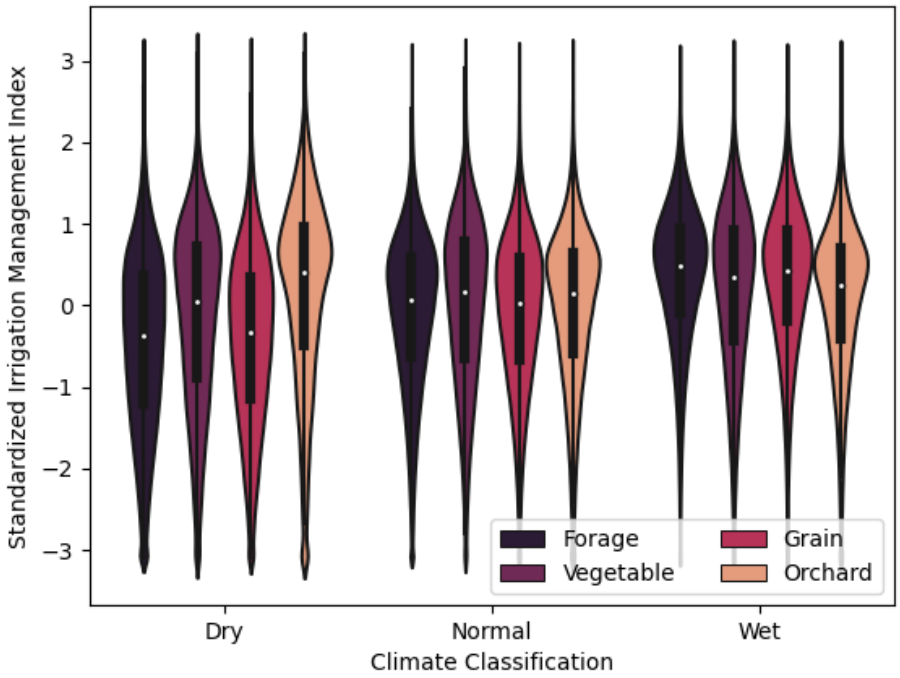

Figure 4.6: Violin diagrams show the response of individual fields categorized by general crop category type during the growing seasons 2008-2021 (n=346,600 fields). The Standardized Irrigation Management Index at each field for each growing season at the study-wide optimal time scales was sorted according to that field's Standardized Precipitation and Evaporation Index (SPEI), where SPEI less than -1.3 was classified as dry, from -1.3 to 0.0 as normal, and SPEI greater than 0.0 as wet. Sample sizes are of 1,448,300 grain, 551,900 vegetable, 2,793,200 forage, and 448,000 orchard crop field-seasons.

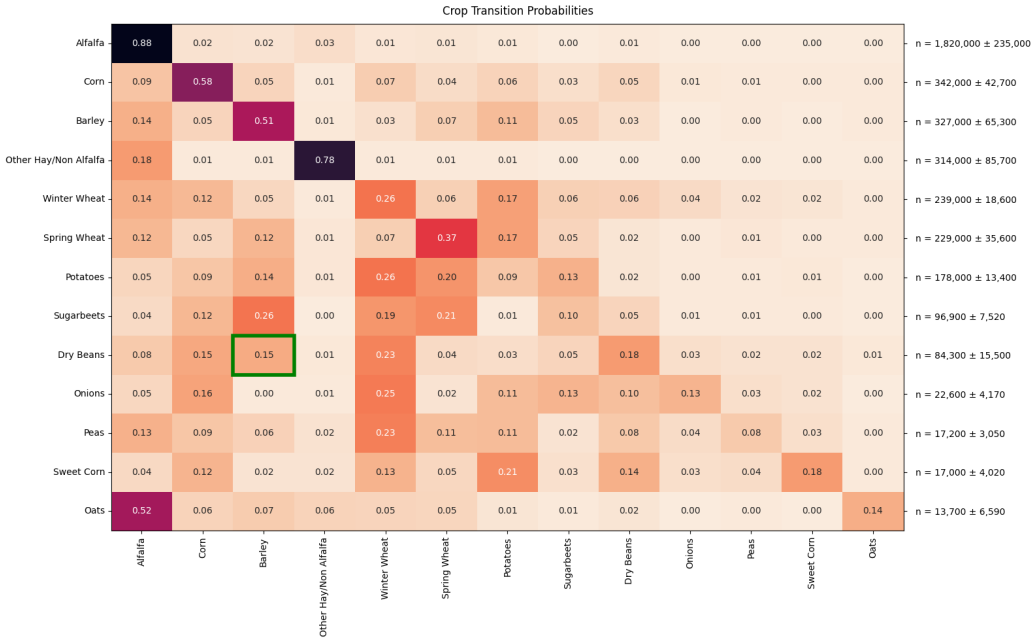

Figure 4.7: Crop transition matrix for the 13 most common field crops grown within the study area, 2008-2021, derived from field-scale majority crop counts. The transition matrix shows the probability of moving from one crop (vertical axis) to another (horizontal axis) from one growing season to the next. For example, the probability of a crop planted as dry beans subsequently planted with barley the following year is 0.15, as highlighted in green. Permanent crops (i.e., orchards, vineyards, hops) have been excluded. Uncertainty estimates (secondary y axis) are F1 scores drawn from a count-weighted average of state-based, annual CDL pixel validation, 2015-2021 (n = 107.3).

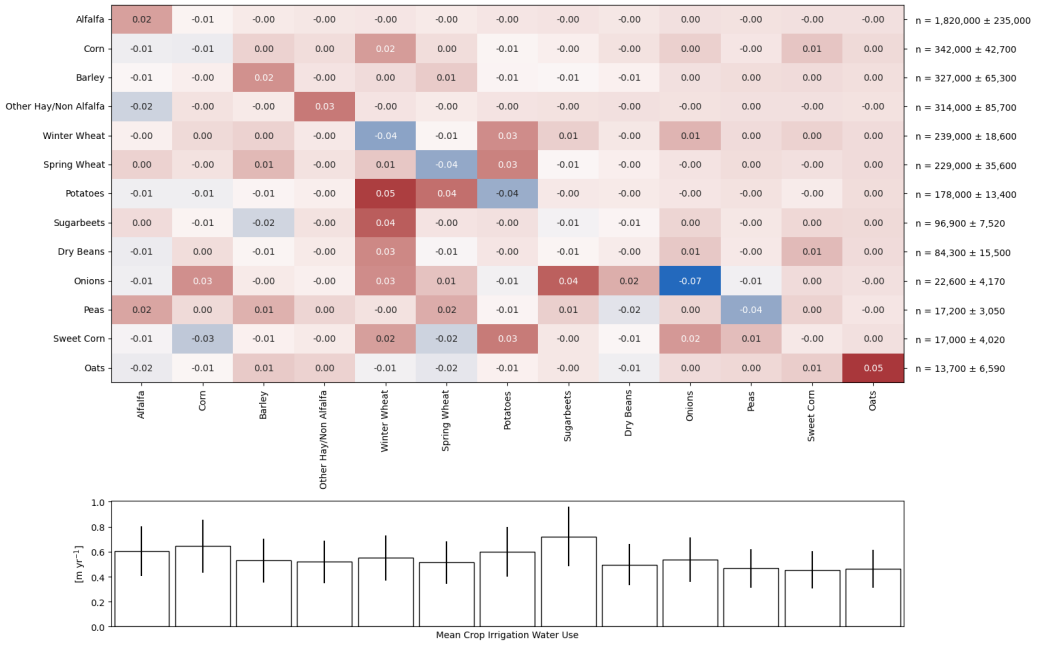

Figure 4.8: The difference in crop transition matrices between dry and wet years for the 13 most common field crops grown within the study area (2008-2021), derived from field-scale majority crop counts. Positive numbers show where the transition probability increases during drought, i.e., where a crop is more likely to be planted during dry years. Permanent crops (i.e., orchards, vineyards, hops) have been excluded. The Lower panel shows the field scale mean irrigation water use for each crop.

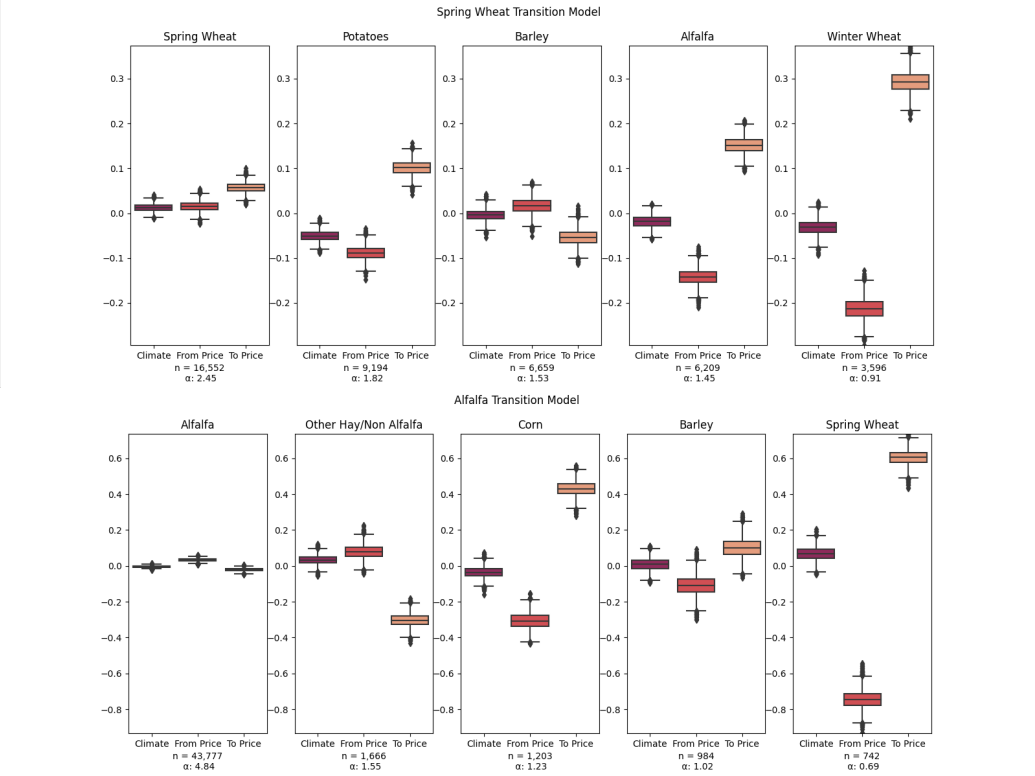

Figure 4.9: Crop transition models for spring wheat and alfalfa, using multinomial softmax regression on SPEI ('Climate'), prices for the previous year's crop ('From Price'), and the price of the crop in interest ('To Price). The leftmost panels show the transition from the crop to itself, the most common course for these crops. The α parameter describes the intercept of the modeled relationship, and is proportional to the frequency of the crop transition and inversely proportional to the magnitude of the coefficients. Most crop transition models, including these, indicate price as a more important predictor of crop planting decisions, as implied by their relatively large coefficients, compared to climate.

Chapter 5

CONCLUSION

The results of this research indicate that irrigation is having a widespread and differentiated impact on water resources in the West. The use of a systematic, sub-continental scale remote sensing-based approach to estimating irrigation water use allowed us to compare the response, via streamflow, of large systems that play a critical role in the West's economy and ecological well-being. To our knowledge, this is the first study to link the rich, high-resolution information contained in long-period remote sensing of our irrigated landscape with the analysis of meteorology and streamflow over climate-relevant timescales at a spatial scale that allows intercomparison of basins. The explicit estimate of irrigation water use at scale is a major advance, as previous estimates of irrigation by the Department of Agriculture only estimate irrigated area and irrigation water application, both of which are insufficient metrics to estimate true water use. We show that IWU may increase even in an irrigated system that sees no expansion in area and a reduction in water application, and that this may lead to the counterintuitive result that modernized, efficient irrigation systems may ultimately consume more water and lead to reductions in streamflow. We further show that the implications of this irrigation efficiency 'paradox' are basin-dependent and thus provide an avenue for water management through targeted deployment of modern irrigation systems, such as center pivots. For example, in the Snake and San Juan basins, where water is effectively exported to outlying irrigation systems, irrigation systems should be modern and efficient such that the diversion of water from the river is minimized. Conversely, our work suggests that water applied in the 'inefficient' systems along the Yellowstone River is not lost, but may return after some delay and augment flows later. These contrasting responses appear to depend both on irrigation infrastructure type and basin physiographic characteristics, such as aquifer properties. Our analysis of hundreds of

thousands of irrigated fields' response to various climate conditions represents a further advance in our understanding of the behavior of our irrigated landscape. We show that while there is a high degree of variance at the watershed scale of field-specific climate response, large-scale patterns are apparent: federal projects, pressurized irrigation infrastructure, and permanent crops are less responsive to drought. Overall, this work shows that humans have a major impact on water resources in many basins throughout the region, and while these systems are influenced by a changing climate, we can expect that management actions will result in future impacts. As such, it is imperative we fully characterize the behavior of these systems so cooperative and proactive management actions can be undertaken. More research is needed to enable optimal management: Careful physical modeling using advanced, high-resolution geospatial data will more fully characterize the response of surface water flow through detailed analysis at the basin scale of aquifer properties, irrigation system dynamics, and climate projections.